NORTHEAST GULF OF ALASKA PROGRAM

by

R. D. Muench, J. D. Schumacher,
S. P. Hayes, and R. L. Charnell

Pacific Marine Environmental Laboratory
National Oceanic and Atmospheric Administration
7606 Sand Point Way, N.E.
Seattle, Washington 98115

Final Report
Outer Continental Shelf Environmental Assessment Program
Research Unit 138

October 1978

PREFACE

Commencing in 1974, the Pacific Marine Environmental Laboratory, NOAA, has been investigating physical oceanographic processes on the continental shelf in the northern Gulf of Alaska. The work has been funded by the Bureau of Land Management as part of the Alaskan Outer Continental Shelf Environmental Assessment Program. The initial phases of this effort addressed processes in the northeastern gulf, in particular the shelf region adjacent to Icy and Yakutat bays. Geographical emphasis has shifted westward with time; the program currently emphasizes the northwest Gulf of Alaska with stress on the region surrounding Kodiak Island. Initially, the program was concerned primarily with obtaining moored current and bottom pressure measurements with only minor attentionto coincident conductivity and temperatures versus depth (CTD) and other data. More recently, the program has shifted emphasis to include collection of CTD data along with ancillary information such as that obtained from satellite-tracked drifters, drift cards and environmental buoys.

The field program in the northeastern gulf was completed in summer 1977 while that in the western section is continuing. However, based on our observations, it is evident that the Gulf of Alaska continental shelf can be divided oceanographically at Middleton Island into an eastern and western regime. The northeastern gulf is a region of relatively broad, diffuse westerly flow. The western gulf, particularly the region off Kodiak Island is characterized by a narrow, high-speed boundary flow, the Alaskan Stream. In addition to the difference in major current regimes, the shelf is narrower off Yakutat and Icy bays than off Kodiak Island and bottom topography is somewhat more irregular, though considerable topographic irregularities also exist off Kodiak Island. We would a *priori* expect shelf circulation off Kodiak Island to be more heavily influenced by shelf break circulation than in the northeastern gulf because of the more intense shelf break current in the former location. Conversely, local meteorological effects and freshwater input might be expected to have relatively greater effect on shelf circulation in the northeastern gulf.

In view of the oceanographic differences between the two regions, we can present in this final report an independent synopsis of the results of the northeast Gulf of Alaska field program without loss of understanding. The stress will be measured currents and bottom pressures, consistent with the major thrust of our field effort.

These will be related to regional circulation where possible, and to coincident temperature, salinity and weather data where appropriate. It is hoped that the end product will provide a useful working document both for environmental planning and for future, more focused, scientific endeavors in the region.

TABLE OF CONTENTS

TABLE OF CONTENTS **(continued)**

Page

LIST OF FIGURES

Figure *Page*

LIST OF TABLES

1. INTRODUCTION

Circulation in the Gulf of Alaska comprises a subarctic gyre in the North Pacific Ocean. It is characterized by a cyclonic (anticlockwise) mean circulation driven by the large-scale atmospheric flow. In the continental shelf region of the northeast gulf (Figure 1.1), we expect to see also the effects of local wind-driven circulation, freshwater input and heating and cooling in generating currents. In addition, we must consider the role of complex geography and bottom topography in modifying currents. This report addresses circulation in the northeast Gulf of Alaska from within this framework.

1.1 History of Oceanographic Research

Taken within the context of large-scale oceanic circulation, the Gulf of Alaska gyre has been indirectly discussed by various researchers (cf. Munk, 1950, Carrier and Robinson, 1962, and numerous others). These studies, which are largely theoretical, established that the gyre is driven by regional wind-stress and that as a consequence of the earth's rotation westward intensification of the Alaskan Stream must occur off Kodiak Island. Within this context, the westward shelf break flow observed in the northeast Gulf of Alaska is simply the northern arm of a cyclonic circulation encompassing the entire gulf.

Research on the northern portion of the Gulf of Alaska has been severly hampered in the past by lack of field data. One of the earliest works was that of McEwen, Thompson and Van Cleve (1930), who used temperature and salinity data obtained along sections normal to the coast from Cape Cleare and Yakutat Bay to discuss regional temperature and salinity structure and currents over the shelf and shelf break. Not until some three decades later, with increased interest in the regional fisheries potential, did significant additional field work occur. The resulting manuscripts used temperature and salinity data to address large scale circulation in the Alaskan Stream southwest of Kodiak Island and westward along the Aleutian Chain, rather than in the northeastern gulf (e.g., Favorite, 1967). Drift-card studies were an exception, however, and provided qualitative support for cyclonic circulation in the Gulf of Alaska and a westerly flow south of the Aleutians (Favorite, 1964; Favorite and Fisk, 1971). An excel "lent oceanographic summary of the subarctic Pacific covering research through about 1972, including a thorough reference list, has been prepared by Favorite, Dodimead and Nasu (1976). As in prior work they discuss primarily larger-scale features and details in the northwest gulf, but find insufficient data to address details in the northeast gulf.

Following inception of the BLM-sponsored Outer Continental Shelf Environmental Assessment Program in 1974, data were acquired *from* the northeast Gulf of Alaska which were sufficient to describe regional oceanographic conditions. The first resultant work was a

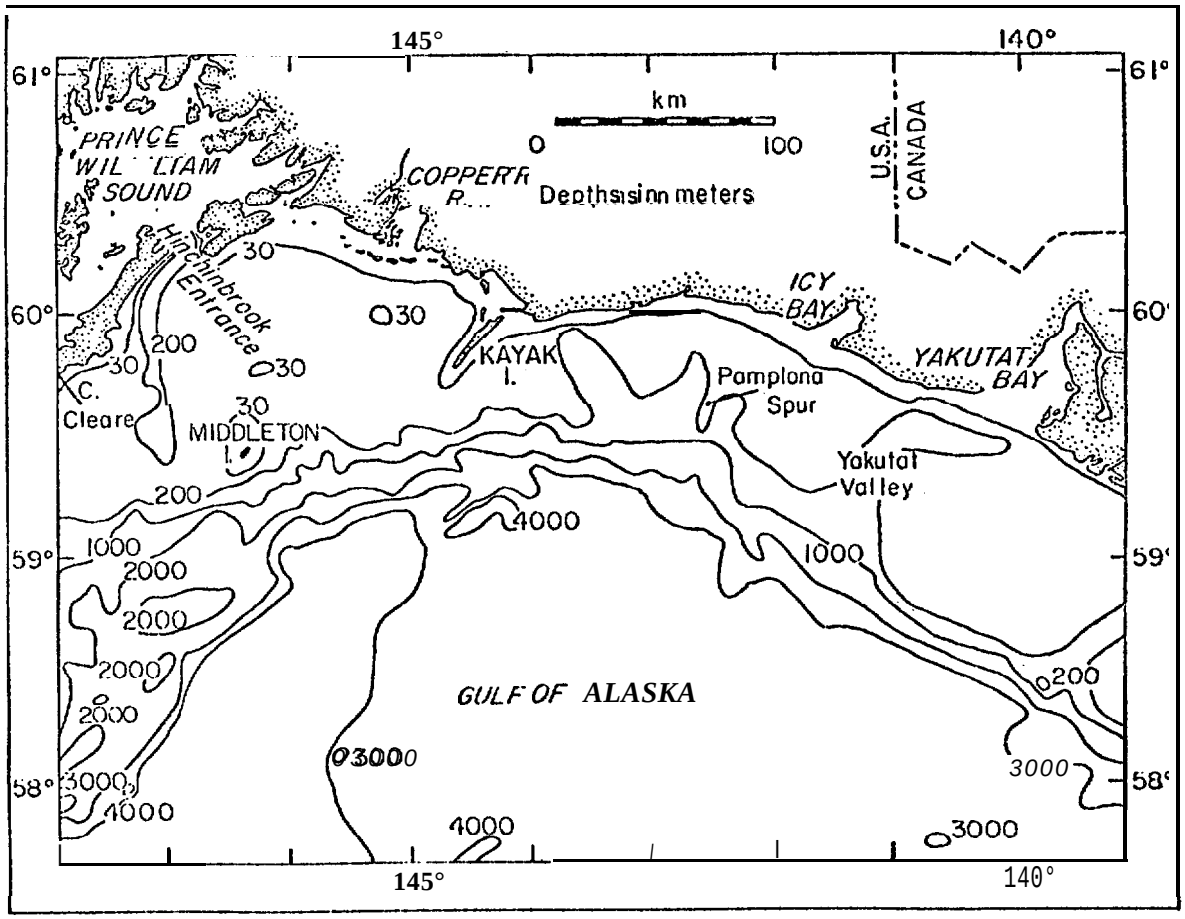

Figure 1.1 - Geographical location in the northeast Gulf of Alaska.

characterization of seasonal variations in the water column in the northern gulf based on time series observations from a single oceanographic station in the northern central gulf (Royer, 1975). Gait and Royer (in press) used current and hydrographic data to discuss large-scale current, temperature and salinity distributions in the northern gulf. Royer and Muench (1977) discussed some large-scale features in the surface temperature distribution and related these to the regional circulation and to vertical mixing regimes on the shelf. Hayes and Schumacher (1976), Hayes (1978), and Holbrook and Halpern (1977) have described and discussed variations in winds, currents and bottom pressures on the shelf off Icy Bay during the period February-May 1975.

1.2 Geographical Setting

The northern Gulf of Alaska is characterized by an arcuate, east-west trending coastline indented with several embayments, the largest of which are Yakutat and Icy bays and Prince William Sound (Figure 1.1). Kayak Island provides an effective southward-extending promontory, more like a peninsula than an island, while Middleton Island occupies the center of a shoal region south of Prince William Sound. The coastline between Yakutat Bay and Kayak Island is characterized by numerous glacial streams which contribute freshwater to the marine system during summer. A major concentrated freshwater source, the Copper River, is present between Kayak Island and Prince William Sound.

Topography adjacent to the coast is generally rugged", with elevations greater than 3,000 m and long, steep-sided valleys which serve to channel strong winter drainage winds. Such valleys are located, for example, at the heads of Yakutat and Icy bays. The Copper River valley also serves as a route for drainage winds. Discussion of the shelf in relation to Prince William Sound is not included in this report; we have chosen the western boundary of our study area to lie along a line between Hinchinbrook Entrance and Middleton Island and the eastern boundary to lie roughly normal to the coastline at Yakutat Bay.

Bathymetrically, the region is complex. The shelf is bounded roughly by the 200 m isobath, seaward of which bottom depths drop off steeply to 3,000-4,000 m. Shelf width is about 50 km between Yakutat Bay and Kayak Island and increases to nearly 100 km west of Kayak Island. The shelf between Yakutat Bay and Kayak Island is marked by major irregularities in the form of valleys and ridges normal to the coastline. The most obvious such features are Yakutat Valley and Pamplona Spur. West of Kayak Island the shelf attains a generally more uniform topography and is somewhat shallower over much of its extent as indicated by the shoal areas (depths of less than 30m) including that surrounding Middleton Island.

1.3 Oceanographic and Meteorological Setting

Since we are concerned in this report with observed circulation, this section will be limited to a brief discussion of those factors which might be expected to directly affect the circulation. In general, we can expect circulation in any shelf region to be affected by both the offshore or shelf break current, via lateral momentum transfer onto the shelf, and by local forcing due to winds and fresh-water input as it affects the baroclinic field. We discuss the former factor first.

1.3.1 Regional oceanographic process

Gulf of Alaska circulation is a subarctic gyre within the North Pacific Ocean. Water for this circulation comes from the North Pacific Drift, which flows easterly from the vicinity of Japan and splits into two branches west of Vancouver Island. The south-flowing branch parallels the coast to become the California Current, while the northerly flowing branch follows the coastline and eventually becomes the Alaskan Current. The lower latitude origin of this water gives rise to characteristic temperature and salinity features which have been discussed by Royer (1975), Royer and Muench (1977) and Gait and Royer (in press). These features include subsurface warm and cold cores, both of which are generated at mid-latitudes and sink beneath the high latitude layer of less saline, less dense water which is locally formed in the northern Gulf of Alaska. "[he temperature maximum can, if we neglect the effects of diffusion, be used to trace the path of flow followed by the shelf break current in our study region (Figure 1.2),

While temperature and salinity distributions can be used to trace flow path, obtaining estimates of current speed proves more difficult. We approach it indirectly, using the known fact that the subarctic gyre derives its energy from the regional atmospheric circulation. Ingraham, Bakun and Favorite (1976) have computed mean monthly wind stress curls over the Gulf of Alaska for the period 1950-1976 and used these to compute total wind-driven water transport recording *to* the method of Sverdrup (1947). This method yields a northward transport throughout the gulf which is dynamically constrained to exit the northern gulf as a concentrated stream along the northwestern boundary (cf Welander, 1959, for a discussion of the dynamics of this mechanism). We recognize this concentrated flow as the Alaskan Stream southeast of Kodiak Island. Mean winter f-low streamlines computed using the wind stress curl by Ingraham *et al.* (1976) are shown in Figure 1.3. It is immediately apparent that our study region in the northeast gulf lies east of the area where appreciable intensification would be expected to occur. Therefore, while there is a westerly flow, current speeds and volume transports would be expected to be a factor of two or three less than computed for the Alaskan Stream farther west. This conclusion is qualitatively supported by the theoretical work of Thomson (1972).

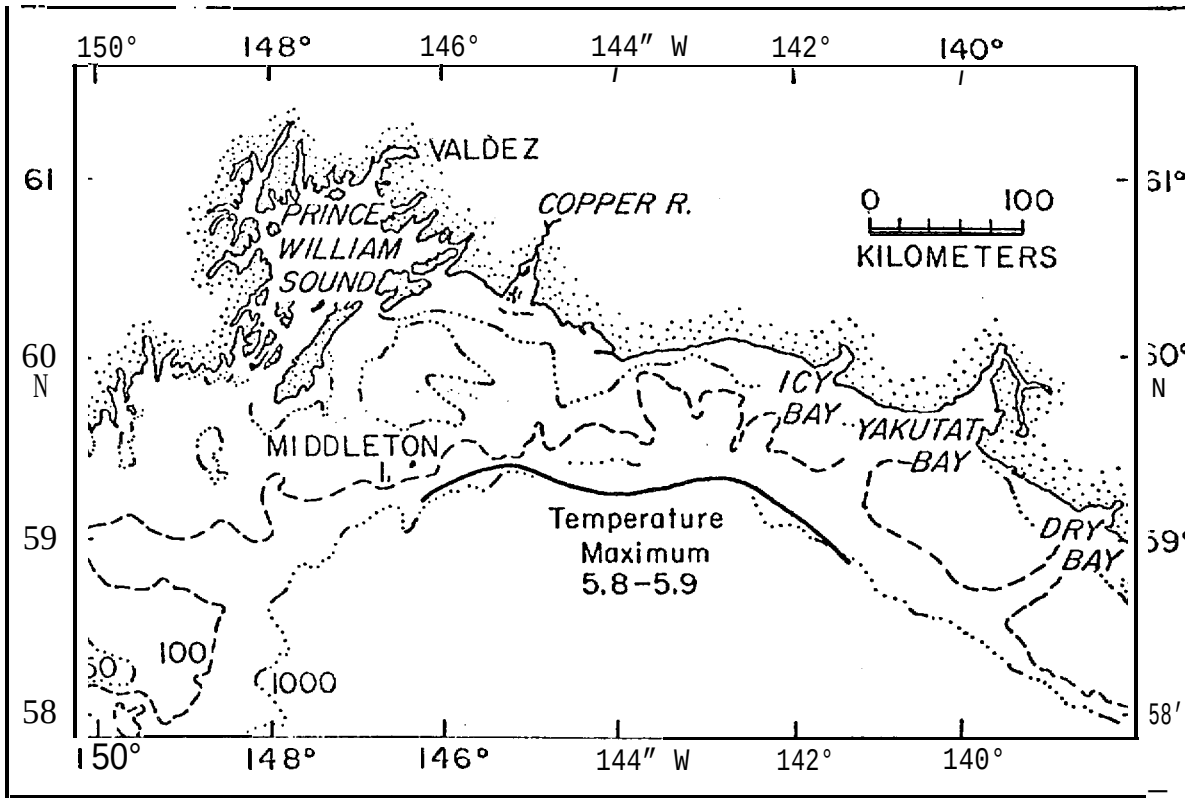

Figure 1.2 - Axis of subsurface temperature maximum used as an indicator of flow streamlines in the Alaska Current in the northeast Gulf of Alaska (from Gait and **Royer,** in press).

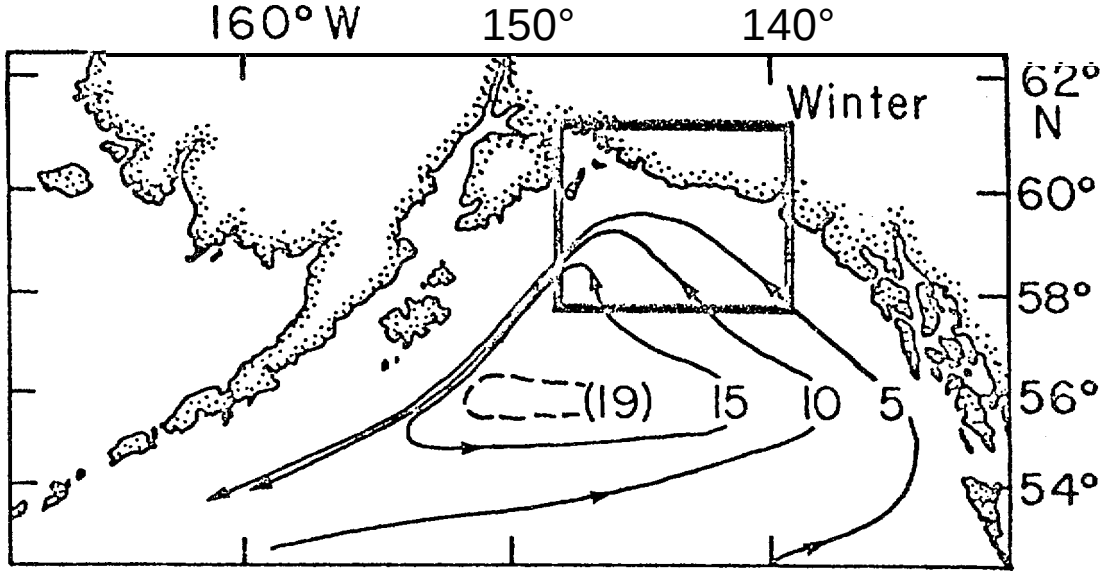

Figure 1.3 - Schematic showing winter water transport in million cubic meters per second computed from wind stress curl (from **Ingraham** et al., 1976) . Rectangle shows our study region, approximately the area included in Figure 1.1.

Computed summer transports were, as opposed to winter transports, virtually zero. This is a consequence of decay of the Aleutian Low atmospheric pressure system during summer and concurrent loss of the wind stress and was also noted, using sealevel data, by Reid and Mantyla (1976). Ingraham *et* aZ. (1976) also noted considerable year-to-year variability in winter transport; values varied from as low as about 9 x $10^6 m^3 s^{-1}$ (in 1963) to as high as 25 x $10^6 m^3 s^{-1}$ (in 1969). We therefore, can expect considerable interyear variability in current speeds along the shelf break in our study region, as well as large intrayear differences.

The method of averaging used by Ingraham *et al.* (1976) in computing wind stress curl likely biased the computed transport toward the low side. Aagaard (1970) carried out wind-driven transport calculaions for the Norwegian Sea, following the procedure of Fofonoff (1960), and analyzed the effect which varying the wind stress averaging period had upon computed transports. He found that the six-hourly mean wind stress curl yielded transports some four times greater than monthly mean curls, and attributed the difference to the importance of wind stress variability in affecting transport. Since the Gulf of Alaska is characterized by highly variable winter winds, it seems likely that the actual transports are larger than those computed by Ingraham *et* aZ. (1976).

Shelf break flow in the northern Gulf of Alaska gyre is important to continental shelf flow only inasmuch as energy from this flow is transferred onto the continental shelf. Since, by conservation of potential vorticity, flow will tend to follow isobath and hence follow the shelf break, indirect means of transferring energy to the shelf must be found. One probability is that a longshore sea level slope connected with the longshore mean flow generates nearshore currents, in similar fashion to that discussed in the Gulf of Maine by Csanady (1974). Another is simply lateral friction transfer of mean flow energy onto the shelf; this might be manifested in the form of eddy-like features splitting off from the current and migrating shoreward as they dissipate energy along their paths as observed for the Florida Current (Lee, 1975). This process, discussed by Csanady (1975), would result in transfer of kinetic energy onto the shelf from the shelf break currents. A considerable volume of material has been written on lateral momentum transfer, and it is not our intention to dwell on this here but rather to emphasize that such processes exist and can be considered significant in the northeast gulf.

1.3.2 Local or shelf oceanographic processes

The study of shelf dynamics currently comprises one of the most active fields in physical oceanographic research. It is this field which deals with processes affecting circulation on the continental shelves. We make no attempt here to present a thorough discussion and bibliography addressing shelf processes; such a task would indeed be monumental. Instead, we present a brief discussion of

those processes which *a priori* may be important to coastal circulation in our study region. We will neglect more esoteric concepts, particularly those whose importance has not been demonstrated by field observations in other regions.

Local winds are a mechanism of major importance for generation of currents on continental shelves. This must be judged especially true in the northern Gulf of Alaska, due to the severity of winter storms transiting the region. Mooers (1976) has given a useful summary of information concerning wind-driven currents on the continental shelves, including a set of references complete up to that date. He classifies locally wind-driven shelf motions as free and forced waves (continental shelf waves} and transient responses (storm surges). A discussion of coastal upwelling/downwelling regimes is included, along with discussion of near-surface and bottom mixed-layer development. All of these phenomena would be expected to occur along the shelf in the northeast gulf. Royer (1975) has characterized the northern Gulf of Alaska shelf as a region of coastal downwelling during winter due to prevailing easterly winds. During summer the wind field relaxes and a weak upwelling tendency is present. More recent observational and theoretical material has enriched our general knowledge of wind-driven shelf waves (Clarke, 1977; Brooks and Mooers, 1977).

The presence of lateral and vertical current shear, in conjunction with density gradients, can lead to certain types of instabilities which are revealed in the current records as periodic motions. Such motions have been detected in the Norwegian current by Mysak and Schott (1978), and we expect similar effects in the northeast gulf, an oceanographically similar region. In addition, the westerly-flowing current must interact with the local bathymetry. There is evidence in satellite imagery, for example, that lee vortices form on the downstream (west) side of Kayak Island (Muench and Schmidt, 1975). It is also likely that the current is perturbed as it passes over the irregular transverse ridge and valley shelf topography between Yakutat Bay and Kayak Island.

Considerable freshwater input to the northeast gulf coastal region occurs during early summer due to snow melt. A second runoff peak occurs in autumn due to local storms which can generate large amounts of precipitation. The resultant low salinity layer is advected westward along the coast (Muench and Schmidt, 1975), and contributes to baroclinicity there. Cessation of most of this freshwater input during winter, coupled with wind and thermohaline mixing, reduces baroclinicity and leads to vertically-uniform temperature, salinity structure on the shelf (Royer, 1975).

1.3.3 Meteorological conditions.

Meteorological conditions over the shelf region of the northeast Gulf of Alaska are subject to strong annual variation. During winter, atmospheric circulation over the Gulf of Alaska is dominated by a low pressure trough, the Aleutian Low. This trough

effectively comprises a trajectory for severe cyclonic winter storms which originate to the west along the Aleutian Islands then migrate northeastward! as they intensify. Typically, migration speeds are 12-25 m see- . Wind speeds during passage of these cyclonic storms can be high; over about a 15 year period, speeds greater than 48 knots occurred for 1% of the time during November-February in the coastal region off Yakutat (Brewer *et al.*, 1977). Though statistics are not complete, the time scales of these storms appear to be of order 5-7 days. During winter the coastal waters will, therefore, be subjected to sequential events of strong easterly winds which, average over periods of a month or more, yield a mean easterly wind stress.

During summer, the Aleutian Low dissipates largely and is displaced by an atmospheric high pressure system, the North Pacific High. While low pressure systems migrate eastward through the system, as in winter, they do not tend to intensify. As a result, winds over the shelf are generally weak and variable, though there is a net eastward component. As in winter, the wind field is event-dominated.

Recent research on near-coastal meteorology in the northeast gulf has clarified the role of the coastal mountain ranges and valleys in directing near-coastal winds (Reynolds *et al.*, in press). The mountains are sufficiently high that they cause bunching of the isobars. This leads to alignment of winds into a direction parallel to the coastline, an effect which has been observed in extreme cases to extend as far as 100 km offshore. Caution must therefore be used when using computed geostrophic winds such as those from Bakun (1975) in the region adjacent to this mountainous coast.

Reynolds *et* aZ., have also investigated the effects of drainage, or katabatic, winds which are funneled seaward through the valleys in the coastal topography. These drainage winds may flow seaward as far as about 25 km, and can comprise considerable perturbations on the large-scale wind field within the coastal region. Particularly low temperatures can occur during these localized wind events, clue to the continental source of air masses. Mean monthly winter temperatures in the coastal region off Icy Bay and Yakutat vary from a minimum of about -10°C to a maximum of about +8°C {in February-March; from Brower *et al* ., 1977).

As a general summary, we can say that winds over the shelf in the northeast gulf are easterly in winter, westerly and weak in summer, and dominated by events. Topographic effects can become significant in the near-coastal regions, therefore, geostrophic winds must be used with caution in such areas.

2. OBSERVATIONAL PROGRAM

In an ideal world, we could recreate the ocean in a computer model and generate the oceanic velocity fields from first principals. However, the real ocean is so rich in variability that a *priori* modeling is impractical. Rather, observational results must be accumulated and events documented in order that the models may be guided into correct approximations. In this manner, models may be used to extend observational results so that we may predict what will probably happen in a given situation.

The experimental program discussed here was designed with this philosphy in mind. The immenseness of the continental shelf in the Gulf of Alaska defies saturation of measurements. Instead, the program provided coverage sufficient to establish statistics of the velocity field at a few points (61 and 62). This was supplemented by process-oriented studies in areas which were selected so that either generic dynamics (Icy Bay Experiment) or site specific problems (west of Kayak Island) could be studied. The dynamical studies related velocity field to wind forcing, bathymetry, sea surface slope, and density field. The process experiments are required in order to interpret statistical observations.

2.1 The Overall Flooring Program

Current meter station locations are shown in Figure 2.1. Aanderaa RCM-4 current meters were used on taut wire moorings with an anchor and acoustic release at the bottom and 1,000-lb subsurface buoyancy float above the top current meter (Figure 2.2). A summary of location, duration and depth of each station's current meters is given in Table 2.1.

Current data were resolved into north and east components and low-pass filtered to remove high-frequency noise. Two new data series were then produced using a Lanczos filter (cf. Charnell and Krancus, 1976). The first series was filtered such that over 99% of the amplitude was passed at periods greater than 5 hours, 50% at 2.86 hours, and less than 0.5% at 2 hours. The second series, filtered to remove most of the tidal energy, passed over 99% of the amplitude at periods of over 55 hours, 50% at 35 hours, and less than 0.5% at 25 hours. This was resampled at 6-hour intervals and *was* used *for* examining non-tidal circulation.

Temperature and salinity data were co-l lected using Plessey model 9040 CTD systems with model 8400 data loggers. This system sampled twice per second for simultaneous values of conductivity, temperature and depth. Data were recorded during the down cast using a lowering rate of 30 m rein-]. Nansen bottle samples were taken at each station to provide temperature and salinity calibration data. The data were averaged to provide l-m temperature and salinity values from which the other parameters were then computed.

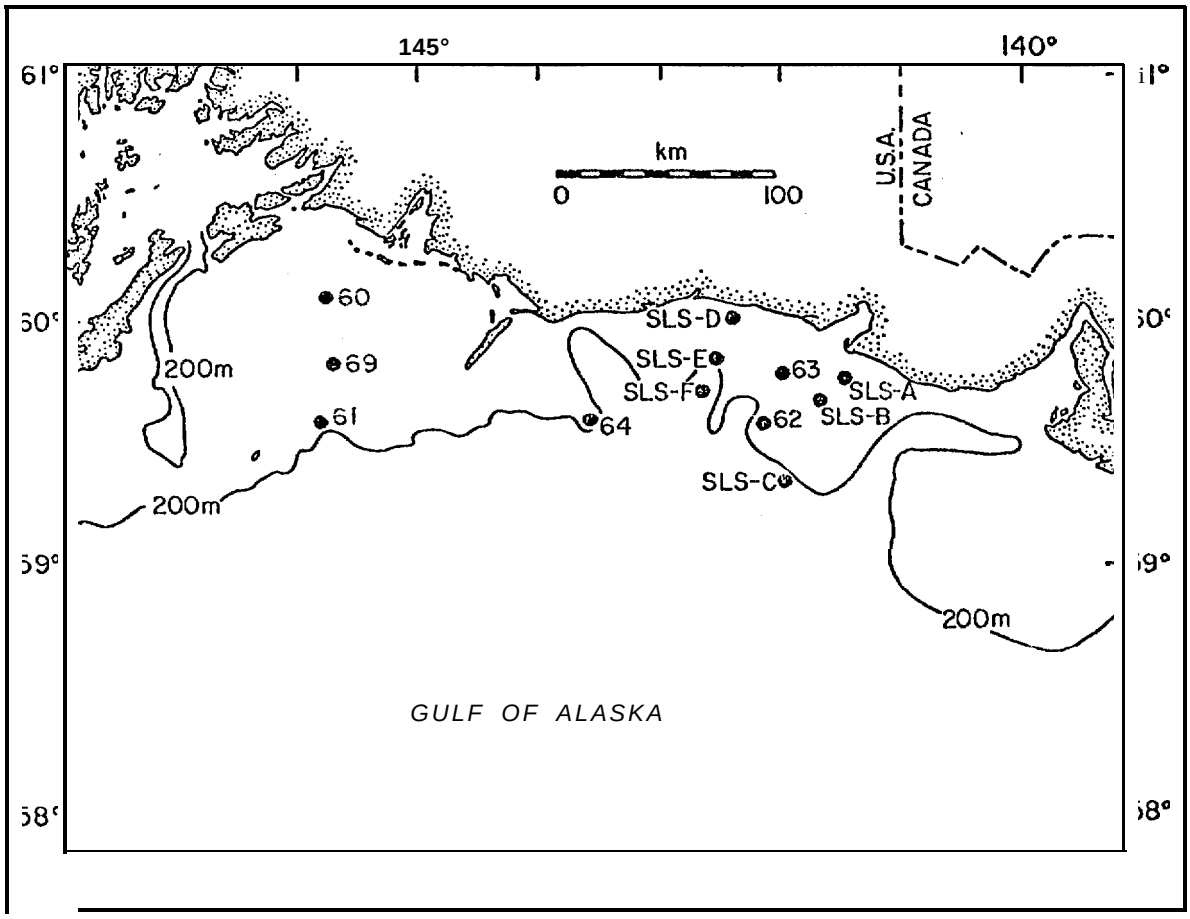

Figure 2.1 - Locations of current meter moorings in the northeast Gulf of Alaska.

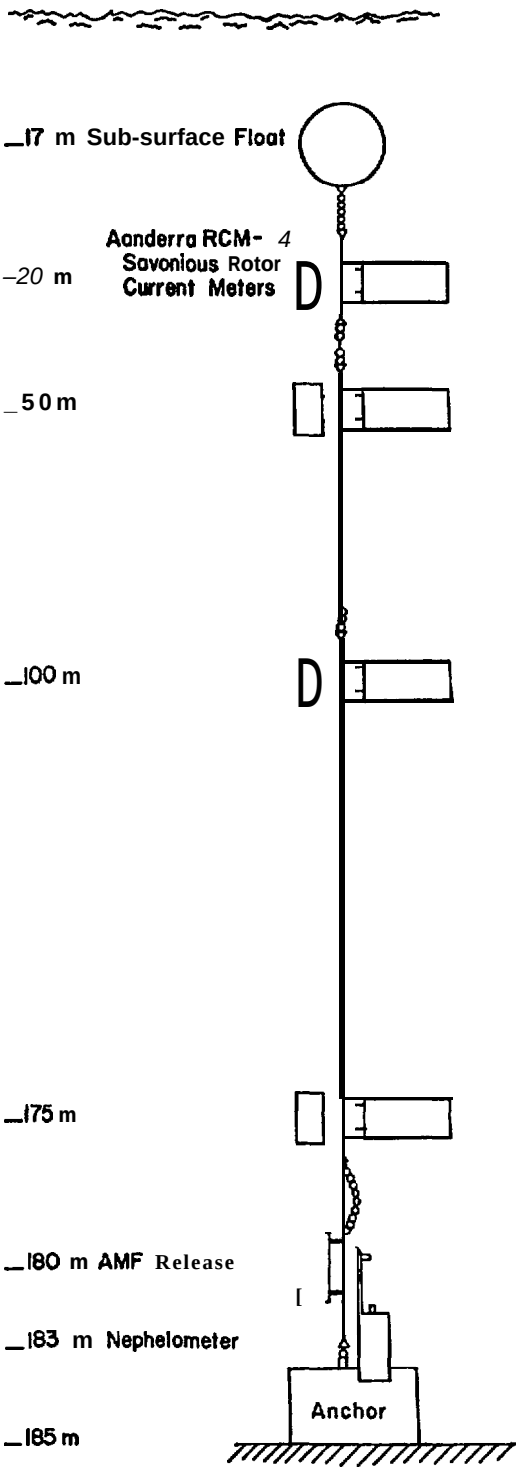

Figure 2.2 - Schematic diagram showing configuration of current moorings used in the northeast Gulf of Alaska (from Feely et al., 1978). Where pressure gauges were used, they replaced the nephelometer.

TABLE 2.1 Northeast Gulf of Alaska mooring deployment information

Sta. No.	LAT(N)	LONG(W)	DATES	Instr. Ser. No.	Instr. Depth
60A	60°05.4′	145°50.7′	7/2/74-9/3/74		
			"	625	20
			7/2/74-9/1/74	412	30
			7/2/74-8/29/74	392	50
			7/2/74-9/3/74	624	90
B	60°07.3′	145°46.1′	3/2/76-5/1 8/76		
			"	1815	20
			"	1451	50
			"	600	100
c	60°07.8′	145°48.7′	5/1 8/76-8/1 9/76		
			"	1679	20
			"	1675	50
			"	1676	90
61A	59°34.0′	145°47.0′	8/16/74-11/20/74		
			"	604	20
			"	601	30
			"	711	50
			"	603	100
B	59°33.9′	145°53.0′	3/11/76-5/17/76		
			"	1454	20
			"	1835	50
			"	1667	100
			3/11/76-3/23/76	1668	162
c	59°32.6′	145°49.7′	5/1 8/76-8/1 9/76		
			"	1687	20
			5/18/76-8/2/76	1804	50
			5/1 8/76-8/1 9/76	1805	90
			"	1807	163
62A	59034.0′″	142°10.5′	8/17/74-2/1/75		
			"	598A	20
			8/1 7/74-1 0/4/74	617A	50
			8/17/74-11/13/74	616A	100
			8[17[74-2/1/75	600A	178

TABLE .2.1 (cent'd)

Sta. No.	LAT(N)	LONG(M)	DATES	Instr. Ser. No.	Instr. Depth	
62B	59°34.0′	145°13.5′	2/2/75-4/27/75			
			"	603B	20	
			"	602A		
			"	604A	1::	
			"	645B	184	
C	59°33.6′	142°11.7′	4/28/75-6/4/75			
			"	598	20	
			"	1451B	30	
			"	1454A	50	
			"	1455	100	
			"	1456A	180	
D	59°33.0′	142°05.3′	6/5/75-9/18/75			
			6/5/75-7/12/75	601	20	(Part I)
			8/2/75-9/18/75	607	20	(Part II)
			6/5/75-9/18/75	603		
			"	1452	1::	
			"	602	178	
E	59°33.0′	142°05.3′	9/19/75-11/20/75			
			"	1682	20	
			"	1681		
			"	1680	1 %	
			"	1679	180	
F	59°34.7′	142°11.4′	11/21/75-3/5/76			
				1811*	20	
			11/21/75-3/5/76	1810	50	
			"	1809	100	
			11/21/75-12/15/75	1807	180	
			"			
G	59°35.6′	142°06.0′	3/6/76-5/16/76			
			"	1683	20	
			"	1684	50	
			"	1669	100	
H	59°37.6′	142°06.2′	5/16/76-8/21/76			
			"	1809	20	
			"	1810	50	
			"	1811	100	
			"	1814	170	

* Recording tape was installed improperly in meter, with backing contacting the recording head rather than the oxide side of the tape. Translation has not yet occurred due to weak recorded signal.

TABLE 2.1 (cent'd)

Sta. No.	LAT(N)	LONG(W)	DATES	Instr. Ser. No.	Instr. Depth
621	59°38.1′	142°05.0′	8/22/76-10/21/76		
			"	1812	20
			"	1977	50
			"	2252	100
			"	2258	180
J	59°38.1′	142°06.1′	10/21/76-3/15/77		
			"	1805	50
			"	1804	100
K	59″38.3′	142°06.1′	3/16/77-6/8/77		
			3/1 7/77-6/8/ 77	1678	20
			"	1685	50
			3/1 7/77-5/22/77	1673	100
			3/17/77-6/8/77	1818	178
L	59°38.5′	142°07.0′	6/8/77-9/1 1 /77		
			"	2160	20
			"	1987	
			"	1833	1::
			"	1804	180
63	59°46.6′	141°59.2′	2/2/75-2/21/75		
			"		3
63½	59°46.7′	141°59.1′	2/3/75-5/10/75		
			"		100
64	59°35.5′	143°36.6′	4/28/75-6/1 1 /75		
			"	625A	20
			"	412B	30
			"	392A	50
			"	624B	114
69A	59°50.1′	145°41.9′	3/3/76 -5/17/76		
			"	604	20
			"	1670	50
B	59°49.2′	.145°43.3′	5/18/76-8/19/76		
			"	1824	20
			"	1828	50
			"	1829	87

TABLE 2.1 (cent'd)

Sta. No.	LAT(N)	LONG(U)	DATES	Instr. Ser. No.	Instr. Depth
SLSA					
#19	59°46.0′	141°29.0′	10/22/76-3/1 7/77		
			"	1824	20
			"	1810	40
SLSB					
#5	59°40.2′	141°39.7′	11/21/75-3/3/76		
			"	1830	50
			"	1828	75
#8	59°39.5′	141°39.2′	3/3/76-5/14/76		
			"	1672	49
			3/8/76-5/13/76	1673	74
#14	59°40.0′	141°40.0′	5/14/76-10/21/76		
			5/15/76-9/22/76	1833	50
			5/15/76-9/24/76	1830	77
#20	59°40.0′	141°40.0′	10/21/76-5/17/77		
			10/21/76-3/16/77	1675	50
			"	1828	75
SLSC					
#9	59°18.8′	142°01.6′	3/7/76-5/13/76		
			"	1677	
			"	1987	1::
			"	1988	240
#21	59°20.0′	142°07.0′	10/22/76-3/16/77		
			"	1811	100
SLSD					
#16	59°59.0′	142°19.0′	8/21/76-3/15/77		
			8/21/76-11/6/76	603	22
			8/21/76-3/14/77	1453	42
SLSE					
#17	59°49.5′	142°31.3′	8/21/76-3/15/77		
			8/21/76-2/24/77	1452	45
			"	1686	70
WIST 1	59°47.5′	141°36.7′	3/17/77-6/8/77		
			"	1680	45
			3/17/77-5/19/77	1681	51
WIST II	59°39.9′	141°40.6′	3/18/ 77-6/8/77	598	58
			"	1812	83
			"	1813	
			"	1817	1:;

2.2 Icy Bay Experiment

The plan for the Icy Bay experiment was to measure bottom pressure at six locations A-F (Figure 2.1) and to measure currents at several depths at B, C, and 62. These measurements span the continental shelf from the 50 m isobath to the shelf break at 250 m. Due to mooring and equipment failures, a complete data set was not obtained. Figure 2.4 lists the records analyzed from each location. In brief, 6 month (March-August) current records at B and 62 and pressure records at B, D, E, and F were obtained. Shorter current records (March-May) were obtained at C. In addition to the moored measurements, CTD stations were taken along the two lines A-C, D-F when instruments were deployed and recovered.

Instrumentation and processing used to measure the pressure fluctuation are described by Hayes *et al.*, (1978). The pressure gauge consisted of a 400 psia full-scale quartz pressure transducer manufactured by Paroscientific Corporation in Redmond, Washington, a temperature sensor, and a digital recording system. The gauges continuously averaged pressure and recorded at 15-min intervals. Temperature corrections were applied to account for the temperature coefficient of the pressure transducer. Final data series were low-pass filtered using the tidal eliminator filter of Godin (1972).

2.3 Kayak Island Experiment-

The current meter mooring 60, 61 and 69 were deployed west of Kayak Island to study the complex flow downstream of this island. The full mooring set was in place from May to October 1976. It provided current meter data at 20 in, 50 m, 90 (or 100) m, and at the shelf break (station 61) 163 in. Earlier observations consisted of a winter deployment at 61. These moored observations were supplemented by CTD sections taken on deployment and recovery cruises.

2.4 Current Observations

Aanderaa current meters were used for the current measurements. Data were reduced using programs described by Charnell and Krancus (1 976).

Moorings at B and C (cf. Figure 2.1) had the uppermost flotation at 45 m depth. This flotation was situated well below the surface in order to minimize contamination due to surface waves (Halpern and Pillsbury, 1976). However, mooring 62 which had a current meter at 20 m depth had flotation 17 m below the surface. There is some evidence that during high wind periods this record may be unreliable. Figure 2.3 shows unfiltered kinetic energy spectra of the current data at 50 m depth on B, C, and 62 for the period 15 March-15 April and on B and 62 for the period 15 July-15 August. Note the order of magnitude difference in the high-frequency energy level between B and 62 during the first period. In summer when winds were generally lighter, the high-frequency spectral levels

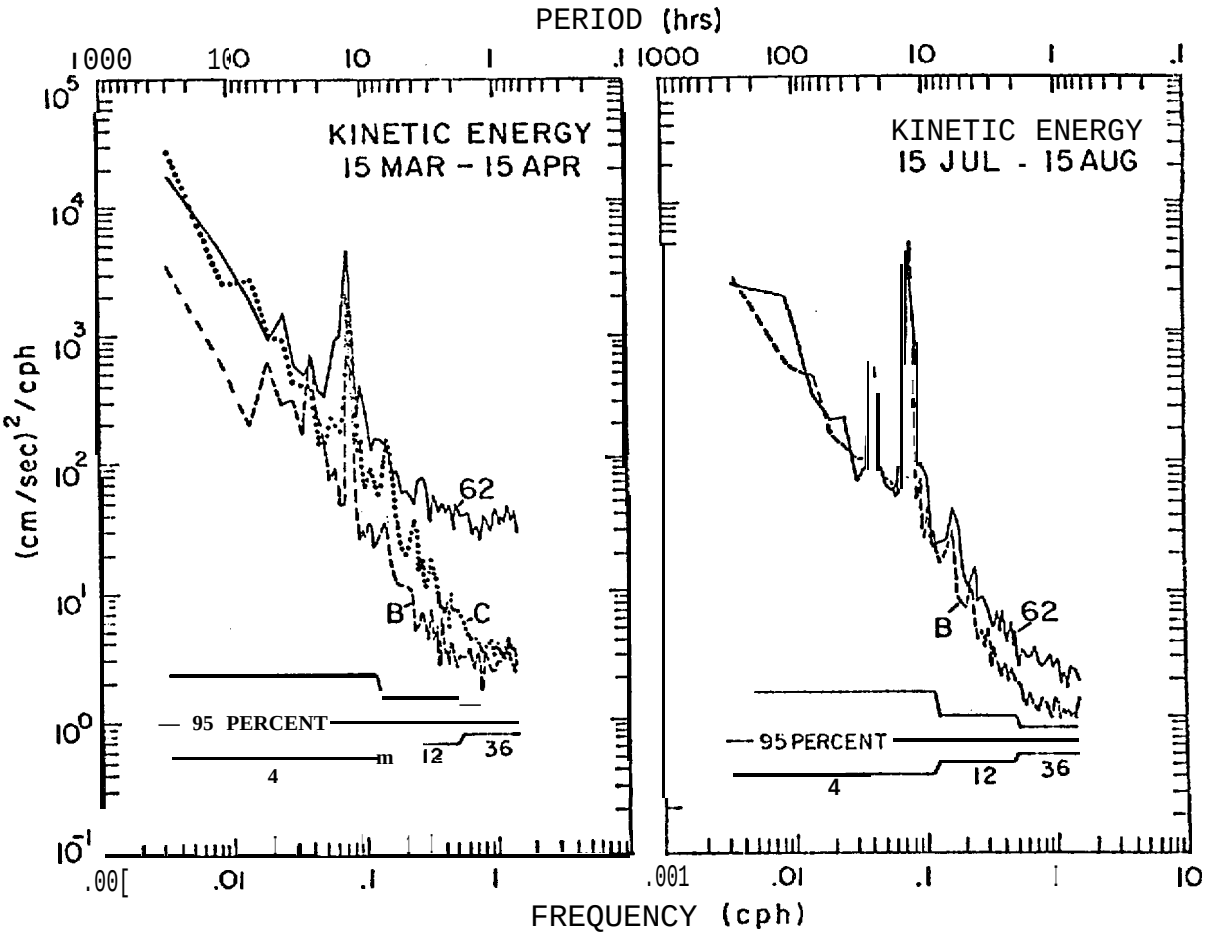

Figure 2.3 - Comparison of the kinetic energy spectra at locations 62, B, and C in spring and at B and 62 in summer. Moorings B and C had upper flotation at 45 m, mooring 62 had flotation at 17 m.

more clearly agreed. The high spectral energy observed in March is similar to that commonly seen when comparing current records obtained on moorings contaminated with high-frequency noise (Halpern and Pillsbury, 1976; Gould and Sambuco, 1975). Since we have no direct, nearby comparison, we cannot ascertain whether the low-frequency oscillations are also erroneous. However, results observed in mooring intercomparison experiments indicate that caution is advisable when interpreting speed data from station 62.

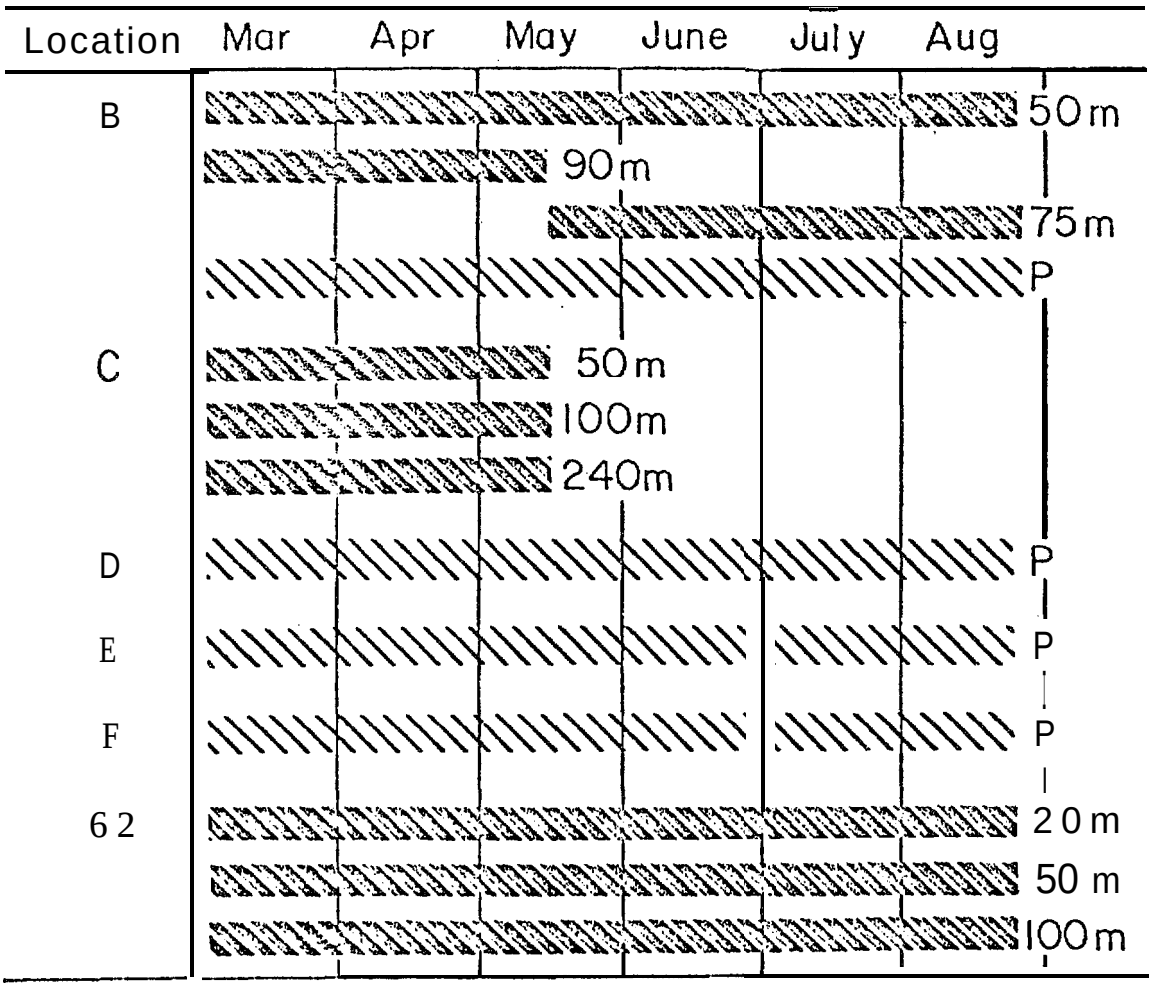

Figure 2.4 - Duration of data records at each 1 ocation for the Icy Bay experiment. Current moorings are solid bars; pressure gauges are hatched.

3. LONG PERIOD TIME VARIATION IN CURRENTS

A major objective of the regional observation program was to obtain a long-term current time series from the seaward boundary of potential lease sites, i.e. the continental shelf edge. This mooring, 62, was designed with current meters located 20, 50, 100 and 180 m below the surface and was moored near the shel f-break (190 m depth) off Icy Bay (see Figure 2.1). Time distribution of current observation at different depths is depicted in Figure 3.1. In this Section, we describe this shelf break current on a variety of time scales and examine its variability. The next section (4) extrapolates the measurements in order to estimate extreme currents.

Monthly averaged currents are shown in Figure 3.2. These vectors were constructed from all speed and direction data from either a 15 rein, 20 min or 30 min sample interval which were obtained during a given month. Two prominent features of flow were a persistent net drift toward the northwest (approximately longshore) and a strong seasonal speed variation. The vectors exhibited negligible directional shear except at the deepest observation level. The tendency for the net flow to veer to the right at the lowest observation level suggests bathymetric steering was important. This effect has been reported (Kundu and Allen, 1976) for flow over the continental shelf off the Oregon coast. A seasonal speed trend was present in all the records and was strongest at the upper level (2011). During winter (approximately October through April) speeds at 20 m were typically 25 to 35 cm/s, decreasing in summer to 10 to 15 cm/s. Consistent net drift toward the northwest, with seasonally modulated speeds is characteristic of shelf edge flow in the Icy Bay region. Only one month (June 1976) was an exception to this generalization.

For periods less than amonth, however, directional variability was a feature of the records. Hayes and Schumacher (1977) reported "eddy-like" features with a period of 1.5 to 3 days and an extended period (~12 days) during June 1976 when flow was reversed, i.e. towards the southeast. Variability at these time scales would have a significant impact on pollutant transport. Using a PVD presentation, we preserve the time history of the extended current reversal in Figure 3.3. This diagram was constructed from 2.86 hour filtered data resampled at 1 hour intervals. Between 17-20 May, there was an offshore pulse, followed by 15 days of predominantly longshelf flow with a small onshelf component. From 4-7 June, flow was onshelf, followed by three days of flow toward the southeast, and then onshelf flow for 2.5 days shifting to approximately southeasterly flow for 6 days, ending 19 June. The mean flow for the record segment described thus far was directed towards 030°T, which was substantially different than any of the monthly averaged flow vectors shown in Figure 3.2. The remainder of this current record indicated four more distinguishable direction changes between 19 June and 5 July. Each of these events were low speed (5 cm/s) and persisted for periods of approximately 3 days. The remainder of this record showed predominantly longshelf flow (13 cm/s) with a smaller (2 cm/s) offshelf component and was typical of summer flow.

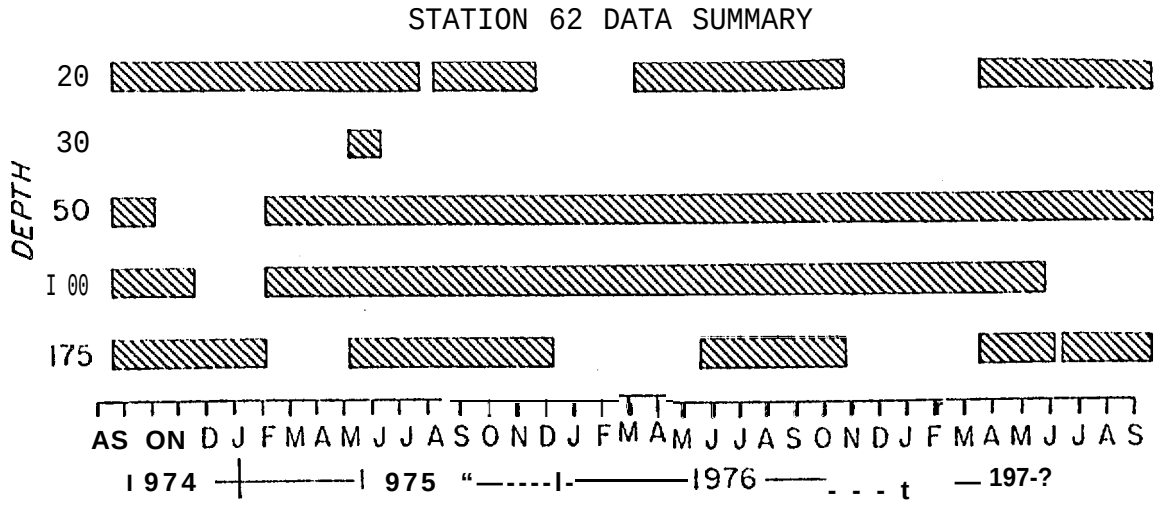

Figure 3.1 - Time distribution of current observations at different depths at station 62.

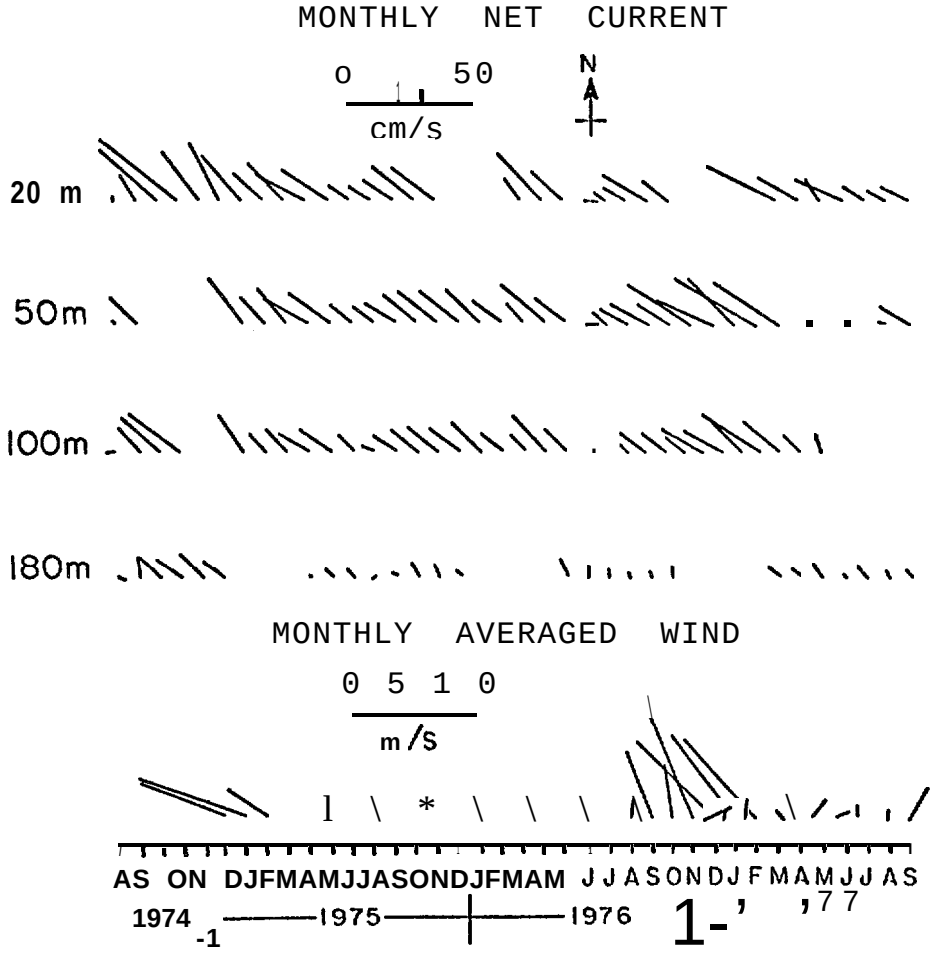

Figure 3.2 - Monthly mean vector-averaged currents at station 62 (upper) and monthly mean averaged Bakun winds at the same location.

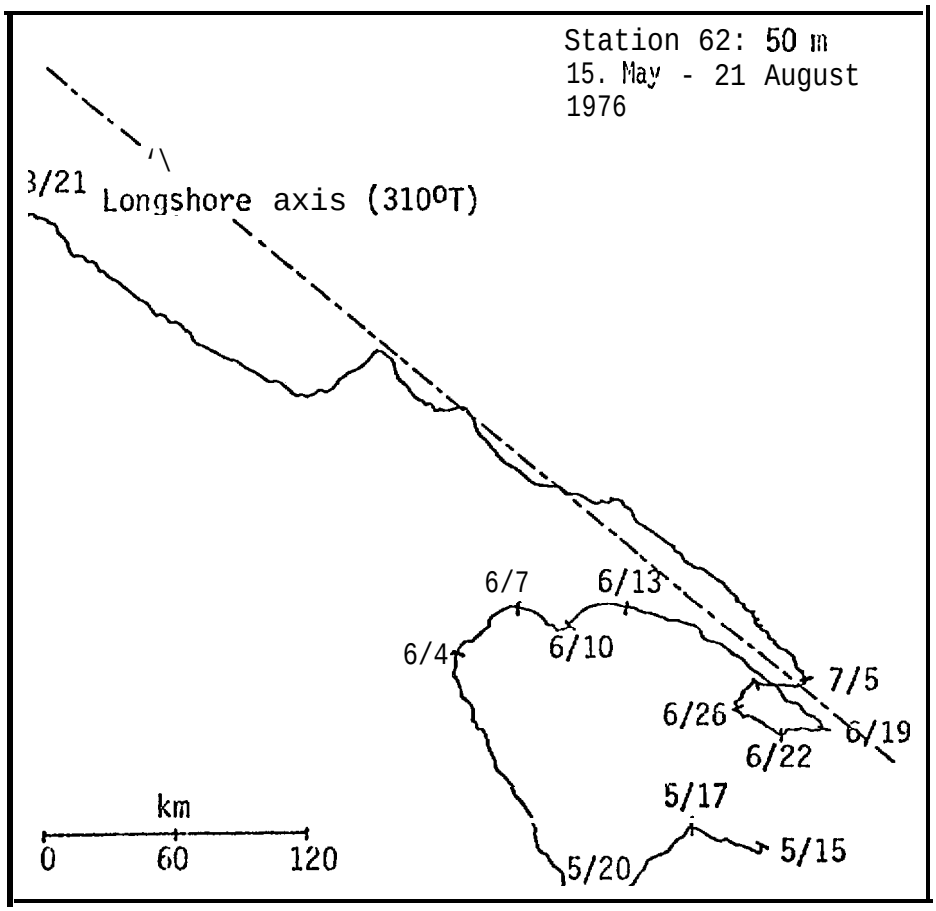

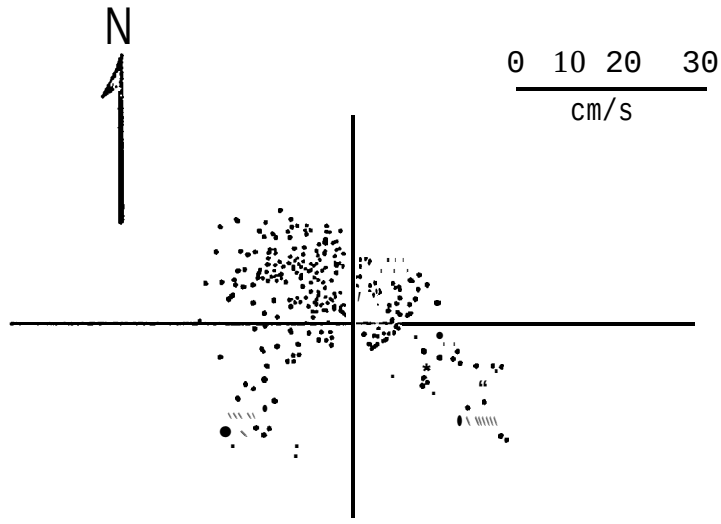

Figure 3.3 - Progressive vector diagram and scatter plot for station 62 during summer.

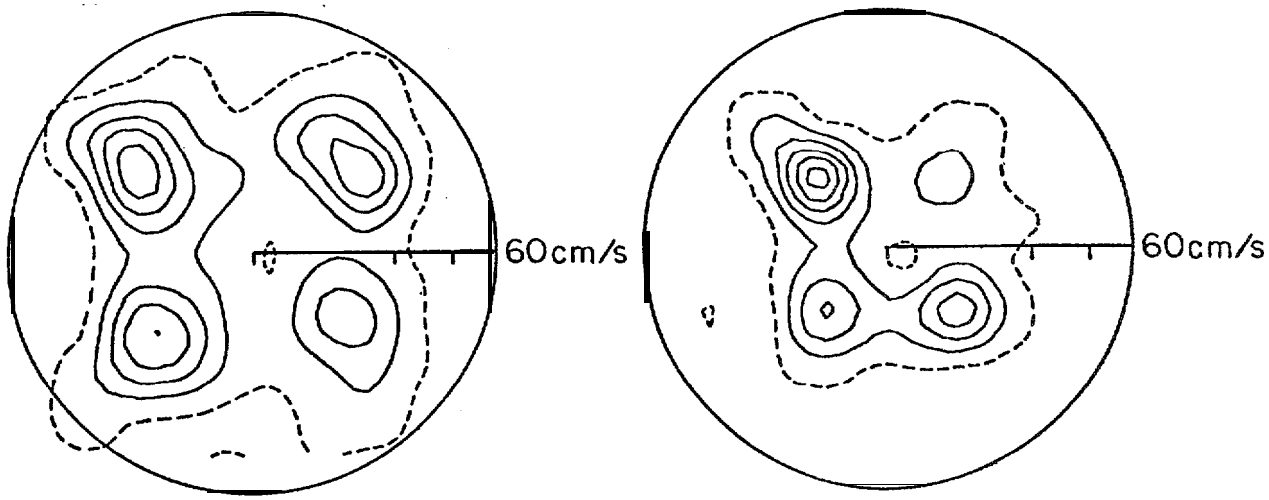

Figure 3.4 - Fabric diagrams showing directional trends in representative winter and summer current records at station 62.

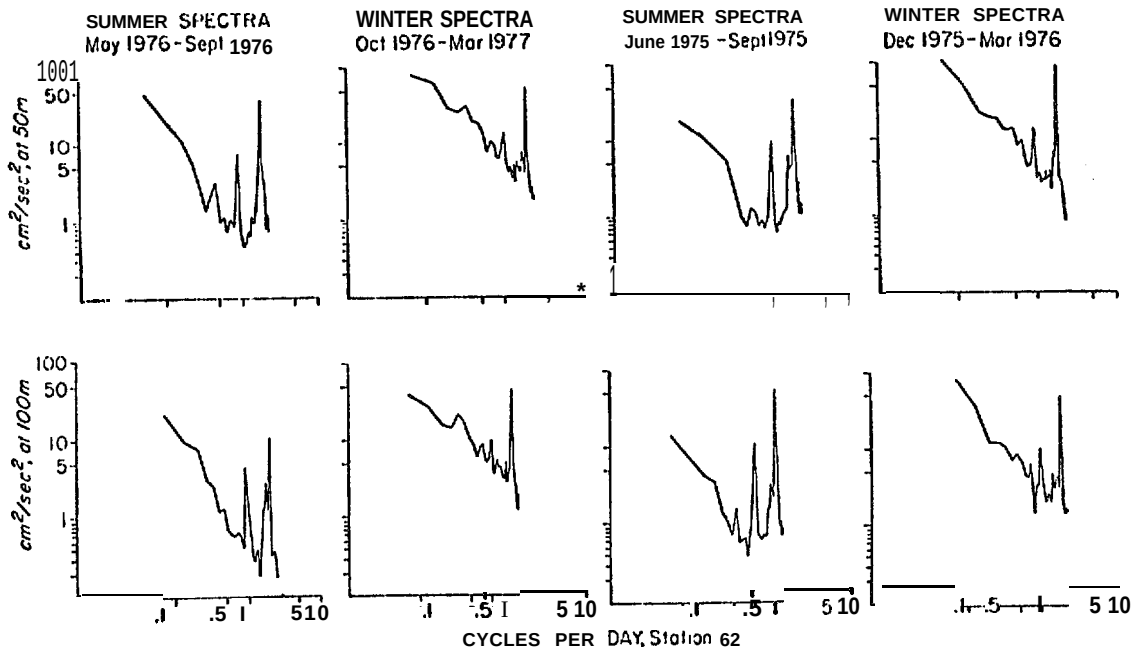

Figure 3.5 - Kinetic energy spectra for winter and summer observations at two depths at station 62.

We present the same record as above in a scatter diagram format in Figure 3.3. This plot was constructed from low-pass (35 hr) filtered data which was resampled at 6 hour intervals. The degree of variability is clearly shown in this format, although time history is lost. The record mean (5 cm/s at 315*T) was substantially less than the scatter and we note that the strongest speeds (30 cm/s) were directed toward the southeast. Another method of showing the variability of the current is the fabric diagram (Davis and Ekern, 1976). We apply this technique to the current records from 50 m depth during a winter and summer (62D) observation period (Fig. 3.4). The contours represent the density of observations by speed and direction. We note a higher density of contours in the northwest quadrant, but it is not dominant. The observations tend to be partitioned into longshelf and cross-shelf domains. The northeast quadrant contained a higher portion of observations during winter than during summer, reflecting seasonal onshore Ekman transport.

The partition of kinetic energy is shown in the spectral energy density diagrams (Figure 3.5) representing winter and summer regimes at 50 m and 100 m depths. During both regimes, semi-diurnal and diurnal tides dominated the short period (less than 30 hr) spectra. Using records from 62J and 62D as representative of winter and summer conditions, respectively, we note that the record variance increased by a factor of six between summer and winter. During summer, variance at the tidal frequencies accounted for approximately 60% of the total, while the variance for periods longer than 30 hours accounted for approximately 35% of the total. The remainder of the variance was contained in short period motions. In contrast, 70% of the total variance during winter was contained in the low frequency bands, with tidal frequency bands accounting for approximately 25% of the total. Thus, the seasonal trend established by the monthly averaged vectors is also apparent in the kinetic energy spectra.

In Figure 3.6, we present the average of the speeds squared as a further measure of kinetic energy, with envelopes of standard deviation calculated during each months averaging. Again, winter flow is shown to be more energetic than that measured during summer. The wide envelopes of the standard deviation suggest that mean flow was not an expected or common value. In fact, we emphasize that kinetic energy and vector components were highly variable, and that standard deviation sometimes exceeded the mean. To demonstrate this fact, we present a plot of the standard deviation as a percentage of the mean kinetic energy for the 100 m record (Fig. 3.7). In this presentation there was no seasonal trend, which suggests that flow was not consistently more uniform during one time of the year as opposed to another time.

The kinetic energy of the large-scale wind field in the vicinity of Icy Bay is shown in Figure 3.8. The wind data shown here were calculated on a 3° grid from atmospheric pressure data using a geostrophic approach. The seasonal nature of the wind signal appears well

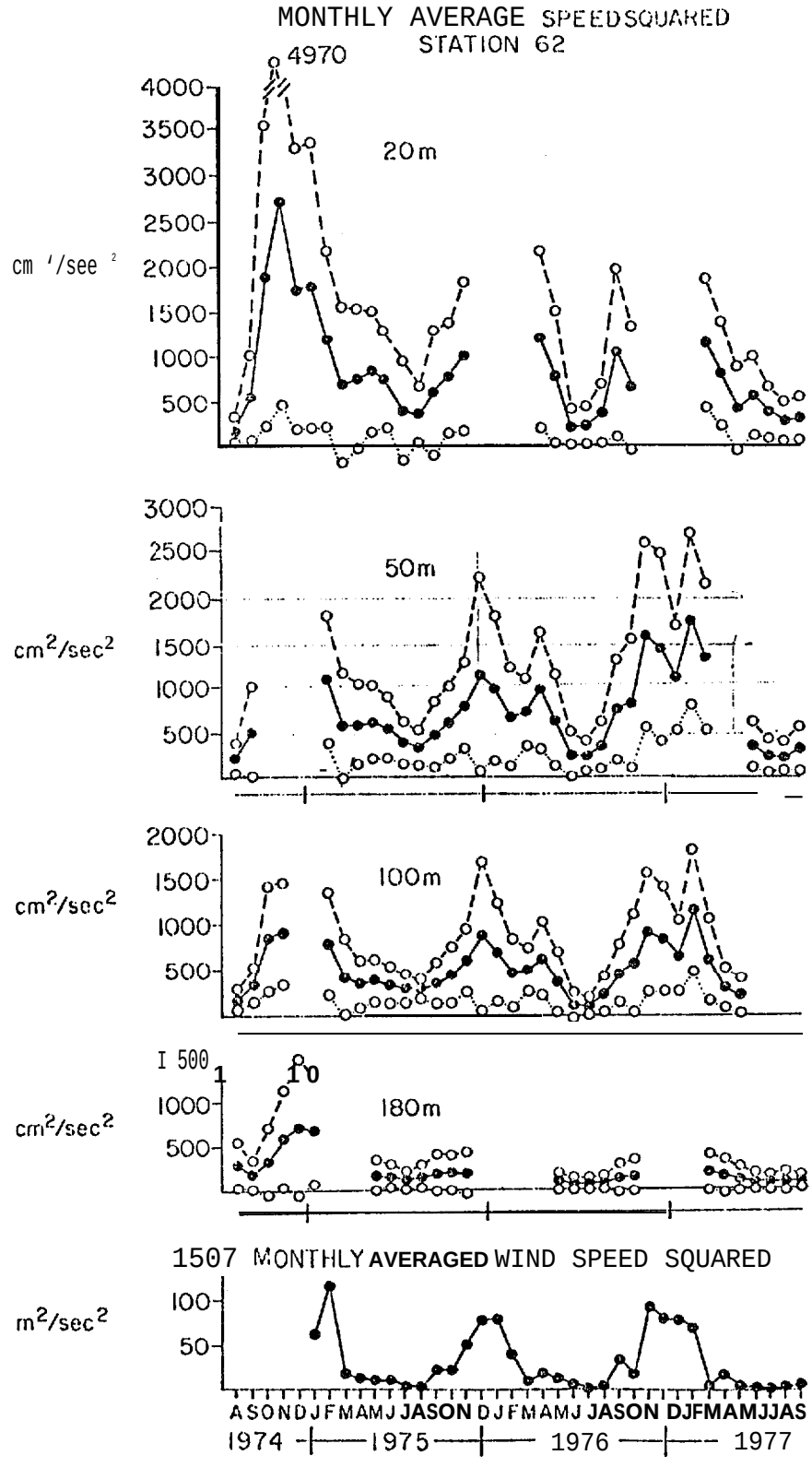

Figure 3.6 - **Average of** current and **geostrophic** wind **speecs** squared, showing **standard** deviation as envelopes.

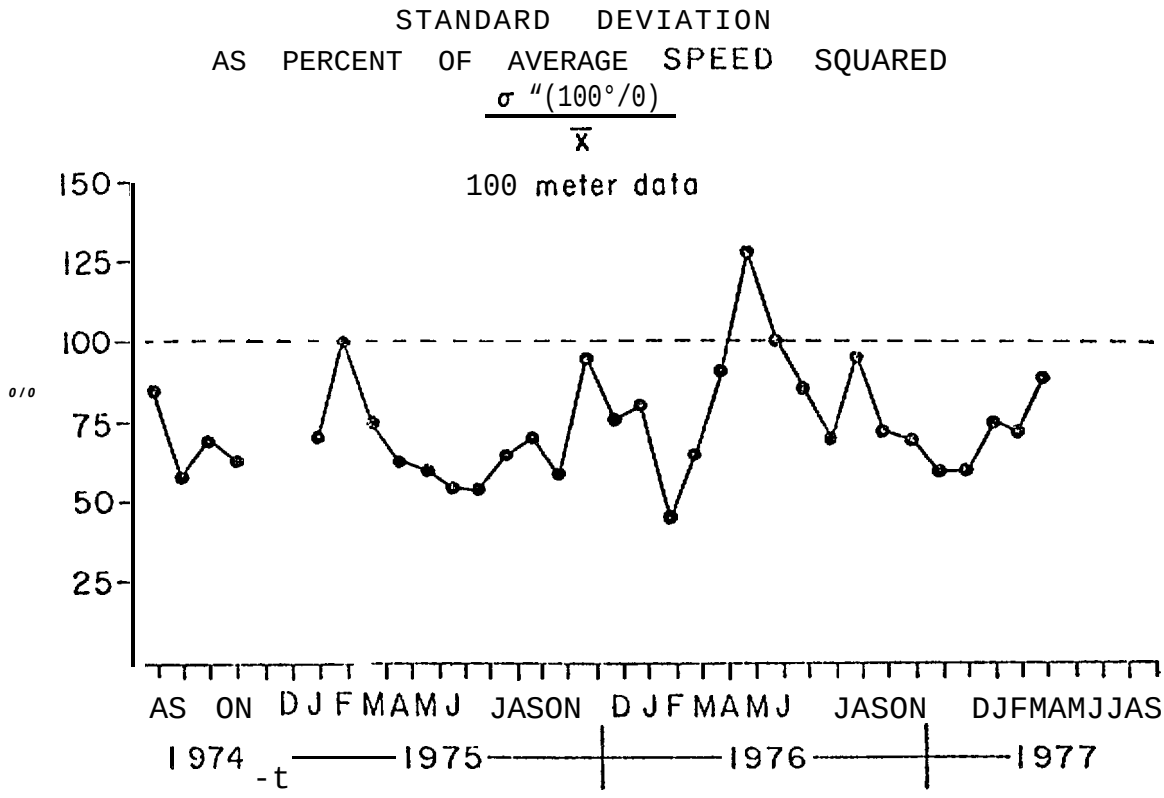

Figure 3.7 - Standard deviation of currents as percent of average speed squared, plotted vs. time.

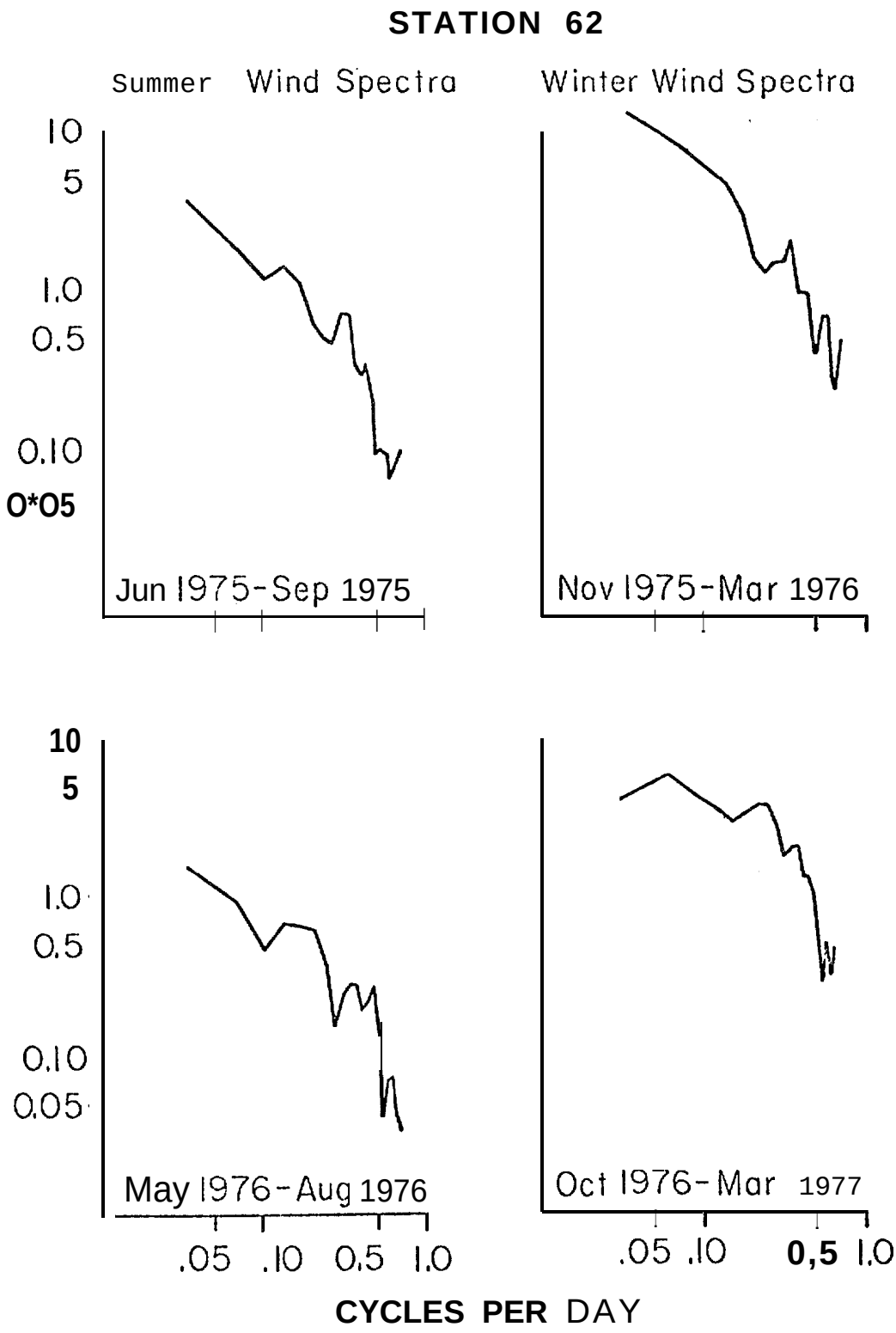

Figure 3.8 - Kinetic energy spectra for geostrophic winds at station 62.

correlated with that of the current kinetic energy. The monthly mean current was found to be correlated to the monthly mean wind speed with $r = 0.80$ at the 95% level. Clearly the winter intensification of the current along the shelf was due in large part to the intensification of the wind field.

In summary, we have shown that on time-scales of a month or more, flow was consistently toward the northwest with a seasonal trend in the speed: higher speeds obtained during winter and were two to three times greater than in summer. No consistent directional shear was evident between the 20 m and 100 m observations, and the kinetic energies at these depths were consistent. The response of the currents to seasonal influences was quite uniform throughout the water column. Only one month out of thirty deviated dramatically from this rather consistent picture. The observed variation in the monthly averaged currents and kinetic energy clearly coincided with the seasonal signal in the wind field. For time scales of the order of months, flow at the shelf-break off Icy Bay was well organized; however, for time scales between tidal periods and 15 days flow was observed to be quite variable. Over half of the sub-tidal frequency variance occurred in periods between 1.5 and 7.5 days. Such variability is clearly shown in current fabric diagrams.

4 . EXTREME VALUE ANALYSIS APPLIED TO CURRENT DATA

The station 62 record was further analyzed in an attempt to describe extreme events. This analysis, while admittedly crude, provides an indication of maximum speeds likely in the vicinity of the shelf break.

4.1 Introduction

The 50 m and 100 m records at station 62 were continuous over 31 months, from February 1975 to September 1977. Figure 4.1 shows 5-day mean speeds over the August 1974 through May 1976 period. The 5-day mean speeds for the 20 m observations ranged from 9-57 cm see-l while for the 180 m observation the mean ranged from 8-28 cm see-l. The data clearly show marked seasonal behavior of flow associated with annual variation in storm activity described by Royer (1975). Data from the 50 and 100 m levels show an increase in the very low frequency flow from a mean of about 15 cm see-l in summer to a mean of over 25 cm see-l in winter; variation about this mean in winter is considerably higher than during the summer. This low frequency flow is due to the effect of the Alaskan Stream on shelf water. Response of shelf water to the passage of storm events during winter at this site is the subject of Hayes and Schumacher (1976).

The ensemble averaged energy spectra for available data at each of the four depths are shown in Figure 4.2. Tidal and inertial periods are indicated. Data from all levels show marked tidal peaks. However, the proportion of diurnal tidal energy is barely above background energy at the 20 meter level but increase with depth. Only the 20 m data show significant energy at the inertial frequency, though most of this occurred during the winter of 1974-75 when records from other levels were incomplete.

Local topography controls the direction of flow, which tends to parallel isobaths at this location. While there are seasonal as well as higher frequency variations in these trends the mean is stable and variations small. Generally, flow strongly adheres to this bathymetric constraint and tends to have a mean direction of around 315°T. Variation of maximum flow about this axis is apparently quite low since mean speeds along this axis for the 50 m data are only 5 percent less than those using mean speed alone. This directional stability allows analysis of extreme flow events to be carried out on a scalar rather than a vector quantity; consequently, subsequent discussion is related to extreme speeds.

4.2 Extreme Speed Analysis

It is desirable to summarize these data in some manner that allows a characterization of significant flow events. A promising technique is that of extreme value analysis. This technique has been used successfully on other environmental data sets and has a large volume

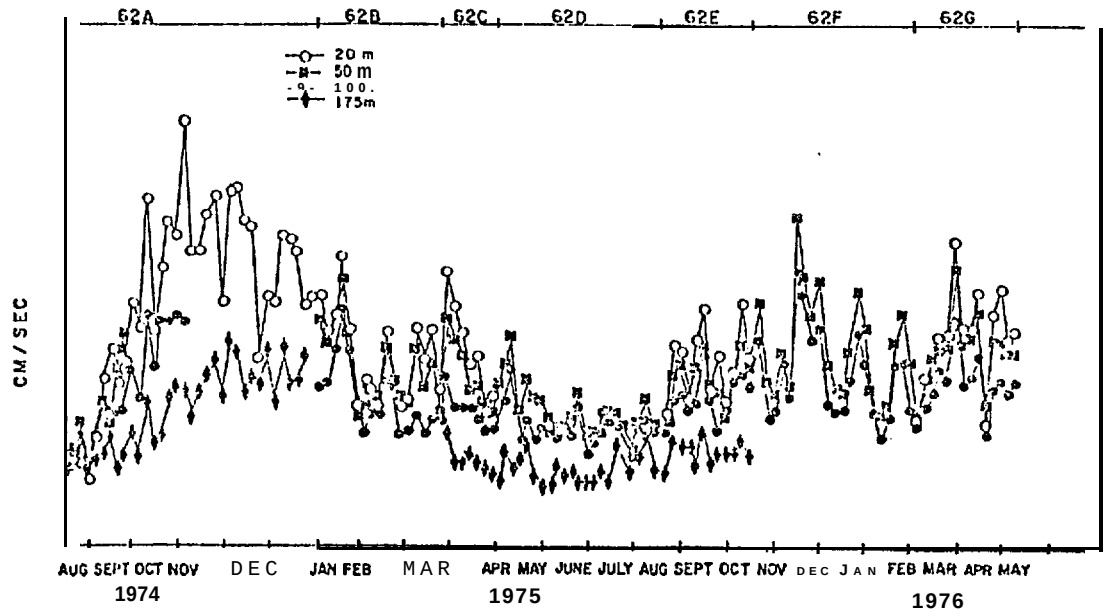

Figure 4.1 - Five-day speeds for data from station 62 from August 1974 through May 1976. Data from the 50-m and 100-m current meters were continuous from February 1975 through May 1976. Mean speeds were higher in winter than in summer.

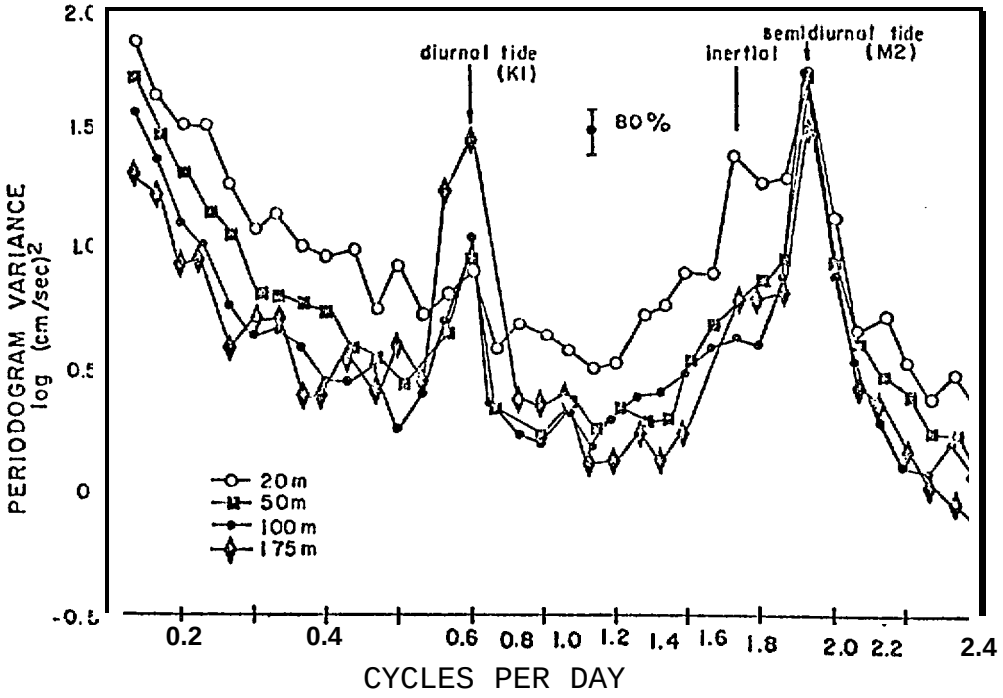

Figure 4.2 - Ensemble averaged energy spectra for the station 62 data. Tidal and inertial frequencies are denoted. Energy is given by logarithm of periodogram variance.

of literature describing its application. Gumbel (1954) presents the technique in detail and can be used readily for application. The theory supposes that magnitude of extreme flow events increases with the logarithm (in) of observation time. Such a distribution fit through observed data allows definition of a return period for extreme values. This concept does not state that the specific value is the largest value to be obtained at a certain time, but only that it is the most probable largest value to be obtained within a certain time and gives limits within which this value may be expected to lie, with a certain probability.

The procedure is to section the record into N segments of length AT, select the largest value of each segment and order the new set by increasing magnitude. For this new data set a mean cumulative probability function, $P(s_m)$, is calculated for each ranked speed, 'm:

$$P(s_m) = \frac{m}{M+1} \qquad (4.1)$$

The Probability of the m^{th} speed equaling or exceeding other speeds of the set thus is equal to $P(s_m)$. A return period, T_R, may be defined for the m^{th} speed as:

$$T_R(s_m) = \frac{\Delta T}{(1-P(s_m))} \qquad (4.2)$$

Significance of the return period is such that on the average, a speed s_m or greater will occur once every $T_R(s_m)$ days. Assuming the data follow the proposed logarithmic distribution, extreme speeds should vary linearly with a-logarithmic function of $P(s_m)$. Gumbel 's model for the logarithmic function is called the reduced variate, Y:

$$Y = \ln(-\ln(P(s))) \qquad (4.3)$$

A straight line can be fit through these data using least squares methods; from the equation for that line, expected extreme speed as a function of return period and segment length can be calculated:

$$s = A+B \text{ “ } y = A+B \text{ “ } (-\ln(-\ln(1-\Delta T/T_R))) \qquad (4.4)$$

A measure of the fit of these data to the probability distribution can be determined from the calculated linear correlation coefficient, r. The percentage of total variation of the expected speeds that is accounted for by the linear relationship with observed speeds can be estimated as $100r^2$. Further, the confidence intervals can be computed using Student's t distribution. For our data, the confidence interval was chosen for a 95% significance level.

There are several restrictions to the technique that require attention and make interpretation for a small data set, such as represented by the Alaska current meter data, somewhat tentative. Application of statistical theory of extreme values is ideally suited to a large data

set covering many years, such as occurrence of flood conditions in streams. For the Alaska current meter data we have 2.5 years of data with many storm events producing extreme flows during that period. The question immediately arises about representativeness of the extremes in this period. While conclusions based on "2.5 years of data offer guidelines, it must be remembered that additional data may modify actual values somewhat. Since obtaining long time series of current meter data is at best difficult, it is worth stretching this technique to the limit to examine typical ranges likely to be encountered in further observations.

Another important restriction is that the data extremes represent independent events. Since extremes are likely to result from storm events, this restriction can be ameliorated by examining extremes in segments of the record coincident with storm frequency. Major storm activity in the Gulf of Alaska is most likely to occur during winter, October through March, so we use data only from that time period to eliminate seasonal variability. Therefore, 6 months of winter extreme speed data represents a full year. Major storm activity during this period is reported to have an average period at roughly 5 days (Hayes and Schumacher, 1976), while tides have a spring-neap cycle of 15 days. To eliminate short period variability, we have chosen a segment length of 30 days.

With these restrictions in mind, extreme value analysis was applied to the Gulf of Alaska data. Figure 4.3 shows speed data for levels 50 m and 100 m of station 62 in such a representation. Extreme values are along the ordinate with return period in years along the abscissa. The fit of each line has a correlation greater than 0.96.

If one remembers the limitations imposed by representativeness of the sample and proper interpretation of the return period concept it is possible to extrapolate these data and estimate the extreme values likely to occur *over* longer periods. For example, data at the 50 m level suggest that with a return period of 5 years we are likely to observe an extreme speed of around 100 cm see-l within $\pm$ 6 cm see-l. Similarly, extreme speed at 100 m is likely to be 89 cm see^{-1} $\pm$ 4 cm sec^{-1} for the same period of 5 years.

Webster (1969) suggested that the mean vertical speed profile has a power law dependence on depth. Were this situation universal, extreme speeds might similarly show this power law dependence. Using this assumption, and extrapolating the 5 year projections of the 50 and 100 meter depths, we might expect a 5 year speed of about 125 cm see-l at the 10 m level. This would be a lower bound, since it does not include wind effect in the Ekman layer.

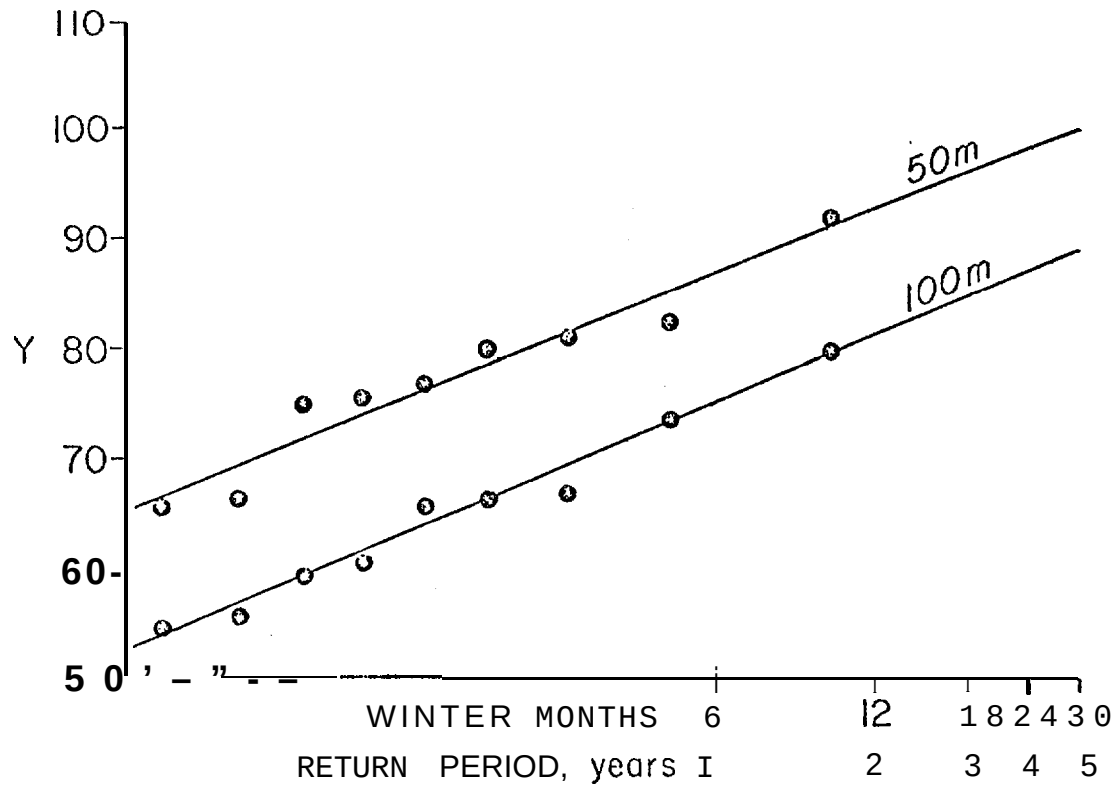

Figure 4.3 - Plot of projected extreme values Y vs. time at station 62.

4.3 Summary

We have carried out an analysis of projected maximum current speeds at 50 m and 100 m depths at station 62 using the technique of extreme value analysis. This has resulted in estimated maximum current speeds, over a five year period, of about 100 cm sec^{-1} at 50 m and 89 cm sec^{-1} at 100 m. It must be stressed that *these are estimates only*, due to the short (relative to inter-year variability) sampling period and resulting uncertainty as to whether or not the sampled data represent "normal" conditions.

5. CURRENT, BOTTOM PRESSURE, AND WIND CORRELATIONS OFF ICY BAY

In the previous two sections (3 and 4), we have examined time variations at a single location in the northeast gulf; station 62. It is now appropriate to examine circulation in the region surrounding this mooring, in order to place the behavior of currents at station 62 in perspective within a larger scale oceanographic milieu. In this section an analysis of the Icy Bay data set acquired during March-August 1976 is presented. The rneasurement.s consisted of moored current meter arrays, including station 62 (cf. Figure 5.1), moored bottom pressure gages, and geostrophic and observed coastal winds. The area included in this analysis is that bounded by the lines connecting moorings SLS A-F (Figure 5.1).

5.1 Introduction

The Icy Bay Experiment was designed to describe low-frequency (f <.025 cph or periods >1.7 days) velocity fluctuations and their relation to bottom pressure and wind variability. In addition to characterizing velocity and pressure fields across the shelf, the usefulness of long- and cross-shelf measurements of bottom pressure in interpretation of the flow field are considered. Several recent studies (Beardsley and Butman, 1974; Smith, 1974; Hayes and Schumacher, 1976) have noted close correlation between long-shelf current fluctuations and sea level measured at a nearby tide gage or bottom-moored pressure gage. A possible interpretation of this result is that much of the low-frequency variability is quasi-barotropic. If so, then direct measurement of cross-shelf bottom pressure gradient fluctuations can provide a time series of barotropic transport.

Allen and Kundu (1977) recently reviewed some dynamical features common to many time-dependent shelf circulation models. In the absence of forcing, equations for the depth integrated velocity components may be written:

$$u_t - fv = -gp_Y \qquad (1)$$

$$fv = gp_X \qquad (2)$$

The coordinate system is shown in Figure 5.1; u is the cross-shelf velocity component shoreward, and v is longshore velocity to the northwest. Subscripts denote differentiation. In the longshore direction, velocity is geostrophically balanced; in the cross-shelf equations the acceleration term may be important. If baroclinic effects are small, then the bottom pressure gradients across and along the shelf approximate P_x and P_y. Velocity and pressure time series will be used to test equations (1) and (2).

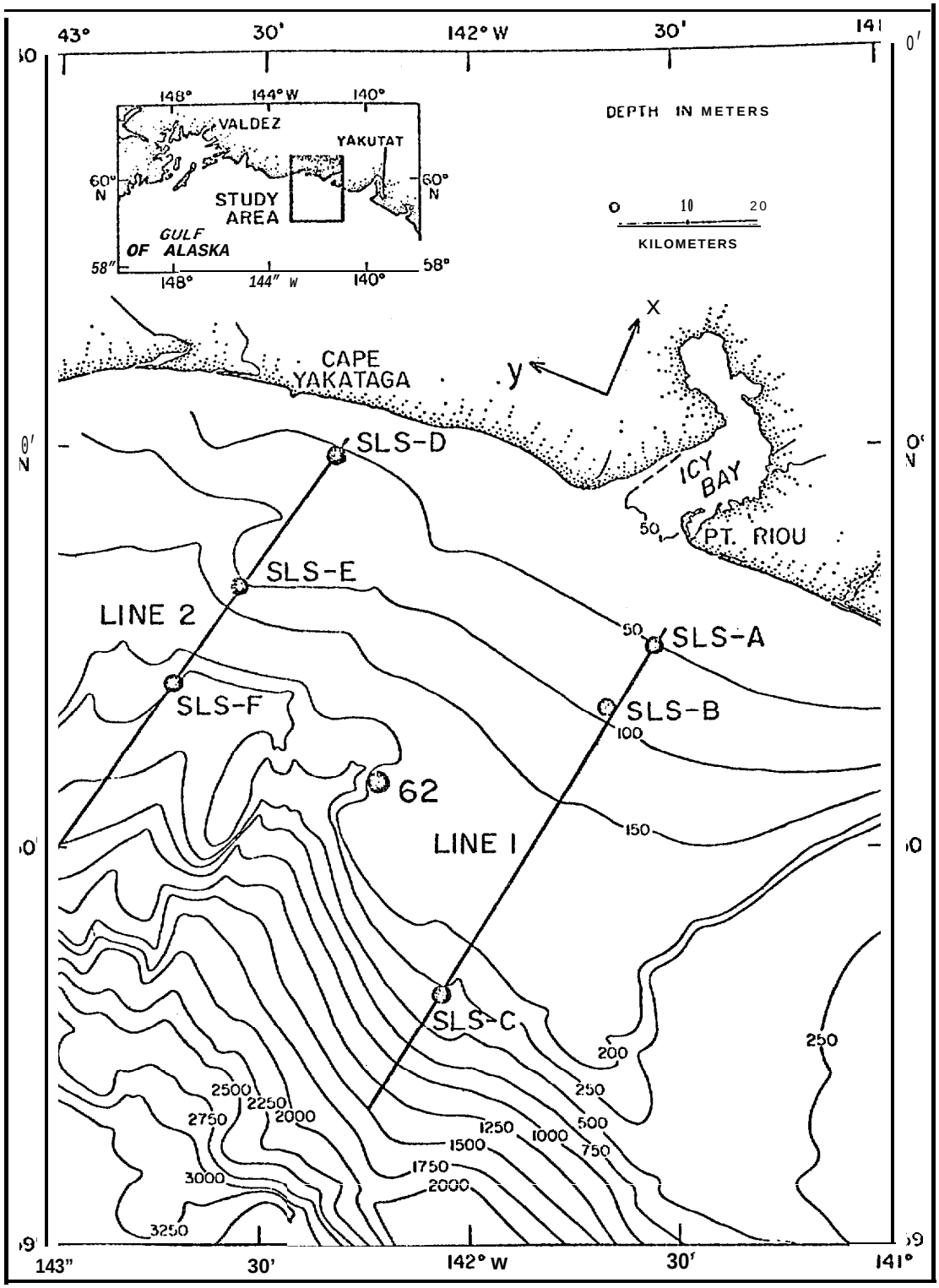

Figure 5.1 - Location of the experiment off Icy Bay, Alaska. The coordinate system indicates the alongshore direction, y, and cross-shelf direction, X.

5.2 Observations

5.2.1 Hydrographic observations

Temperature and salinity data were obtained from hydrographic sections made during March, May and August as discussed in section 2. Additional sections from Royer (1977) provided data in February, April and September. Representative density sections for winter, spring and summer are shown in Figure 5.2. The February and May sections show weak vertical stratification and downwelling. By summer, a shallow seasonal pycnocline had developed. Figure 5.3 compares temperature, salinity and density stratification at the three depth contours where bottom pressure measurements were made. Through May, little vertical gradient was observed at the 50 and 100 m locations. Salinity stratification largely determines the density gradient, and temperature gradient can be of either sign. At 50 m the temperature increased 3.2° from March to May. This increase was probably due to advection rather than seasonal heating. In August, a seasonal thermocline was seen at all locations. However, at 50 m, effects of river runoff produced a shallow, cold, low-salinity layer.

Surface water near the shelf break had a seasonal structure similar to that on the shelf. However, at about 150 m the permanent halocline of the Gulf of Alaska gyre occurs. This halocline can be expected to isolate deep from surface flow. Temperature in the halocline is variable and has been used as a water mass tracer (Royer, 1975).

5.2.2 Wind observations

Measurements of surface wind over the Northeast Gulf of Alaska region are available from Yakutat and as geostrophic winds calculated from 6-hourly synoptic surface atmospheric pressure analyses produced by Fleet Numerical Weather Central (Bakun, 1975). Yakutat winds are not representative of oceanic winds because of the mountainous coastal topography (Hayes and Schumacher, 1976; Reynolds *et al.*, 1976). The FNWC winds have received considerable attention recently (Hickey, 1977; Halpern and Holbrook, 1978). In the vicinity of Icy Bay the coastal mountains form a barrier to storms propagating to the northeast; the resultant packing of isobars may yield actual winds which are stronger than those inferred from large-scale (3° grid) pressure gradients used by FNWC. In addition, katabatic winds which blow offshore from the coastal glaciers have been observed near Icy Bay by Reynolds and Walter (1976). Such winds are not included in the FNWC calculation. With these reservations, the FNWC winds are presented in Figure 5.4. The wind vectors have been lowpass filtered (40-hr cutoff) and rotated into approximate onshore and longshore axes. Visually, the record can be divided into a spring period (March-May) when the wind is large and variable with a significant longshore component toward the west and a summer period (June-August) when the wind is smaller and often has an eastward longshore component. The vector mean wind

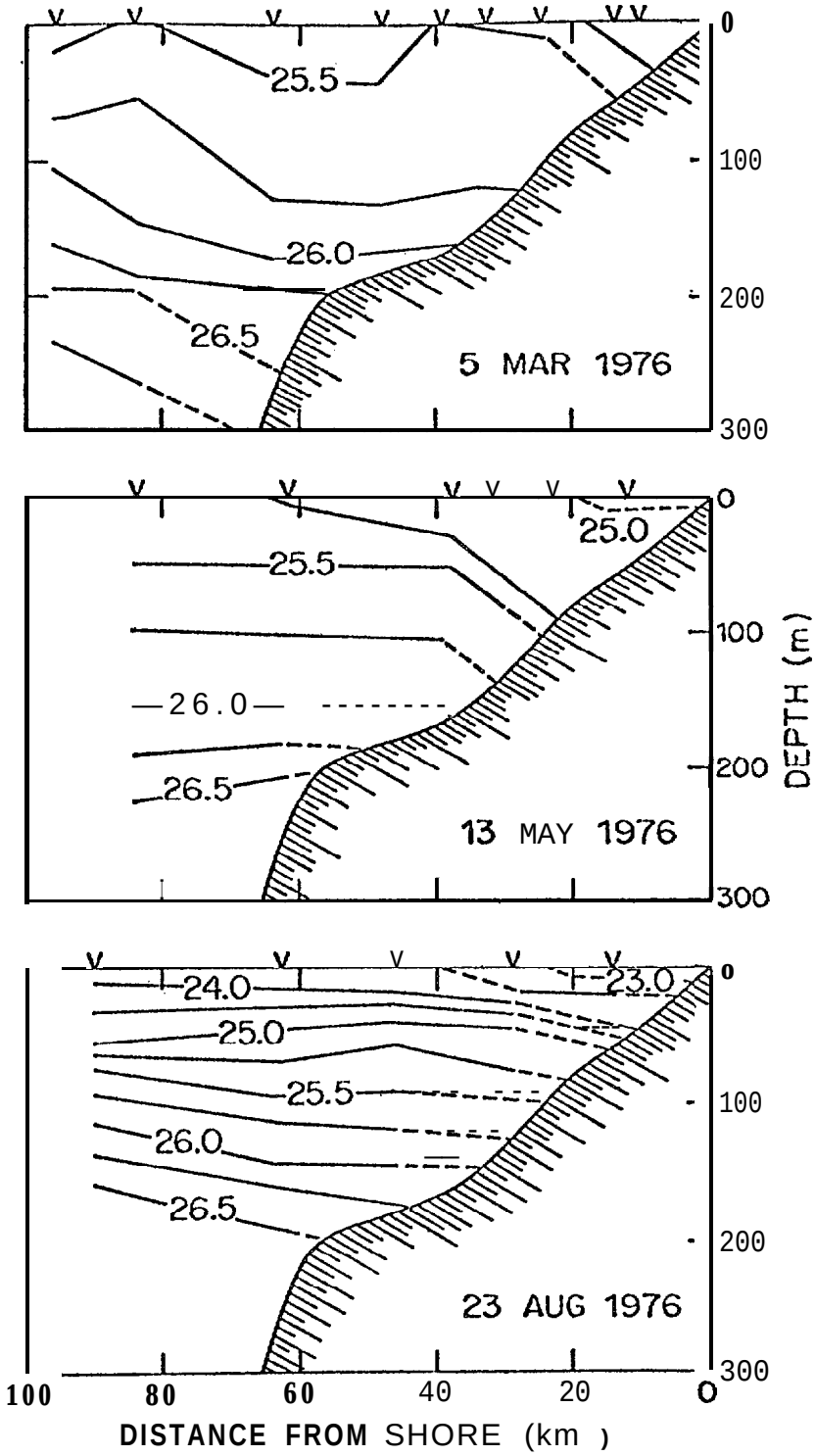

Figure 5.2 - Typical cross-shelf density sections for February, May and August .

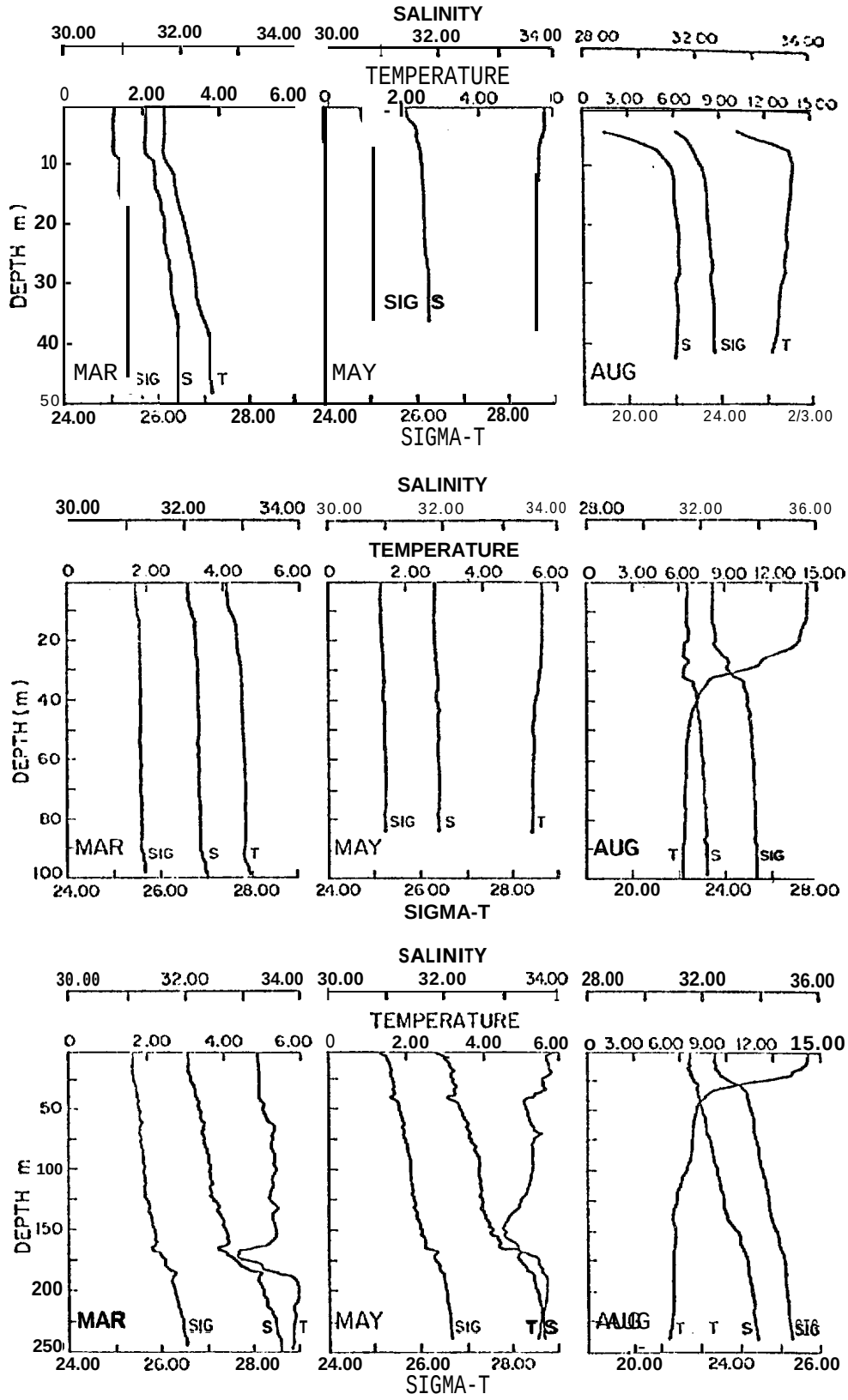

Figure 5.3 - Seasonal variation of the temperature, salinity, and sigma-t profiles at the three depths **where bottom pressure was measured.**

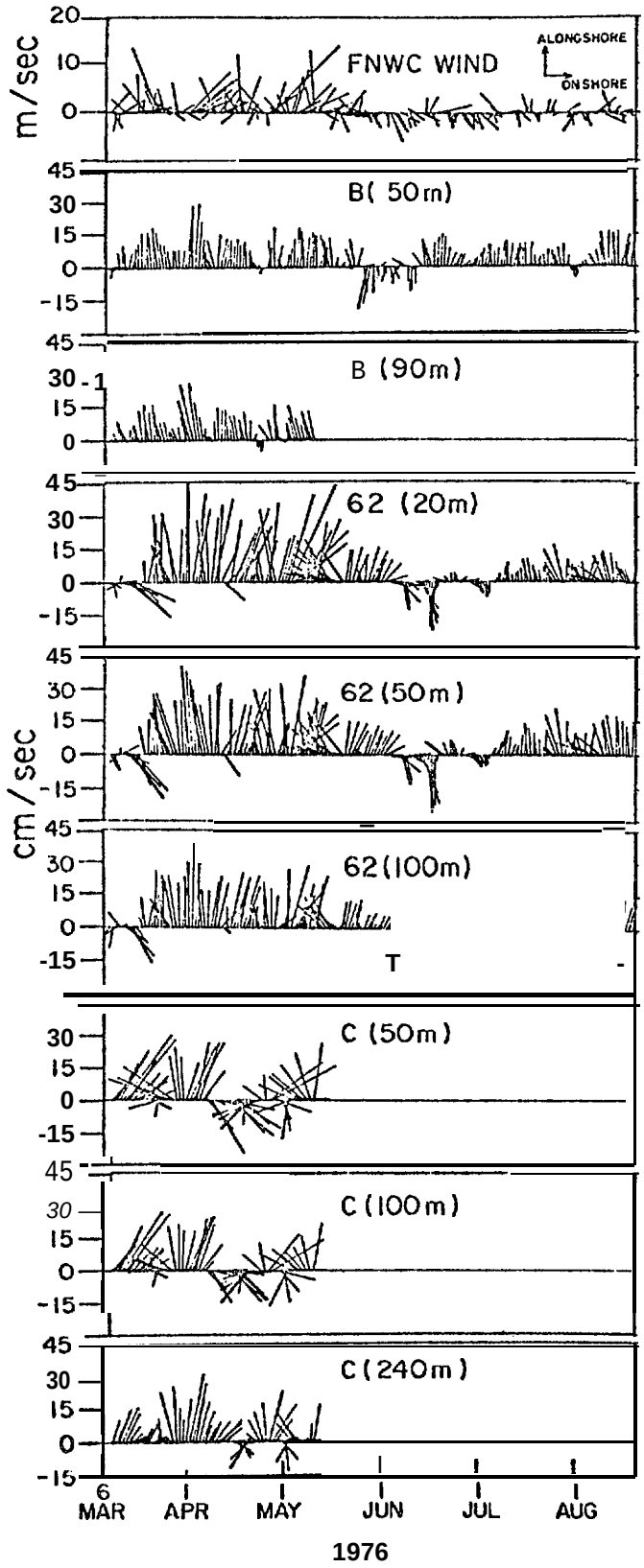

Figure 5.4 - FNWC vector time series for the calculated wind and measured currents. All vectors have been low-pass filtered and rotated into alongshore and onshore axes as discussed in the text.

speed was 5.8 m/s in spring and 2.9 m/s in summer. This variation is typical of seasonal wind patterns as described by Ingraham *et al.* (1976).

5.2.3 Bottom pressure observations

The low-pass filtered (0.025 cph cutoff) time series of atmospheric pressure at Yakutat, adjusted sea level (atmospheric pressure in millibars added to sea level in centimeters) at Yakutat, and bottom pressure at sites B, D, E, and F are shown in Figure 5.5. Mean pressure calculated over the record length was subtracted from each time series. At site B, the total record was constructed by joining records from two consecutive deployments; at other locations the data are continuous measurements by a single gage.

In Table 5.1 the mean trend and detrended variance are given for filtered bottom pressure records. Adjusted sea level from Yakutat was not included in this table because tide gage data from the Yakutat station had numerous gaps. However, the Yakutat series was similar visually to bottom pressure recorded at site D. Mean trend, based on least squares linear regression, varied between sites. At the 100 m isobath (sites B and E) the trend was negligible; however, at 50 m (D) and 250 m (F) the trend was about 1 cm/me. These trends were not constant throughout the record.

The measured bottom pressure is composed of several terms related by the equation:

$$P_B = \bar{P} + P_a + g\int_o^H \rho'(z,t)dz + \rho_o g\eta \qquad (3)$$

$\bar{P}$, mean pressure at the mean depth H of the gage, can be ignored since we are only concerned with time-dependent pressure. Pa, the atmospheric pressure, is often assumed to be compensated for by the inverse barometer effect (i.e., an equivalent change in sea level). However, if sea level compensation is depth-dependent, then atmospheric pressure fluctuations will produce changes in the bottom pressure gradient. Such an effect is difficult to isolate, since winds accompanying the changes in Pa are expected to dominate (Buchwald and Adams, 1968). The third term in (3) represents the density effect. Local changes in the density distribution could affect the measurement of bottom pressure. Finally, the last term represents pressure changed due to sea level variation η. Using equations (1) and (2), this term can be related to the barotropic current. Thus, before assigning dynamical significance to the measured bottom pressure gradient, the influence of all other terms must be considered.

The observed trends can be compared with water density variations at each site. CTD casts near each mooring showed an increase in dynamic height from spring (February-April) to summer (August-September) of 12.5 cm, 6.6 cm, and 4.8 cm at the 50, 100 and 250m isobaths, respectively, If sea level were constant over this period,

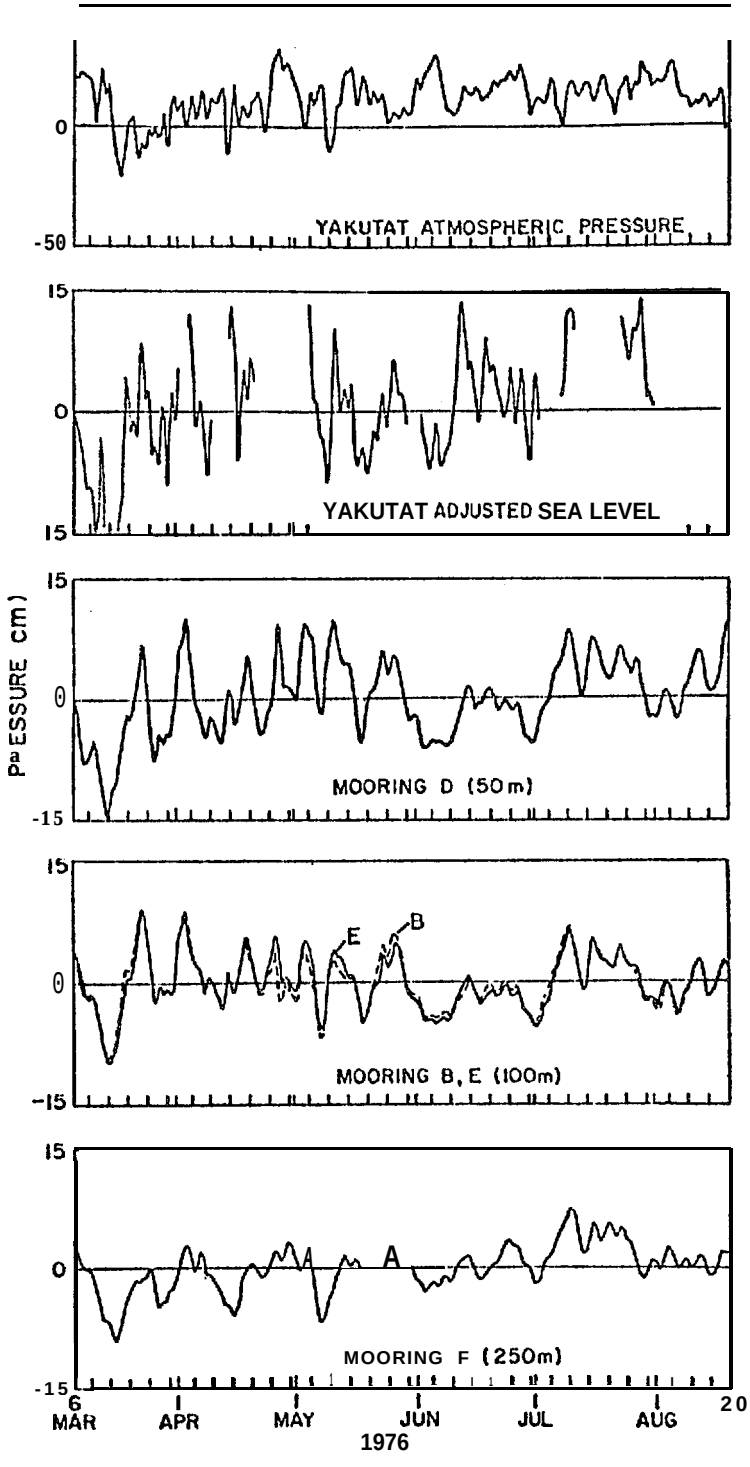

Figure 5.5 -Time series of atmospheric pressure and adjusted sea level at Yakutat and of bottom pressure at B, D, E, and F. All records have been low-pass filtered. The gaps in adjusted sea level are caused by missing tide gauge data. It is assumed that 1 cm = 1 mb.

Table 5.1 - Statistics of bottom pressure for the period 6 March-20 August 1976. The variance was calculated after removing the linear trend.

Location	Variance (cm^2)	Trend (cm/me)
B	11	0.04
D	19	0.99
E	11	0.05
F	5.8	0.93

then bottom pressure at each site would show a decrease comparable to the dynamic height increase. None o-f the bottom pressure records show such a decrease, thus shallow water density changes do not appear important in local sealevel variations.

Reid and Mantyla (1976) found good agreement between seasonal changes in Yakutat adjusted sea level and deep water density variations off the continental shelf. Based on historical data, monthly mean adjusted sea level at Yakutat increased by 5 cm between April and August. This change is similar to the pressure trend observed at 50 and 250 m. Using CTD observations in 1,500 m of water, we calculated a spring-summer change in dynamic height between 1,000 dbar and 50, 100 and 250 dbar surfaces to be 6.2, 5.1, and 4.2 dyn cm, respectively. These observations support the conclusion of Reid and Mantyla (1976) that seasonal sea-level changes observed on the shelf are related to the deep water" density field.

Bottom pressure variance across the shelf varies inversely with water depth H (Fig. 5.6). If one assumes that bottom pressure fluctuations represent sealevel oscillations associated with a nondivergent wave, then the inverse relation of pressure variance with depth implies that the depth-integrated horizontal kinetic energy is constant across the shelf, i.e., $V \sim H^{-1/2}$. As pointed out by Kundu and Allen (1975), theories of continental shelf waves lead to such a velocity-depth relationship.

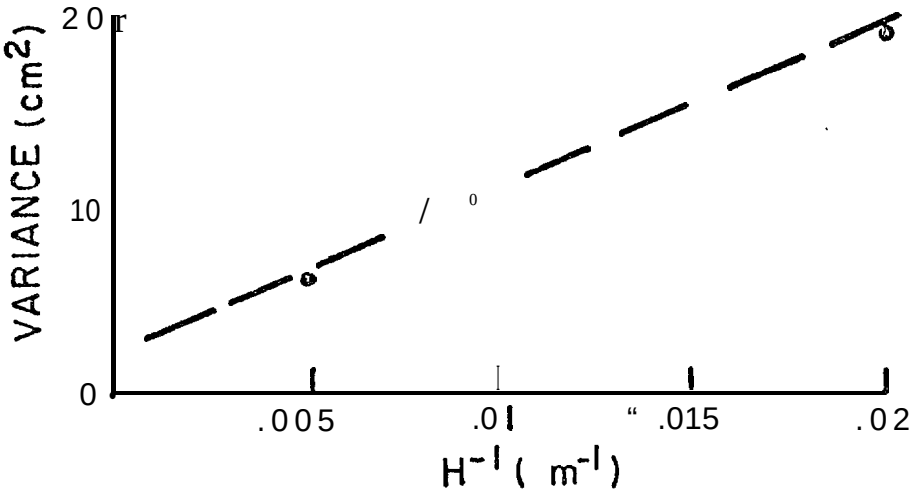

Figure 5.6 - Low-frequency bottom pressure variance plotted as an inverse function of water depth H. A linear trend was removed from the time series before computing variance.

5.3 Analysis

5.3.1 Current time series, vertical and cross-shelf structure

Current vectors were rotated into an approximate cross-shelf (u) and along-shelf (v) coordinate system determined from principal axes of the data (Fofonoff, 1969), local bathymetry, and the mean velocity vector. The principal axes were significant (based on the stability of the ellipse; Gonella, 1972) at the 50 m and deeper current meters on B and 62. At C only the near-bottom (240 m) current record had a stable axis. At all locations the principal axis of the deepest current record was within 10° of the orientation of the local bathymetry. This direction was therefore chosen as the alongshore coordinate. and current vectors at all depths were rotated accordingly. For the three locations, B, C, and 62, the alongshore axes were 300°T, 300°T and 310°T, respectively.

The rotated velocity time series were filtered using a tidal eliminator filter (Godin, 1972). This filter was chosen since it removed the strong tidal component seen in the pressure records. However, its half-power point is at a period of about 72 hours. Therefore, in calculating spectra or coherence the unfiltered time series are used and only the low-frequency (<.025 cph) estimates are presented. Filtered data are used in time series Plots and correlation function calculations.

Figure 5.4 shows the low-pass filtered vector time series of the velocity observations considered here. The data have been subsampled to give daily values. Statistical characteristics of these records are given in Table 5.2. In all cases a bar indicated mean value over the length of the series, while a prime' refers to time-dependent velocity with frequencies below .025 cph. Mean kinetic energy (per unit mass) $\overline{KE}$ is defined as $\frac{1}{2}(\bar{u}^2 + \bar{v}^2)$ and eddy kinetic energy $KE' = \frac{1}{2}(\overline{u'^2} + \overline{v'^2})$. In referring to velocity series a subscript indicates mooring location, and depth of the current meter is given in parentheses.

Mean velocity at all locations is predominantly longshore. The shear in this component is small; the largest velocity difference (5 cm/s) occurred between $\bar{v}_{62}$ (20) and $\bar{v}_{62}$ (100) during spring. In the cross-shelf direction, vertical structure during March-May was consistent with downwelling circulation. On the shelf at B and 62, the near-surface current $\bar{u}_{62}$ (20 M) was onshore and the near-bottom current $\bar{u}_B$ (90) was offshore. However, at the shelf break (C) flow at all depths was onshore which may indicate that the downwelling circulation did not extend this far offshore. Cross-shelf flow was small at all locations, and a slight error in assigning axis orientation could affect this interpretation.

In summer, the seasonal thermocline could support larger mean shear. If such shear occurred, it must be above 20 m, since in the mean there was negligible gradient between the 20 and 100 m currents in May-August . The dominant difference between spring and summer was a reduction in mean flow speed. At B, the mean speed dropped by a factor of 2; at 62 it dropped by a factor of 4. (However, mooring motion may affect this result.)

Vertical structure of the time-dependent velocity components varied across the shelf. At B and at 62, the rms speeds had little vertical structure; however, at C these rms speeds decreased from 21cm/s at 50 m to 11.5 cm/s at 240 m. Presumably, shear across the permanent pycnocline is responsible for this decrease. Linear cross-correlation between longshore velocities at different depths show high correlations at B and 62, For the spring period (March-May) the correlation coefficient 0.95 between v_B (50) and v_B (90) and ().93 between v62 (20) and v62 (100) was not significantly reduced (O. 88). At C, the correlation between velocity components was 1 ess than observed on the shelf (0.71 between v_C (50) and v_C (240)); however, the rature of the flow at the shelf break makes the correlation of the rectilinear components less useful.

Figure 5.4 shows a clear difference in the current field as we proceed across the shelf. At the 100 m isobath, mean flow and low-frequency oscillations were largely parallel to the coast. At the 250 in isobath the flow was still predominantly longshore, but there was significant: cross-shelf flow. Even the near-bottom current meter (240 m depth) showed this effect. There is little visual correlation between velocity at B and C; however, B and 62 appear related both to each other and to the wind.

Table 5.2 - Statistics of velocity time series. Overbars indicate mean values, u′ and v′ are the standard deviations of these components. Standard error estimates on the mean values, $\overline{KE}$ and KE' are discussed in the text.

Location	Date	Depth (m)	ii (cm/s)	$\bar{v}$ (cm/s)	u' (cm/s)	v' (cm/s)	$\overline{KE}$ $(cm/s)^2$	KE' $(cm/s)^2$
B	7 Mar-14 May	50	.1±.5	11.1±1.4	2.6	7.3	62	30
		90	-1.6±.3	8.8±1.1	1.4	6.0	40	19
	15 May-20 Aug	50	.1±.7	4.9±1.2	4.1	7.7	12	38
	7 Mar-20 Aug	50	.1±.2	7.2± .9	2.0	7.6	26	31
c	9 Mar-13 May		3.2±3.7	5.6±3.7	14.9	14.8	21	221
		1%	2.9±3.0	5.6±3.3	12.2	13.1	40	160
		240	2.2±1.4	7.1?2.5	5*5	10.1	28	66
62	7 Mar-14 May	20	4.6±1.9	19,523.3	9.0	15.9	201	167
			0.5±1.7	16.9±3.1	8.0	14.8	143	142
		1%	1.2±1.2	14.0±2.5	6.0	11.8	99	87
	15 May-20 Aug	20	-.121.1	3.8±1.6	6.5	9.1	7.2	62
			.2*1.2	5.2±1.8	6.6	10.0	14.1	72
		1;:	.4±.6	4.2±1.3	3*7	7.6	8.9	36
	7 Mar-20 Aug	20	1.6±1.0	9.9±1.8	7.1	13.6	50	117
		50	.4±.9	10.1±1.7	6.5	12.9	51	104
		100	.9±.5	8.4±1.4	4.0	10.2	36	60

The statistics in Table 5.2 characterize cross-shelf variations. In spring at the 50 m depth, $\bar{v}$ increased from B (11cm/s) to 62 (17 cm/s) and then decreased at C to 6 cm/s. In view of possible contamination of the record at 62 by surface waves, we cannot be certain of the relatively high mean velocity (3o cm/s) to C (22 cm/s). Also, the balance between contribution from longshore and cross-shelf fluctuations changed; at B the alongshelf fluctuations dominated, whereas at C the two components contributed equally. Flow 10 m off the bottom had less cross-shelf variability; however, KE' still increased by a factor of 3.5 between B and C.

In order to compare time scales of low-frequency velocity fluctuations, auto-correlation functions were calculated. The low-pass filtered velocity time series were used with a time step At of 4 hours. Results for sites B and C are shown in Figure 5.7. The integral time scale T_{ij} for each velocity series was estimated from the equation:

$$T_{ij} = \sum_{n=-N}^{N} r_i(n\Delta t)\ r_j(n\Delta t) \qquad (4)$$

(Allen and Kundu, 1977), where r_i (t) and r_j (t) are the auto-correlation function for series i and j. N was chosen to be 8 days so that the contribution to T from n>N was negligible. The integral time scale determines the time required to obtain independent measurements. At 50 m, v' had a time scale of about 2.5 days at B and 4 days at C. Similarly, the u' time scale increased at the shelf break. Figure 5.7 also shows the autocorrelation functions for the near-bottom currents at the two locations. Although details vary, motions at C had longer time scales than those at B.

Having established T for each velocity series, root-mean-square error in the mean velocities can be estimated from:

$$\sigma_1 = \sigma/\left(\frac{\tau}{T}\right)^{\frac{1}{2}} \qquad (5)$$

(Kundu and Allen, 1975), where σ_1 is the rms error of the mean and u is the standard deviation of the time series of length T. Integral time scales of 2.5, 3 and 4 days at B, 62, and C were used to obtain the error limits shown in Table 5.2. These error limits indicate that the differences in $\bar{v}$ at B, c and 62 (during spring) are probably not due to random fluctuations.

Spectral decomposition of the kinetic energy is shown in Figure 5.8 for the 50 m velocity at B, c and 62 in spring. As expected, at the lowest frequency the energy density at the 100 m isobath (B) was an order of magnitude smaller than that observed near the shelf break (C). At higher frequencies the spectra at C falls rapidly with insignificant peaks. However, at B there is a significant energy density peak at about 0.017 cph (60 hr. period).

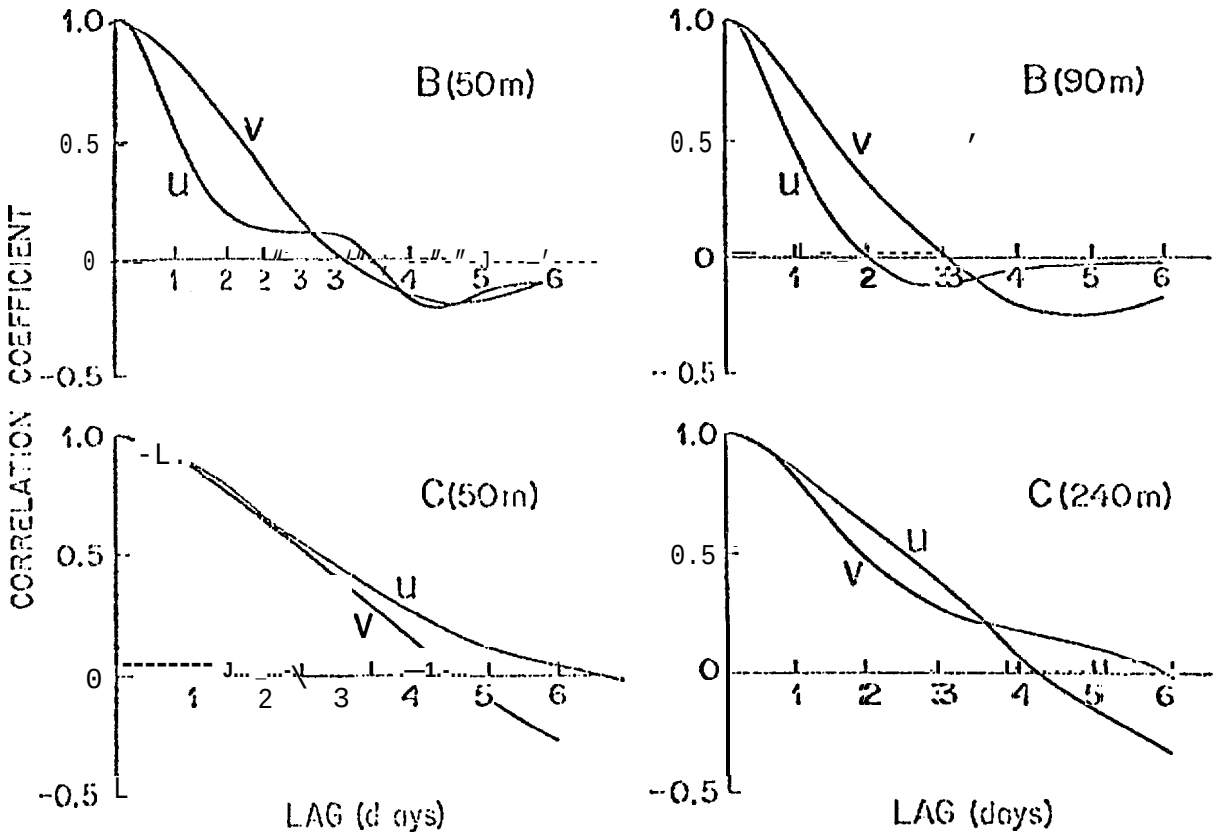

Figure 5.7 - **Autocorrelation** functions of the low-pass filtered velocity components at B and **C.** Results for records at 50 m depth and at 10 m above the bottom are shown in each case.

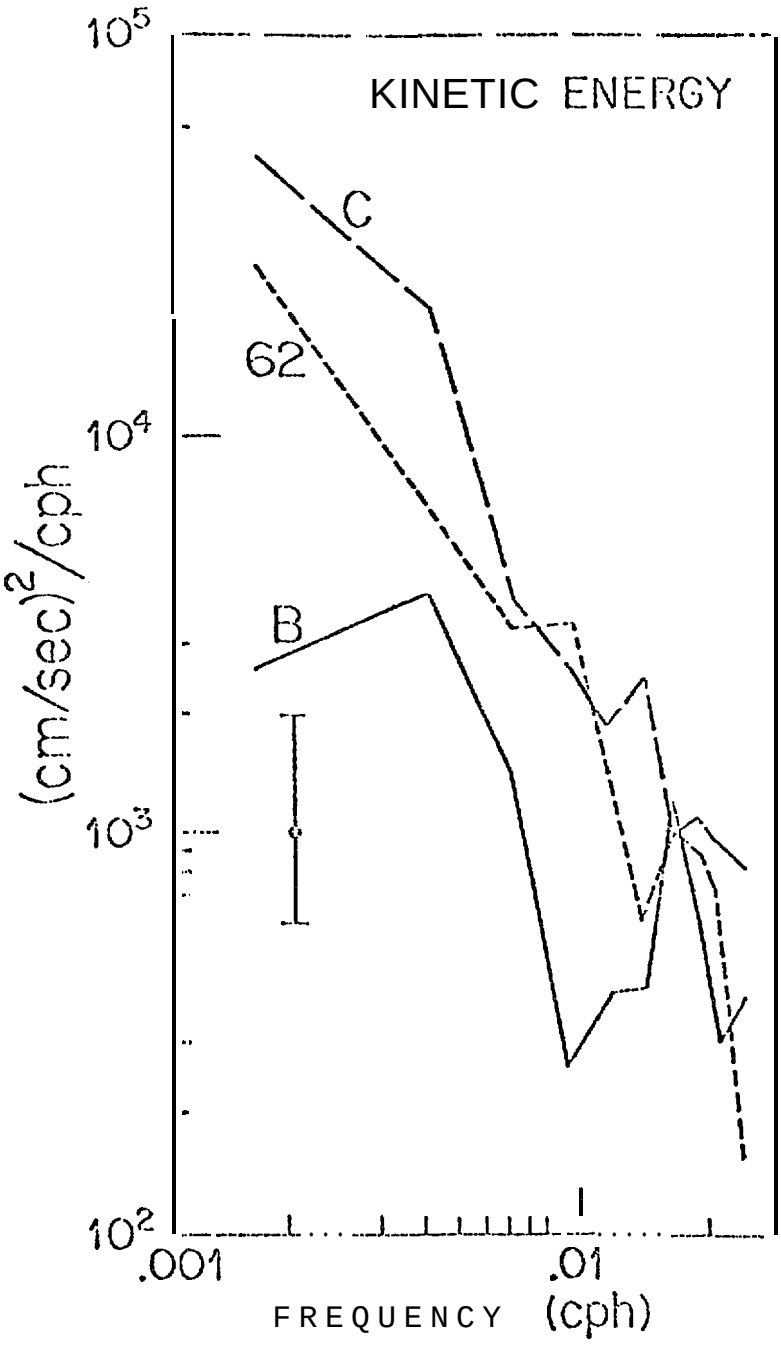

Figure 5.8 **- Kinetic energy spectra of the low-frequency** fluctuation at B, C, and 62 for the period 15 March - 15 May.

Spectra at B and C are further compared in Figure 5.9 where rectilinear and rotary spectra are shown. At B the *low-frequency* flow paralleled the isobath so that the v spectra exceed the u spectra; at C the flow was rotary with a clockwise rotation. Near-bottom kinetic energy spectra are similar to those shown even though the 240 m velocity at C was more nearly aligned with the bathymetry. Clockwise polarization was still observed. These spectra indicate that flow on the shelf was directly steered by the bathymetry, while at the shelf break where the bottom gradient is greater, the flow was rotary.

Cross-correlations for currents at the three sites were computed, but were not large for any of the series. In spring, 50 m cross-correlation coefficients were $r_u = .2$, $r_v = .4$ between B and 62 and $r_u = .1$, $r_v = .3$ between B and C; subscript indicates the velocity component. Similar results were observed between near-bottom currents at 5 and C. Based on a joint time scale of about 3 days, the 10% significance level for these correlations is about .35. Therefore, observed correlations are at best marginally significant. The change in polarization of the flow across the shelf may have resulted in small correlation of u and v components even if rotary components were coherent. To test this, rotary coherence between the velocity series, independent of the coordinate system, was computed (Mooers, 1973). To obtain a measure of overall coherence, spectral estimates with periods greater than 3 days were ensemble-averaged. These coherence estimates have a 95% confidence level for zero coherence of 0.40 (Carter *et al.*, 1973). In spring at the 50 m level the counterclockwise (C_+) and, clockwise (C_-) coherence were $C_+ = .50$, $C_- = .19$ between B and C; $C_+ = .49$, $C_- = .35$ between B and 62; and $C_+ = .23$, $C_- = .06$ between 62 and C. Thus, the dominant clockwise oscillations observed at C (Figure 5.9) apparently did not propagate onto the shelf. These oscillations were coherent and had no phase shift in the vertical ($C_+ = .25$, $C_- = .86, \phi = 3°$ between 50 and 240 m). The motions at C apparently represented quasi-barotropic motions along the shelf break.

5.3.2 Pressure time series, spectra and correlations

Low-frequency (<.025 cph) spectral estimates of the unfiltered pressure records are *shown* in Figure 5.10. At the lowest frequencies these spectra are similar; they have a weak slope up to about .003 cph and then a sharp falloff (ω^{-3}) with frequency. This frequency dependence is stronger than that observed for kinetic energy (Fig. 5.8). Pressure spectra at sites D (50 m) and E (100 m) show a significant peak at 0.017-0.020 cph (60-50 hr. period). This peak is not seen in the shelf break record at C (250 m). A similar peak was noted in the velocity spectra at B (Fig. 5.8). In the frequency band of this spectral peak, pressure variance across the shelf fell more rapidly than H^{-1}. The ratios of variance estimates at the 100 mand 250 m isobath to the 50 m variance were 0.55 and 0.15. This rapid falloff is consistent with an exponential depth dependence.

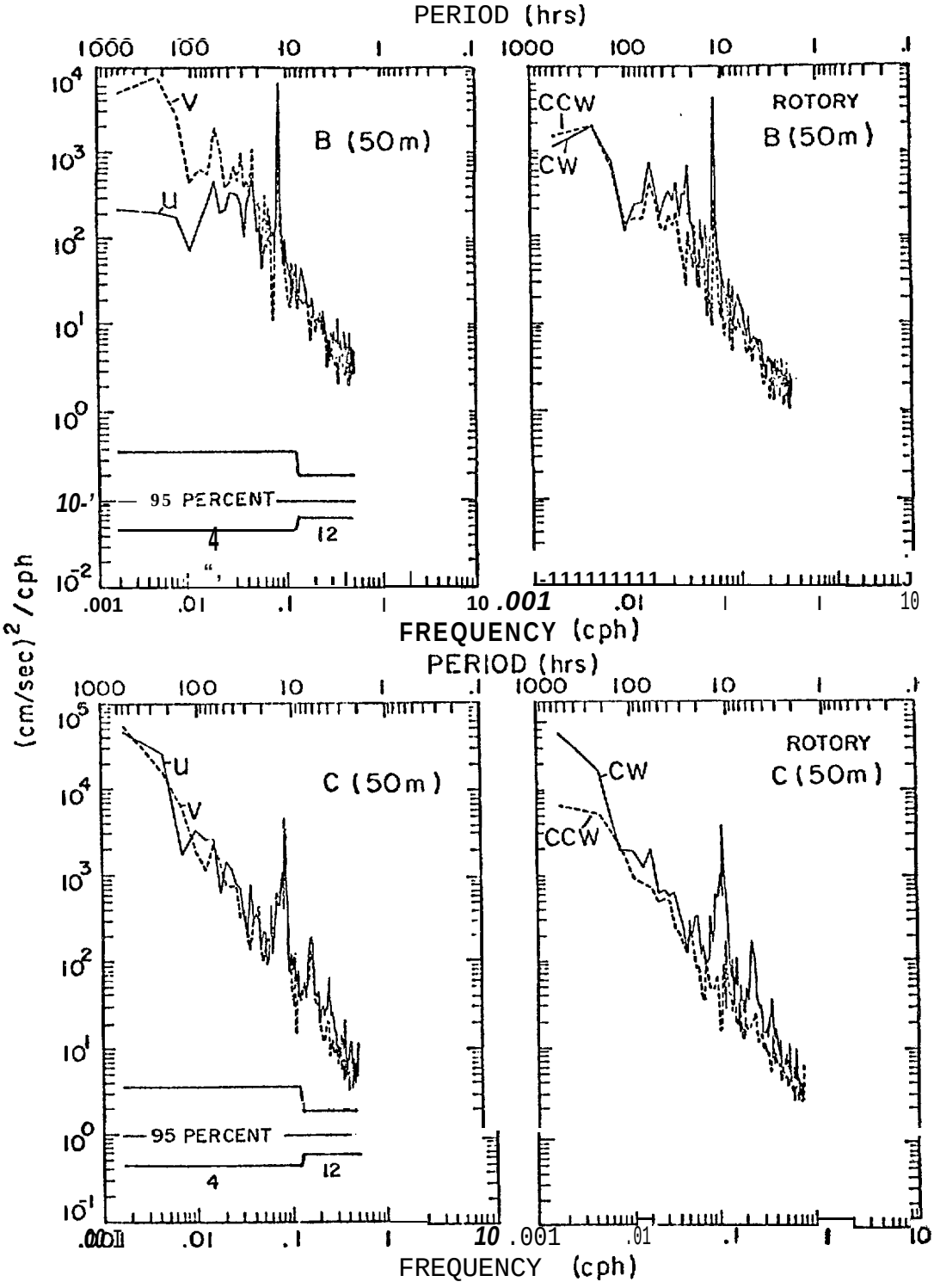

Figure 5.9 - Rectilinear and rotary kinetic energy spectra at the 50-m depth at locations B and C.

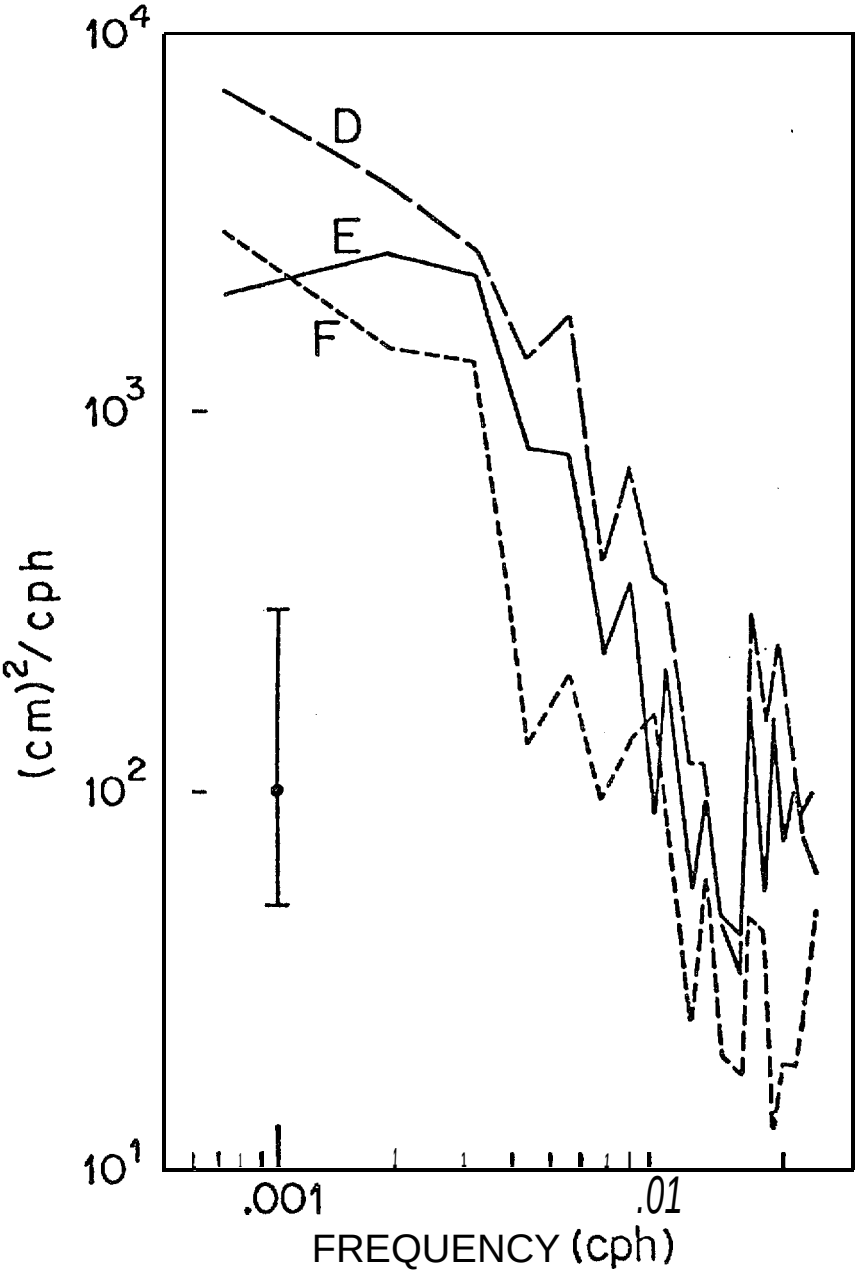

Figure 5.10 - Spectra of bottom pressure records at sites D, E, and F. The error bars indicate 95% confidence interval.

Pressure records may be compared in both cross-shelf and long-shelf directions. The pressure field has a larger cross-shelf coherence scale than velocity. The cross-correlation coefficient between 50 m and 250 m records was 0.59. This larger scale could reflect pressure fluctuations unrelated to shelf effects, such as a seasonal variance associated with changes in deep water structure of the Alaska Current. Though the data records presented here are probably highly influenced by shelf circulation, the 250 m record should reflect to some degree off-shelf pressure fluctuations. Except for the .017 cph energy peak, pressure variance spectra are similar at all locations and offer little hope of separating shelf effects on the basis of frequency (Fig. 5.10). However, coherence between locations D and F shows that only the lower frequency variance ($f < .006$ cph) is significantly coherent across the shelf (Fig. 5.11). This suggests that oscillations with periods longer than about 7 days are more likely associated with off-shelf (or, in any case, very broad) current structures.

The single pressure comparison obtained in the along-shelf direction indicated high coherence. Time series at sites B and E are nearly identical; the cross-correlation coefficient at 100 m depth is 0.98. A phase lag of 2 hours suggests propagation from E to B, counter to the direction expected for free shelf waves. It may be related to the eastward propagation of most storm systems.

5.3.3 Velocity-pressure correlations

Comparison of variations in bottom pressure gradients and currents can provide information on dynamical balances in the equations of motion (1) and (2). We first consider the velocity field. Accelerations u_t and v_t were calculated from the low-pass filtered time series using a central difference approximation with a time increment of 12 hours. The rms longshore velocity term, fv, exceeded acceleration by a factor o-F 20 for both the 50 m current at B and the 100 m. Thus neglect of u_t in equation (1) is reasonable. In equation (2) the rms value of fu exceeded rms v_t by factors of 5 and 10 at sites B and 62, respectively; cross-shelf velocity dominates, but acceleration terms may not be negligible.

Table 5.3 compares longshore velocity with the pressure time series. Cross-correlation coefficients have been calculated between longshore velocity measurements at four currents meters (B (50 m), 62 (100 m), C (100 m and 240 M)) and bottom pressure and bottom pressure gradients. Correlations using low-pass filtered data are presented for three periods: the total record, spring (15 March-15 May), and summer (15 June-15 August). The 5% significance level for the correlation coefficient was estimated using integral time scales defined by auto-correlation functions of the component series (equation (4)). For the total record the 5% significance level was 0.25; for each subinterval it was 0.45.

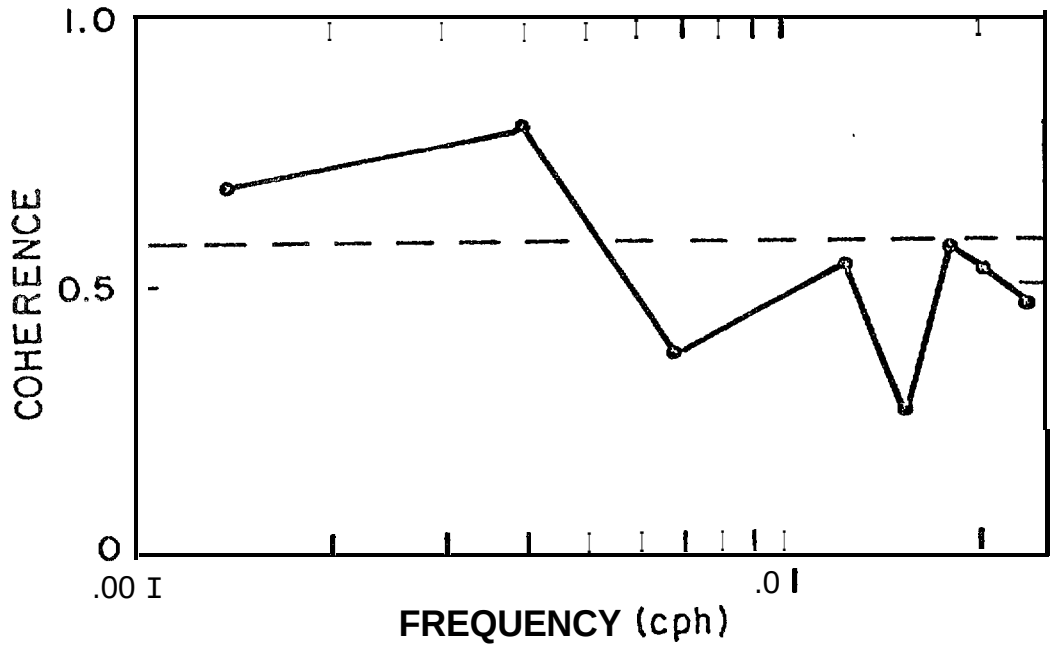

Figure 5.11 - Coherence between bottom pressure measured at sites D (50-m depth) and F (250 -m depth). The dashed line indicates the **95% confidence** level **for zero coherence.**

Table 5.3 - Linear correlation coefficients between velocity and pressure or pressure gradient. The 5% level of significance is approximately 0.45 for the 2-month pieces and 0.25 for the total record.

Velocity	Pressure	7 Mar-14 May	15 June-15 Aug	7 Mar-15 Aug
B-50 m	P_D	0.52	0.56	0.47
	P_E	0.33	0.35	0.36
	P_F	0.02	-0.02	0.08
	P_D-P_E	0.52	0.87	0.49
	P_D-P_F	0.63	0.68	0.56
	P_E-P_F	0.54	0.45	0.47
c-loo In	P_D	0.01		
	P_E	-0.08		
	P_F	-0.04		
	P_D-P_E	0.14		
	P_D-P_F	0.(-)5		
	P_E-P_F	-0.08		
C-240 m	P_D	0.21		
	P_E	0.25		
	P_F	0.27		
	P_D-P_E	0.05		
	P_D-P_F	0.09		
	P_E-P_F	0.12		
62-100 m	P_D	0.75	0.39	0.61
	P_E	0.77	0.41	0.58
	P_F	0.32	0.13	0.18
	P_D-P_E	0.40	0.11	0.41
	P_D-P_F	0.68	0.41	0.63
	P_E-P_F	0.77	0.74	0.67

Results can be summarized by considering the largest velocity-pressure correlations. At the 100 m contour (B) for the total record interval , the highest correlation (0.56) was with the pressure gradient estimated ever the entire shelf (PD - PF). This correlation was better than that obtained with the pressure measurement at 50 m alone (P_D). In spring, similar results were obtained. However, during summer a distinct improvement in correlation was found when the 50 m velocity at B was compared to the pressure gradient between the 50 and 100 m isobaths (P_D - P_E). This correlation (.87) was the highest observed. At the 180 m isobath (62) the best correlation (.67) for the total record was with the pressure gradient between the 100 m and 250 m isobaths. Again, this pressure gradient correlation was only slightly better than the correlation (.61) with the single pressure measurement at 50 m. During spring, results were similar. The summer period was characterized by poor correlation with individual pressure measurements, but correlation with the pressure gradient between 100 m and 250 m isobaths was large (.74). Finally, at the 250 m isobath (C) correlations for all pressure-velocity combinations were below the 5% significance level.

The seasonal pattern of pressure-velocity correlations suggest that the pressure field across the shelf is simpler in spring than in summer. During March-May, correlations using a single pressure measurement on the shelf were almost as high as those which involved pressure gradient measurements. Thus, in spring a reasonable model for the pressure-velocity relation is a linear sealevel slope across the shelf with little or no response at the shelf break. The slight enhancement of the correlation at 62 (180 m depth) when the outer shelf pressure gradient (P (100m)-P (250m)) is used indicates that this model is not entirely adequate and that there is some difference in shallow water sea level response. During summer, individual pressure measurements gave lower correlations with velocity than did pressure gradients. Also, the difference between pressure gradients measured over the inner (P (50 m)-P (100 m)) and outer (P (100 m)-P 250 m)) shelf region was large. The interior gradient correlated with velocity at 62 (r = 0.63).

Summer stratification contributes to increased complexity Of the pressure field. For example, the pressure gradient between 50 m and 100 m isobaths includes a cross-shelf density gradient term as well as the sea surface gradient. Variations in this density gradient term reflect baroclinic velocity fluctuations which would be observed by the current meter at the 50 m level at B. To measure these baroclinic effects the shear in v was correlated with the pressure gradients. No significant correlations were found. However, since we expect the barotropic term to dominate both velocity and pressure fluctuations, the small correlation coefficients do not necessarily preclude baroclinic effects.

In summary, comparison of the longshore velocity and pressure measurements indicates that on the continental shelf 50-70% of the current variance can be accounted for by equation (1). At the shelf break,

current and bottom pressure are uncorrelated. The cross-shelf velocity coherence and these pressure-velocity correlations show that the shelf break separates the circulation into two distince regimes.

With the present data a definitive test of equation (2) is not possible. Figure 5.12 shows v_t, fu and P estimated from the 50 m velocity at B and the long-shelf pressure difference between B and E. Although there are periods when v, or fu appear correlated with P, the overall correlations are not significant. Similarly, the sum, v_t + fu, is not correlated with pressure difference $P_E - P_B$. This lack of correlation is not surprising considering the small magnitude of the quantities. Errors in axis orientation could contaminate the u series: density and local topography could influence the longshelf pressure gradient.

5.3.4 Wind correlations

Wind has been neglected in the above discussions. We expect, particularly in spring, that atmospheric forcing will be important both in driving currents and in setting up sea level slope. FNWC calculated winds and observed winds and pressure at Yakutat are used to investigate the gross features of the response.

A wind energy spectrum for the March-August period (Fig. 5.13) was calculated after detrending the time series by joining the end points (Frankignoul , 1974). At the 95% confidence limit no significant peaks were observed. The energy density had a frequency dependence of about ω^{-1} at low frequencies. This frequency dependence and the energy level are similar to the wind spectrum presented by Hayes and Schumacher (1976). However, the latter spectrum had significant structure near .02 cph.

Variations in atmospheric pressure Pa exceeded variations in any of the bottom pressure series (Fig. 5.5). The low-frequency" variance in P_a was 81 cm^2, a factor of 4 greater than the bottom pressure variance at D. The inverted barometer effect has been shown to reduce bottom pressure fluctuation in the deep ocean. (Brown *et al* ., 1975) and at the shelf break (Beardsley et d., 1977). Here we see that the reduction in bottom pressure variance occurs across the shelf. In addition, linear correlation between bottom pressure fl actuations and Pa was insignificant at all sites (r = -.13, -.14, -.18 between P_A and P_D, P_E, P_F). We thus feel confident in neglecting the contribution of the atmospheric pressure term in equation (3).

Table 5.4 shows correlation coefficients between wind and current or pressure measurements over the 6-month record. At both B and 62, longshore current components are significantly correlated with longshore wind, but cross-shelf wind and current components are uncorrelated. No significant correlation of wind and current at C was found. These velocity correlations substantiate what is clear from the time series plots (Fig. 5.4); longshore shelf flow is related to longshore winds, but flow at the shelf break is not,

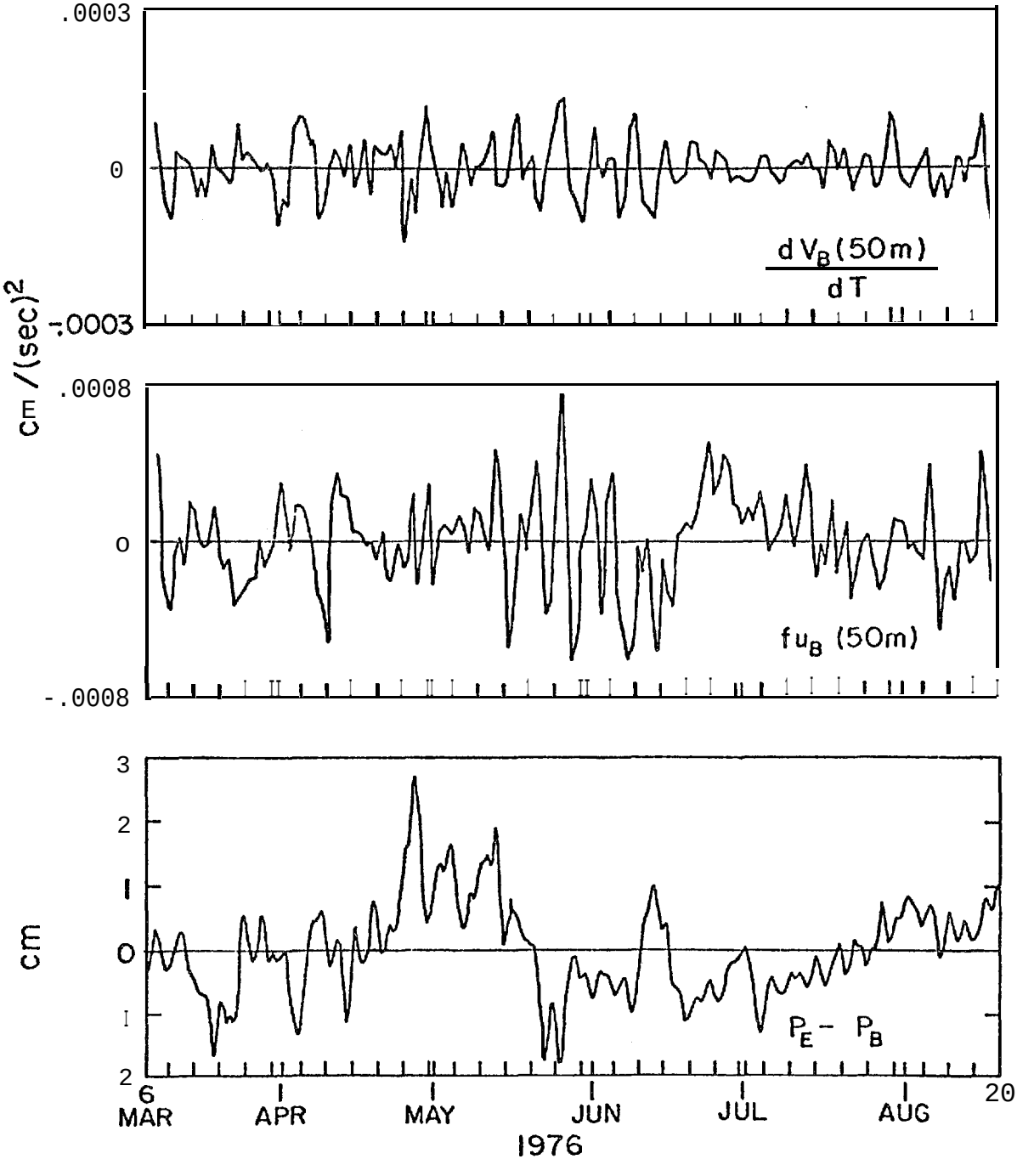

Figure 5.12 - Acceleration of the alongshore velocity compared with the cross-shelf velocity and the alongshelf bottom pressure difference. Measurements were made at the 100-m isobath. Velocity records are from 50-m depth; f is the Coriolis parameter.

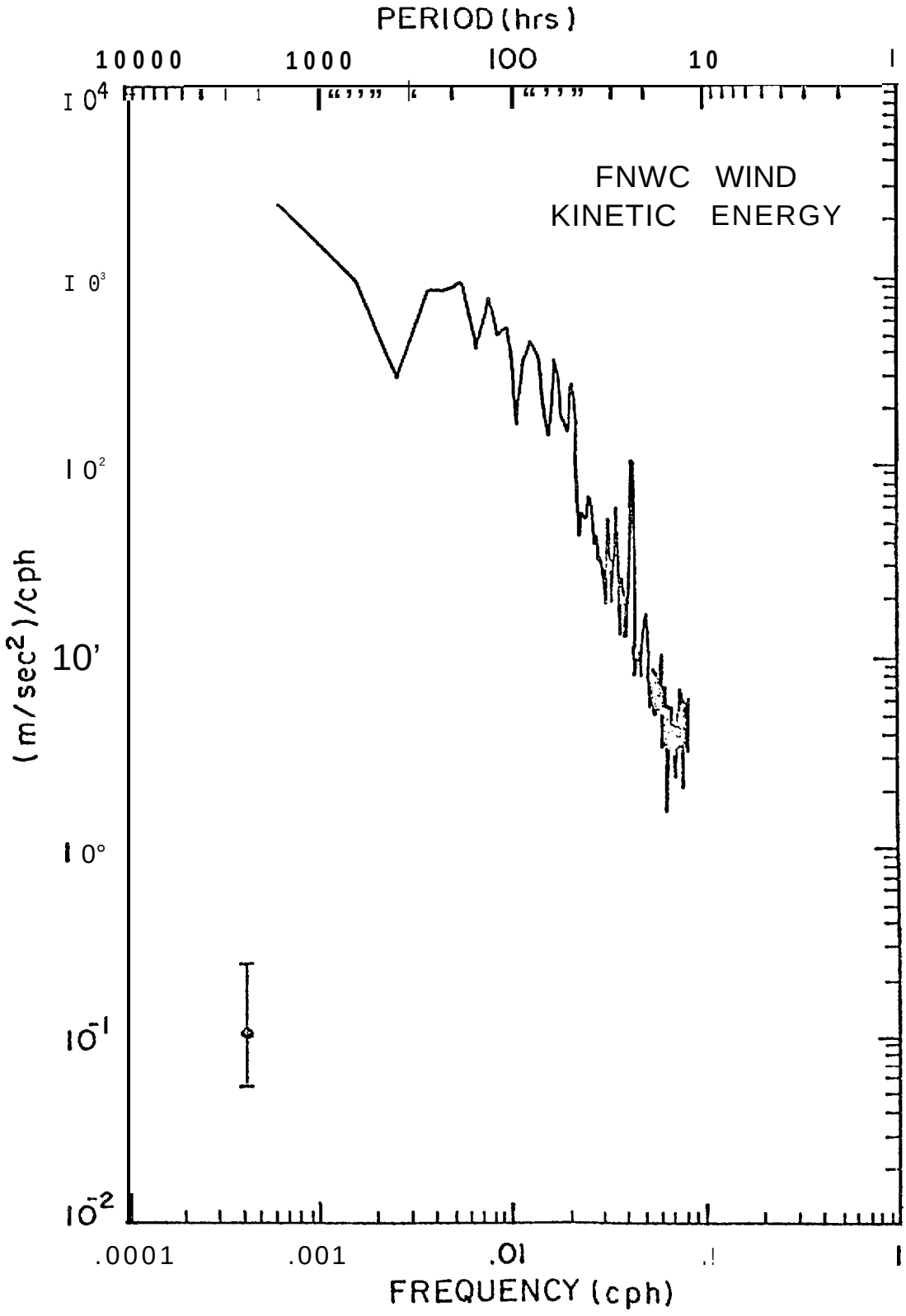

Figure 5.13 - Kinetic energy spectrum of the FNWC wind. The error bars indicate 95% confidence interval.

Table 5.4 - Linear correlation coefficients between wind components and velocity or pressure series.

Series	r_{wind}	r_{wind}
u_B (50 m)	0.10	-0.03
v_B (50 m)	0.27	0.51
u_{62} (100 m)	-0.12	0.20
v_{62} (100 m)	0.08	0.52
$P_D - P_E$	0.33	0.15
$r_E - r_F$	0.05	0.63

The pressure, gradient correlations suggest an interesting difference in response across the shelf. On the inner shelf (between 50 m and 100 m isobaths) pressure gradient was significantly correlated (assuming a 5% significance level of 0.25) with onshore wind; on the outer shelf (between 100 and 250 m isobaths) the significant correlation was with the longshore wind. This relationship is further described by binning the pressure differences according to the component wind speed using 2m/s bins. Resulting scatter diagrams between pressure difference and wind (Fig. 5.14) show a clear tendency for shallow water to respond to onshore wind while deep water responds to longshore winds. This relationship is consistent with simple dynamical ideas. In deep water the Ekman response produces onshore transport accompanying an longshore wind (Ekman, 1905). If however, Ekman depth is equal to or less than water depth, direct wind setup becomes more important (Welander, 1957). It must be kept in mind that wind estimates are crude, particularly for the onshore component. Until more accurate measured winds are available in conjunction with bottom shelf pressure gradient measurements, distinctions between inner and outer shelf response to wind forcing must be treated with caution.

5.4 Discussion and Summary

This section has focussed upon low-frequency ($f<0.025$ cph) variations in current and bottom pressure on the continental shelf in the Northeast Gulf of Alaska. The analysis has shown:

(1) Flow on the shelf differed from flow at the shelf break. At the 100 m contour, mean and fluctuating velocity components were aligned with bathymetry and depth dependence was small. At the 350 m contour,

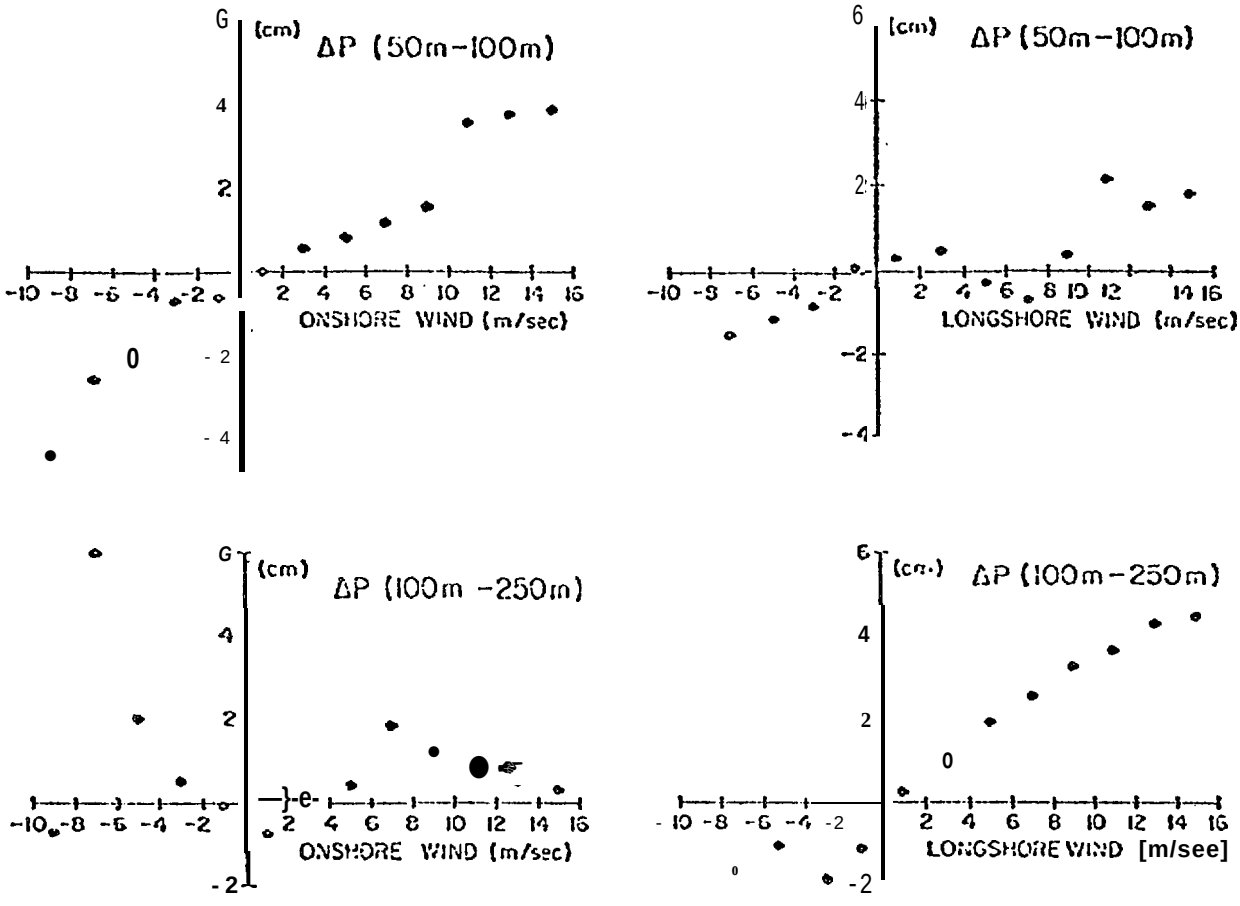

Figure 5.14 - Cross-shelf pressure gradient between indicated depth contours versus onshore and alongshore wind.

mean longshore flow was reduced by 50%, f"1 uctuating components were rotary and "largely anticyclonic, and eddy kinetic energy increased by a factor of 7. These anticyclonic low-frequency motions were vertically coherent, bunt did not propagate onto the shelf. In general, cross-shelf coherence between all velocity series was small.

(2) The bottom pressure field across the shelf was more coherent than the velocity. Along the 100 m isobath the correlation coefficient was 0.93 for a separation of 50 km and the pressure differences did not exceed 3 cm. Cross-sheld bottom pressure variance was an inverse function of water depth. The correlation coefficient of 0.59 between pressure measurements at 50 m and 250 m isobaths indicates large cross-shelf scales for a significant

fraction of the variance. These larger scale fluctuations were predominantly low-frequency (periods greater than 7 days) motions.

(3) On shelf, the 50 m and 100 m isobath bottom pressure variance and 100 m horizontal kinetic energy spectra had a significant peak at about 0.0?7 cph. Station separation was not sufficient *to ob*serve propagation (if any). The oscillations may be a local forced response.

(4) On the continental shelf, bottom pressure and velocity correlations can be interpreted in terms of a simple geostrophic barotropic model. Alongshore velocity fluctuations were balanced by cross-shelf bottom pressure gradients. However, cross-shelf velocity and alongshelf pressure gradients were too small to permit a test of this component equation. Alongshore current-cross-shelf pressure correlations were simpler in spring than in summer, In the former case, a single nearshore pressure measurement was representative of the sea level slope across the shelf. In summer, possibly because of increased baroclinicity, pressure gradient measurements enhanced the velocity correlation.

(5) The contribution of atmospheric pressure to the bottom pressure changes can be neglected even in water depths of 50 m.

(6) Simple dynamical models describe features of the sea 1 evel response to wind forcing. In shallow depths, sea level slope responded directly to onshore winds; in deeper water only the alongshore wind component caused setup. This depth-dependent response can be expected to yield a near-shore coastal current which differs from the current over the outer shelf.

Low-frequency variance on the continental shelf has been shown to correlate with the wind. The Alaska Current is an additional, potentially important, source. Royer and Muench (1977) noted temperature structures in this current which they interpreted as anticlyclonic eddies with spatial scales of tens of kilometers. These eddies could correspond to the anticyclonic flow observed at the shelf break. As discussed above, this flow does not propagate onto the shelf. A possible explanation for this result is provided by the theory for topographic Rossby wave transmission across an exponential shelf break (Kroll and Niiler, 1976). By choosing exponential shapes which fit the Northeast Gulf of Alaska shelf and shelf break, we calculated that the maximum transmission coefficient for low-frequency (.014 cph) waves corresponds to a longshore wavelength of 400 km. Ignoring friction, this transmission coefficient is a broad function of longshore wavelength; however, the coefficient does indicate that small-scale waves (50 km) will tend to be reflected at the shelf break. Thus, assuming scales similar to those noted by Royer and Muench, the observed lack of cross-shelf current coherence is expected. In order to improve our understanding of the relative importance of various low-frequency sources better spatial resolution of the current field and direct nearby wind measurements are required.

6. CURRENTS WEST OF KAYAK ISLAND

In the preceding sections of this report, attention has been focused primarily on circulation in that portion of the northeast gulf east of Kayak Island. In this section, we devote attention to the region between Kayak Island and an imaginary north-south line across the shelf from about Hinchinbrook Entrance to Middleton Island. We expect *a priori* that circulation here will be affected by the presence of Kayak Island on the upstream side (relative to flow in the Alaska Current) and by summer freshwater influx from the Copper River.

6.1 Introduction

General circulation over the shelf west of Kayak Island may be classified as highly complex. The visible surface manifestation of this complexity, as indicated by surface suspended sediments on ERTS satellite imagery (Muench and Schmidt, 1975), was a series of vortex-like features suggesting an anticyclonic flow tendency on the downstream or western side of Kayak Island and extending several hundred kilometers southwest from the island. This complexity was also reflected in the trajectories of four satellite-tracked drifters drogued at 30-50 m depths in the region during summer 1975 (Fig. 6.1). These drifters suggested existence of an eastward counterflow directly downstream from Kayak Island and a westerly near-shore flow. One drifter, #1174, executed several circular loops 30-40 km in diameter just west of Kayak Island, suggesting presence of an eddy-like feature. Since the other drifters did not duplicate this track, the eddy was likely a transient feature associated with vortex shedding on the downstream side of the island.

6.2 Observations

n an effort to better define circulation west. of Kayak Island, current meter mooring 6(I, 61 and 69 were deployed during March-October 1976 (cf. Table 2.1, Section 2). We note that mooring 61, at the shelf break, had in addition been deployed during the previous winter. At each mooring, currents were measured at depths of 20 m, 50 m, 90 (or 100) m and, at the shelf break station 61, 163 m. Data acquired were therefore adequate for estimating cross-shelf and vertical distribution of currents spanning winter-summer (March-August) 1976. Based on the above discussions dealing with time variability, it appears that 1976 was not an unusual year in *terms* of currents, with the possible exception of the current reversal at station 62 during June 1976. With this caveat, we proceed.

Time-series current data can be conveniently presented as vectors showing mean velocity during the measurement period, upon which are superposed bars indicating variance in low-pass filtered current speed both parallel and normal to the mean 'flow direction. This presentation is used for selected March-August 1976 data (Fig. 6.2) and is the basis for the following discussion. We present only the 20 m data, which were generally representative of deeper motions,

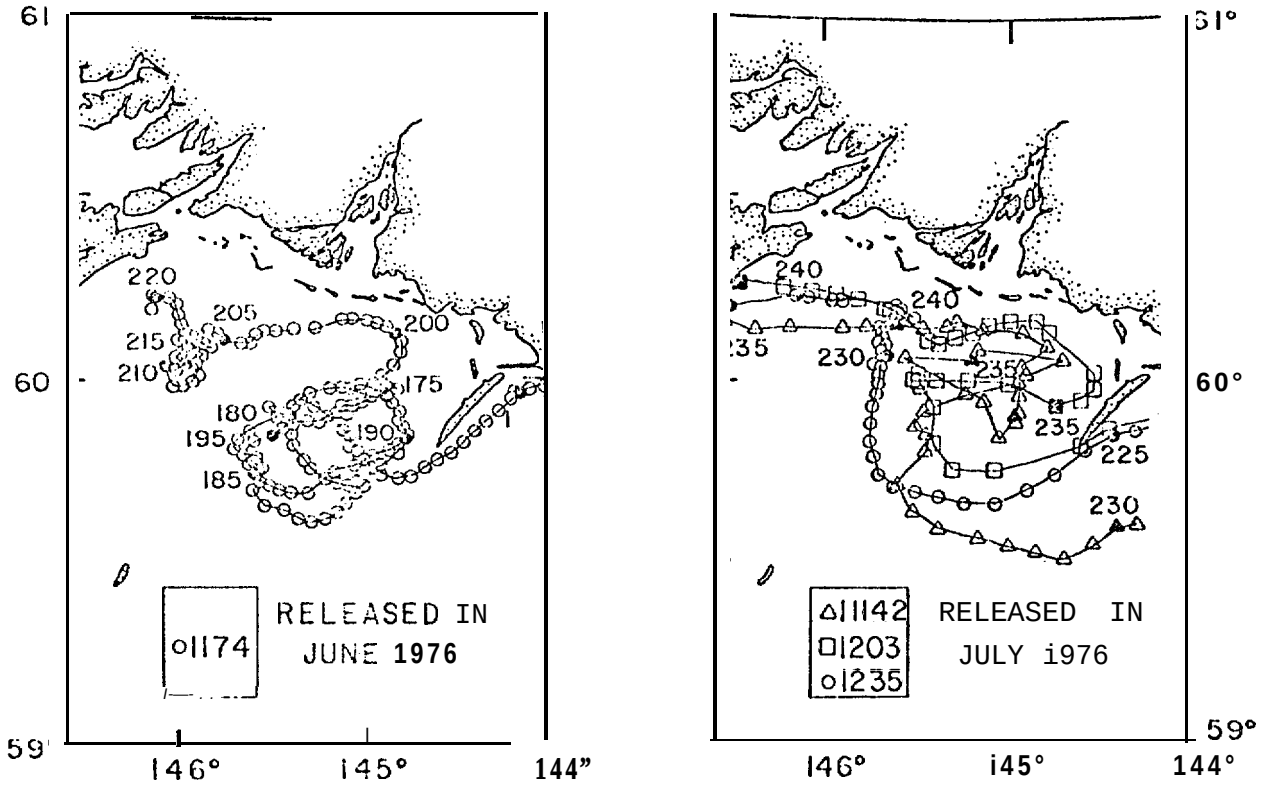

Figure 6.1 - Satellite-tracked drifter trajectories west of Kayak Island in summer 1976.

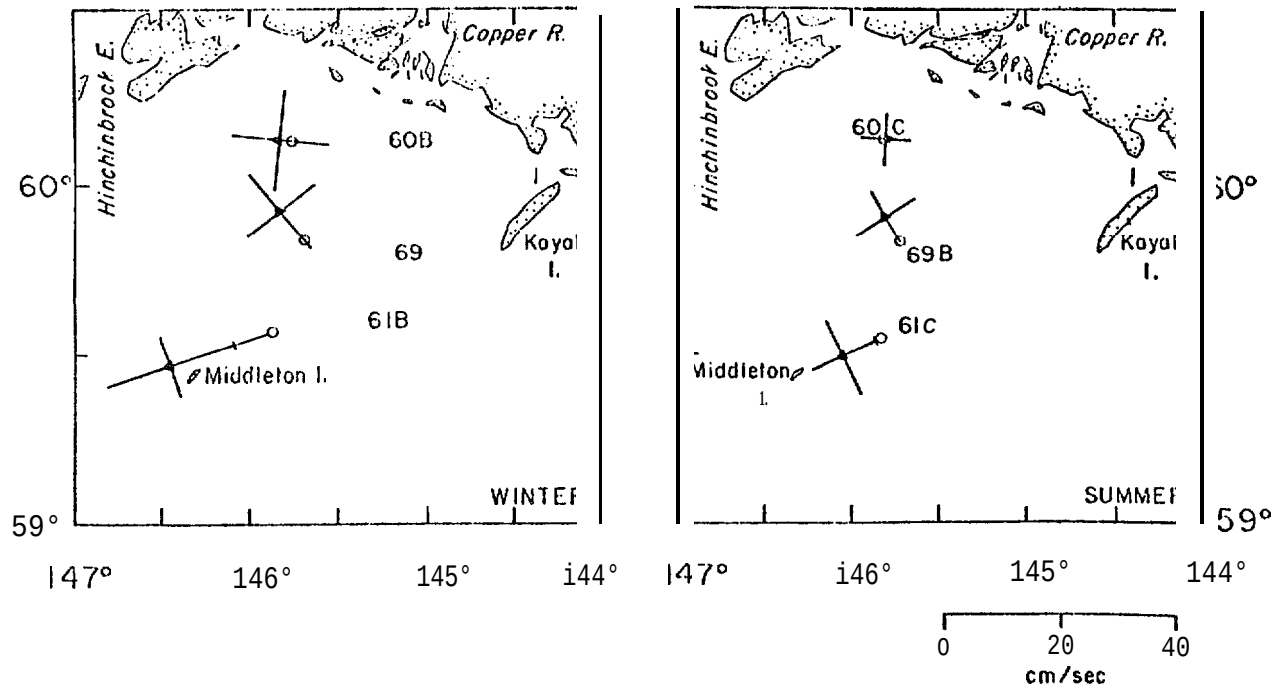

Figure 6.2 - Arrows indicate mean current vectors, while cross-bars indicate variance, at three locations west of Kayak Island during winter and summer 1976.

for stations 60, 61 and 69. Mean flow at the shelf break station 61 reflected the influence of westward longshelf flow due to the Alaska Current, being directed westward. Mean speed was greater during the winter than during summer, as was the variability, noted also for station 62 off Icy Bay (cf. Section 3). The relatively constant direction of flow at station 61 reflected the role of bathymetry in steering water motion; flow paralleled isobaths at the shelf break. Currents at 50 m paralleled those at 201n and have similar speeds. Flow at 100 m was about 45° to the left of the 20 m and 50 m flow during both winter and summer, while speeds were lower than at shallower depths. Referral to the bathyrnetry (Fig.1.1) suggests that bathymetric steering was more effective in controlling current direction at deeper levels. An alternative possibility is that an offshore flow component was present at depth, at least during winter, in response to the known tendency for winter coastal downwelling which would require an onshore near-surface flow and a compensating offshore deep flow (Royer, 1975). Offshore near-bottom flow in this region was also reported by Feely *et al.* (in press), based on near-bottom suspended sediment transport. Such causal factors are impossible to assess here, given the local flow complexity and small number of observations. We also note, *en passant*, that a portion of the flow variability at 20 mwas likely due to wave noise acting on the 17 m deep subsurface float with consequent transfer of energy to the uppermost current meter. This would have been particularly likely during winter, when sea state is at its highest in the northern gulf (cf. Section 2).

At station 69, approximately 25 km shoreward of station 61 and at the same latitude as the western tip is Kayak Island, the mean flow lacked any significant winter-summer speed variation, such as observed at stations 6"1 and 62 along the shelf break. Current direction at station 69 was consistently northwesterly toward Hinchinbrook Entrance at both 20 m and 50 m depths. This northwesterly flow tendency agrees qualitatively with the trajectories of the satellite-tracked drouges (cf. Figure 6.1) in that same area. Apparently this region is one of persistent shoreward cross-shelf flow. This is probably a consequence of the pressure gradients set up by intrusion of Kayak Island into the regional westerly flow and is thus a normal situation.

Currents at station 60, that nearest the coastline, were highly variable and exhibited only a weak mean flow with current speeds of order 2 cm see-l or less. During the spring-summer period, however, flow was easterly. This change in direction was of the proper sense to result from local winter-summer wind variations; winter easterly winds would have driven a westward flow, with the converse true in summer.

Relative variability in the 20m deep currents at stations 60, 61 and 69 is qualitatively shown by progressive vector diagrams for the summer 1976 period (May-October). While currents at stations

61C and 69B show some fluctuation, the overall direction of flow was consistent. Such was not the case at station 60C. One way in which current variability can be addressed quantitatively is by use of rotary spectra (Mooers, 1973), which give an indication both of the frequency components and of the rotational sense! (if any) of the motion. Spectra for the 100 m deep records at stations 60B and 61B during w-inter (March-May 1976) are typical and are shown as an example (Fig. 6.3). Both spectra contain a clearly defined semi-diurnal tidal peak with no other significant peaks. At near-coastal station 60B, the total variance was only about 20% of that at station 61B at the shelf break. At station 61B some 65% of a total variance of 597 cm^2 SeC^{-2} was contained in periods between 12.00 and 12.86 hours, with about 30% in periods between 1.25 and 15 days. Tidal energy at station 60B, like overall energy, was lower- than at station 61B. The overall correlation between the two data sets indicates that, at the 95% significance level, only flow at the semi-diurnal tidal frequency was correlated.

While the hydrographic structure of the water can be used to give an indication of large-scale, long time period motions, it will generally not reflect the shorter period flow fluctuations which characterize currents in the northeast gulf shelf region. With this limitation in mind, we present vertical sections showing density distribution along a transect normal to the coastline just downstream from Kayak Island (Figure 6.4). These sections clearly show evolution of vertical stratification during winter-summer 1976. Using;

$$\Delta\sigma_t = \sigma_{t_{15}} - \sigma_t$$

as a measure of vertical stratification, there was an increase of σ_t from '0.5 to 2.0. This can be attributed primarily to freshwater addition consequent to summer snowmelt in the continental interior, while some of the change is clue to temperature increase from isolation.

In addition to the change in stratification, the vertical density sections show a consistent pattern which must reflect long period flow. The sloping isopycnals indicate a westward baroclinic flow at the shelf break, an eastward counter-flow in the center of the section due west of the southern tip of Kayak Island and a weak westward coastal flow which was best defined during October. Since the current moorings were located west of the sections, a direct comparison between density structure and measured currents was not possible. We note, however, that the persistent westward shelf break flow suggested by the density field is consistent with the westerly flow observed at station 61. Comparison between density distribution and the drifters (cf. Fig. 6.1) is however more satisfying; drift trajectories on the downstream side of Kayak Island generally agreed well with the currents deduced from density distributions.

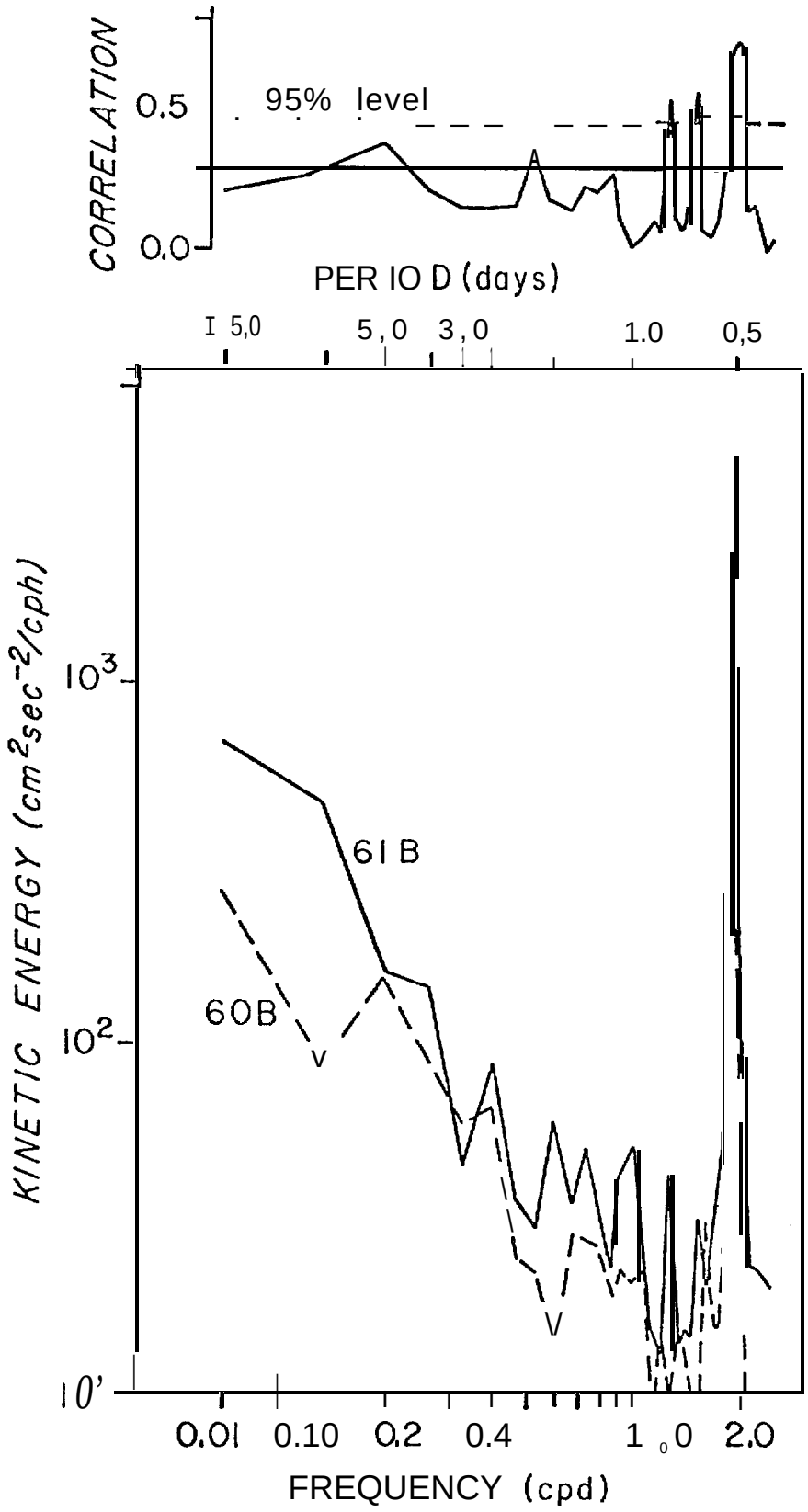

Figure 6.3 - Kinetic energy spectra and rotary correlations for 100 m winter current records at stations 60 and 61 west of Kayak Island.

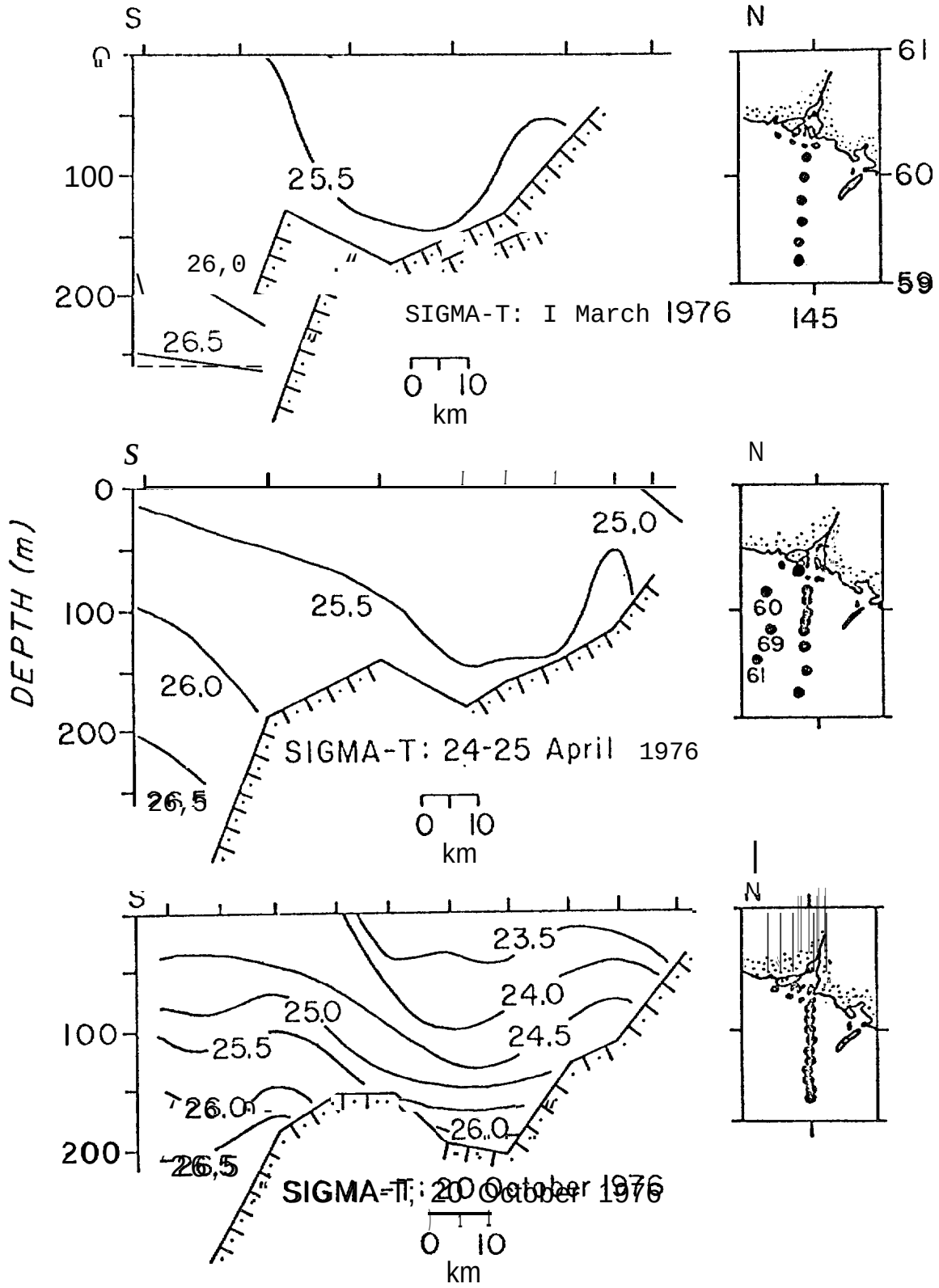

Figure 6.4 - Vertical distribution of density (as sigma-t) west of Kayak Island for three periods in 1976.

6.3 Conclusions

Our measurements have substantiated that there was a persistent westerly shelf break flow southwest of the southern tip of Kayak Island. Typical observed mean flow speeds were approximately '10-15 cm sec^{-1}, and were higher during winter than in summer. These compare well with speed estimates south-southwest of Kayak Island of 17-23 cm see^{-1} based on buoy drift (Feely *et al.*, in press). Speed variability was also greater during winter. These seasonal variations are due to variations in the regional wind field, which drives the mean flow, and in the local winds which contribute to the shorter period fluctuations.

Shoreward from the shelf break, lee effects on the downstream side of Kayak Island confuse the flow field. Our moorings were too far west to aid in defining an easterly counterflow which was suggested both by drifter trajectories and by the density field. This counterflow has a consequence of pressure gradients established in the water by the blocking effect of Kayak Island, which protrudes southward into the westerly flow. The westerly coastal flow was 1 ikely contributed to, in addition, by a coastal low density wedge due to freshwater input. Current measurements in the lee of the island showed large variability which, in the case of the mooring nearest the coast (60) was considerably larger than the mean flow; mean flow at that location must be considered to have little real physical meaning.

The mid-shelf current station, 69, showed persistent shoreward flow which agreed qualitatively with the drogue trajectories. Since this flow persisted through winter-summer, it appears to be a permanent feature.

In summary, the shelf region west of Kayak Island was characterized by a westerly net flow which was greatest at the shelf edge. Flow variability increased shoreward, as mean-flow decreased. The overall flow pattern was considerably more complex than to the east of Kayak Island, due to the blocking effect of the island itself.

7. DISCUSSION AND SUMMARY

Time series current data were obtained from moorings situated in the northeast Gulf of Alaska between Yakutat and Prince William Sound over periods varying from several months to about 2.5 years. These data show the major regional flow characteristic to be a westward mean current extending over the width of the shelf. This flow persisted throughout the year, but speeds were greater during winter than in summer.

The winter speed increase is due to winter increase in regional wind stress curl over the Gulf of Alaska. The Aleutian Low pressure system intensifies during winter, leading to migration of cyclonic storms over the gulf and consequent generation of large positive wind stress curls. This leads to increased cyclonic transport in the Gulf of Alaska gyre with a concurrent increase in westerly flow within the Alaska Current along the northeast gulf shelf break. The westerly flow on the shelf results from lateral transfer of momentum from the shelf break flow and from longshore sealevel slope set up by the shelf break flow. This shelf flow is abetted by local wind forcing and modified by local bathymetric effects, resulting in considerable complexity at the scales which we are considering.

7.1 Spatial Variability

Given a generalized westerly flow on the shelf, more detailed features can be discussed in terms of both spatial and temporal variability. The former will be addressed first. Spatial variations in currents in the northeast gulf are due primarily to constraints imposed by local bottom and coastline topography and, in some cases, to local winds. We first address the topographic, or non time-variant, effects.

The northeast Gulf of Alaska continental shelf can be divided into two segments, which have different physical oceanographic characteristics, by the southward extending promontory formed by Kayak Island. East of this island the shelf is relatively narrow, deep and broken by major bathymetric irregularities in the form of transverse troughs and ridges. West of the island the shelf is broader, shallower and, with the exception of a deep hole just west of Kayak Island, more regular in depth. The width differences in particular are pertinent to continental shelf physical processes. On broad shelves current regimes connected with the shelf break occur independently from the coastal current regimes; on narrow shelves the coastal and shelf break current systems merge and can generate considerable complexity.

Part o-f the difference in flow regimes between those regions east and west of Kayak Island requires consideration of the larger scale topography of the northern Gulf of Alaska. The northern coastline of the gulf is arcuate, curving in direction from northwesterly-southeasterly through east-west to southwesterly-northeasterly. Large-scale oceanic dynamics require that the Alaska Current intensify,

due to this coastline configuration, as it flows westward. While the major intensification occurs to the west of our immediate study area, off Kodiak Island, it is likely that the shelf break flow west of Kayak Island may be stronger than that east of the island. Our observations are, however, insufficient to make conclusive statements about this hypothetical longshore flow variability. A cross-shelf flow west of Kayak Island might, in fact, tend to divert flow from the shelf break current and hence tend to mask this effect.

Currents on the shelf east of Kayak Island were westerly across the entire width of the shelf. At the shelf break, some anticyclonic rotary motions were present, probably due at least in part to the shear zone on the landward side of the Alaska Current. On the shelf itself, currents tended to parallel the local isobaths more closely and lacked the rotary component. West of Kayak Island, the flow was considerably more complex. While westerly flow was observed at the shelf break, as expected due to presence there of the Alaska Current, flows north of the shelf break were characterized by dominant shoreward components through the observation period and vertically through the water column. With the exception of the shelf break observations, currents west of the island showed considerably greater variability in speed and direction than east of the island. This increased complexity west of the island is due to lee effects from Kayak Island, which extends southward and blocks the flow along the shelf. This blocking leads to several features. One of the more obvious effects was vortex shedding in the downstream direction. These vortices were at times manifested as transient eddy-like features appearing first downstream from the island then propagating westward with the mean flow as they decayed. These features were observed both in satellite imagery and in satellite-tracked drifter trajectories.

A second effect of Kayak Island was to establish by its blocking effect a hypothetical (we have not observed it directly) mean sea-level slope leading to an easterly mean counterflow in the lee of the island. This counterflow was observed in drifter trajectories and as a persistent feature in the baroclinic (density) field. An easterly flow requires by volume continuity a compensating westerly flow, and there are two possible choices for such a counterflow. One option would be entrainment into the westerly flow off the southern end of Kayak Island, closing an anticyclonic eddy there. A second option would be inclusion in a westerly coastal flow. Such a coastal flow was observed in drifter trajectories and in the baroclinic field during late summer. The coastal flow appears to be in large part due to presence of a 5-10 km wide freshwater wedge consequent to freshwater input from the Copper River, so would be expected to be a seasonally appearing feature. The spring density section did not indicate presence of such a feature, and no drifter data were obtained during winter to verify its absence. We hypothesize that it may not be present during winter, or would be in greatly reduced form if present.

The strong shoreward component of flow observed at the mid-shelf current mooring west of Kayak Island and indicated also by one of the drifter paths is of uncertain origin. This flow was apparently too far west to reflect the counterflow behind Kayak Island, but it is likely that it reflected the perturbing influence of the island on westward flow.

7.2 Time Variations

It is apparent from examination of the long time series current record obtained from station 62 that time variability is a major factor to consider in any discussion of flow on the northeast Gulf of Alaska continental shelf. Standard deviations were at times larger than mean flow, particularly during summer when mean flow was weakest. Time variations can be subdivided and discussed according to the dominant time scales ranging from seasonal down to 5-7 day scales typical of synoptic weather patterns.

Seasonal variations are the most obvious both as to nature and source, therefore are easiest to characterize. They are manifested both as variations in the mean flow itself and as variations in intensity of perturbations upon the mean flow. Seasonal variations in mean flow were readily observable from the monthly means computed for station 62 (Section 3), and were also evident as differences between mean values computed for summer versus winter moorings at other locations (Sections 5 and 6). Seasonal variations in flow variability are reflected on the plots of variance (as mean speed squared) against time of year at station 62; the winter increase in variability was considerable, and was due to the effects on the water column of severe cyclonic storms migrating eastward through the system. It must be noted that, while the record from station 62 was long enough to qualitatively identify seasonal variation, the record was not long enough to statistically define the annual cycles. Since there was no reason to believe that the years sampled were abnormal, the variations observed are probably representative.

Shorter term fluctuations in current speed and direction, those which contribute to the large variability about the mean at station 62, are due to variations in local wind forcing and to interaction of the mean flow with topographic features such as Kayak Island and the ridges and troughs which cross the shelf transversely off Icy Bay. East of Kayak Island the flow regime is more heavily controlled by the westerly shelf break flow than west of the island because the shelf is narrower in the former location and also because the blocking action of the island itself influences downstream flow. Short-term (2-10 days) flow fluctuations east of the island are largely due to fluctuations in local wind forcing (Section 5), though some portion of the variability reflected fluctuations in the shelf break flow clue in turn to offshelf disturbances.

West of Kayak Island, fluctuations were large relative to the mean flow. Due to the greater width of the shelf, local winds can be expected to play a larger role in driving variable currents relative to the shelf break-driven mean flow. Fluctuations downstream from the island would also reflect the effects of vortex shedding from the interaction of the island with the westerly flow, i.e., a topographic effect. Wind observations west of Kayak Island were inadequate for comparison with currents. It is therefore impossible to assess quantitatively the relative importance of local winds and topography upon flow variability west of Kayak Island.

Based on the foregoing, it is apparent that the concept of a "mean current" is a statistical entity which does not necessarily have any physical significance. This is due to the observation that the mean current was, in many cases, considerably less than the fluctuations about the mean. This was particularly true during summer, when the concept of mean current would have had little meaning if taken within a predictive context, and at current stations closer to the coast and farther from the shelf break.

The northern Gulf of Alaska coastal region has been characterized as a coastal upwelling regime during summer which reverses during winter to a downwelling regime. These are driven by the regional wind field. The current measurements off Icy Bay indicate that this was true some of the time during late winter-summer. There was a bimodality in the flow, however, which indicated that currents could be off- *or* onshore depending upon the particular wind event. As on other shelf regions, upwelling phenomena tend to occur as discrete events with periods of relaxation in between. Therefore, while the "mean" seasonal characterization might accurately be an upwelling or downwelling regime, the instantaneous situation at a given time can be quite otherwise in much the same way in which instantaneous currents need not bear any relation to mean currents. The topographic complexities west of Kayak Island make it difficult to determine whether upwelling or downwelling were in fact operative mechanisms. Near-bottom flow on the central shelf tended to be offshore, which would have supported a downwelling regime, but there did not appear to be a shoreward near-surface flow, necessary by continuity to maintain such a regime. The mid-shelf shoreward flow at station 60 downstream from Kayak Island extended through the water column. This barotropic feature was apparently a consequence of extension of Kayak Island southward into the westerly flow and was not related to wind-driven upwelling or downwelling. We conclude by characterizing the flow in the shelf region west of Kayak Island as generally northwesterly but with numerous temporal and spatial variations, large relative to the mean, superposed upon this flow.

When considering near-shore regions, it is necessary to take into consideration the rapid response of nearshore waters to local wind events. In light of the strong katabatic winds which occur in coastal regions of Alaska during winter, nearshore dynamics would

be highly influence! by these outbreaks. Since such winds are not necessarily related to the regional wind field, they must be considered on a case by case basis when addressing the response of near-coastal waters.

Tidal currents have not been specifically addressed in this report except inasmuch as their presence has been noted as peaks on the energy spectra. Tidal currents represent fluctuations having time scales of a clay or less, considerably shorter than those connected with meteorological forcing. In terms of trajectories for either water parcels or pollutants, they represent a mechanism for dispersion rather than for advection, taken in comparison with other advective terms such as instantaneous non-tidal flow.

7..3 Summary

Major features observed in the current distribution on the northeast Gulf of Alaska shelf can be summarized:

- Flow at the shelf break was westerly, with mean speeds on the order of 15 cm see-]. Large variations are however superposed on this mean speed and, coupled with directional variability, can lead to flow reversals.

- Westerly flow was strongest and most persistent at the shelf break. Nearer the coast, westerly flow weakened and directional variability became greater.

- Currents on the downstream (west) side of Kayak Island showed a mid-shelf eastward counterflow which appeared to be a permanent feature. During mid-late summer, a westerly near-coastal flow was observed shoreward of the counterflow. On one occasion, the westward shelf break flow interacted with the easterly counterflow to form a transient eddy-like feature on the downstream side of the island. West of this flow-counterflow system, flow across mid-shelf was northwesterly through the water column.

- Flow variability was larger relative to a weak mean flow during summer. During winter the mean flow was stronger and variability, while larger than during summer, was smaller relative to mean flow. The larger mean flow during winter was due to regional wind stress acting on the Gulf of Alaska gyre. The large winter variability was due to local winds acting on the shelf waters.

- Flow friability west of Kayak Island was due in part to vortex shedding off the southern tip of the island where it impinges into the westerly shelf break current.

- In all parts of the study region, flow variability was appreciable relative to, and at times larger than, mean flow. This was true with respect to both speed and direction. Mean flow figures must therefore be used with considerable circumspection when applied in a predictive sense.

8. REFERENCES CITED

Aagaard, K. 1970. Wind-driven transports in the Greenland and Norwegian seas. Deep-Sea Res., 17, 281-291.

Allen, J.S., and P.K. Kundu 1977. On the momentum, vorticity, and mass balance off the Oregon coast. J. Phys. Oceanogr. (In press).

Bakun, A. 1975. Wind-driven convergence-divergence of surface waters in the Gulf of Alaska. (Abstract) EOS Trans. Am. Geophys. Union, 56, 1008.

Beardsley, R.C., and B. Butman 1.974. Circulation on the New England continental shelf: Response to strong winter storms. Geophys. Res. Lett., 1, 181-184.

Beardsley,R.C.,H. Hofjeld, M. Wimbush, C.N. Flagg, and J.A. Vermersch, Jr. 1977. Ocean tides and weather-induced bottom pressure fluctuations in the middle-Atlantic bight. J. Geophys. Res., 82, 3175-3182.

Brooks, D.A. and C.N.K. Mooers *1977.* Wind-forced continental shelf waves in the Florida Current. Jour. Geophys. Res., 82, *2569-2576.*

Brewer, W.A. , Jr. , H.F. Diaz, A.S. Prechtel, H.W. Searby, and J.L. Wise 1977. Climatic atlas of the outer continental shelf waters and coastal regions of Alaska; Volume I-Gulf of Alaska. AEIDC Pub. B-77, Anchorage, Alaska, 439 pp.

Brown, W., W. Munk, F. Snodgrass, Il. Mofjeld, and B. Zetler 1975. mode bottom experiment. J. Phys. Oceanogr. , 5, 75-85

Buchwald, V.T. and J.L. Adams 1968. The propagation of continental shelf waves. Proc. R. Sot. London, A305, 235-250.

Carrier, G.F. and A.R. Robinson 1962. On the theory of the wind-driven ocean circulation. Jour. Fluid Mech., 12_, 49-80.

Carter, G.C., C. Ii. Knapp and A.}{. Nuttal 1973. Statistics of the estimate of the magnitude-coherence function. IEEE Trans. Audio Electro-acoust., AU-21, 383-389.

Charnell, R.L. and G.A. Krancus 1976. A processing system for Aanderaa current meter data. NOAA Tech. Memo. ERL PMEL-6, Seattle, Washington, 49 pp.

Clarke, A.J. 1977. Observational and numerical evidence for wind-forced coastal trapped long waves. Jour. Phys. Oceanog., 7, 231-247.

Csanady, G.T. 1974. Barotropic currents over the continental shelf. Jour. Phys. Oceanog., 4, 357-371.

Csanady, G.T. 1975. Lateral momentum flux in boundary currents. Jour. Phys. Oceanog., 5, 705-717.

Danielson, E.F., W.V. Burt and M. Rattray, Jr. 1957. Intensity and frequency of severe storms in the Gulf of Alaska. EOS Trans. AIn. Geophys. Union, 38, 44-49.

Dodimead, A.J., F. Favorite and T. Hirano 1963. Salmon of the North Pacific Ocean region. Bull. 13, Inst. N. Pac. Fish. Comm., Vancouver, B.C., 195 pp.

Dodimead, A.J. and G.L. Pickard 1967. Annual changes in the oceanic-coastal waters of the eastern subarctic Pacific, J. Fish. Res. Bd. Canada, 24, 2207-2227.

Ekman, V.W. 1905. On the influence of the earth's rotation on ocean currents. Arkiv for Matematik, Astron. ock Fys., 2, 1-52.

Favorite, F. 1964. Drift bottle experiments *in* the northern North Pacific Ocean, 1962-1964. "Jour. Oceanog. Sot. Japan, 20, 160-167.

Favorite, F. 1967. The Alaskan Stream. Int. N. Pac. Fish. Comm. Bull. 21, 1-20.

Favorite, F. and D.M. Fisk 1971. Drift bottle experiments in the *north* Pacific Ocean and Bering Sea 1957-60, 1962, 1966 and 1970. U.S.Dept. Comm., NOAA/NMFS Data Rep. 67, 20 pp.

Favorite, F. 1974. Flow into the Bering Sea through Aleutian passes, Oceanography of the Bering Sea. occas. Publ. 2, Inst. of Mar. Sci., Univ. of Alaska, Fairbanks, 623 pp.

Favorite, F, A.J. Dodimead and K. Nasu 1976. Oceanography of the subarctic Pacific region, 1960-71. INPFC Bull. No. 33, Vancouver, B.C., 187 pp.

Feely, R.A., E.T. Baker, J.D. Schumacher and G.J. Massoth 1978. Processes affecting the distribution and transport of suspended matter in the northeast Gulf of Alaska. Deep-Sea Res., 25, in press.

Fofonoff, N.P. 1960. Transport computations for the North Pacific Ocean. Ms. Rep. Ser., Fish. Res. Bd. Canada, 77, 87 pp.

Fofonoff, N.P. 1969. Spectral characteristics of internal waves in the ocean. Deep-Sea Res., 16, 59-71.

Frankignoul, C. 1974. A cautionary note on the spectral analysis of short internal wave records. J. Geophys. Res., 79, 3459-3462.

Gait, J.A. and T.C. Royer (in press). Physical oceanography and dynamics of the NE Gulf of Alaska. In; Proc. Symp. on Science Resources and Technology in the Gulf of Alaska, AINA.

Godin, G. 1972. The Analysis of Tides. Univ. of Toronto Press, Toronto, 264, pp.

Gonella, J. 1972. A rotary-component method for analyzing meteorological and oceanographic vector time series. Deep-Sea Res., 19, 833-846.

Gould, W.J. and E. Sambuco 1975. The effects of mooring type on measured values of ocean currents. Deep-Sea Res., 22, 55-62.

Gumbel, E.J. 1954. Statistical theory of extreme values and some practical applications, NBS Applied Mathematics Series, 33, 51 pp.

Halpern, D. and R.D. Pillsbury 1976. Influence of surface waves on subsurface current measurements in shallow water. Limnol. and Oceanogr., 21, 611-616.

Halpern, D. and J.R. Holbrook 1978. Moored near-surface current measurements during February 1975 on the Gulf of Alaska outer continental shelf. J. Geophys. Res. (in press).

Hayes, S.P. and J.D. Schumacher 1976. Description of wind, current and bottom pressure variations on the continental shelf in the northeast Gulf of Alaska from February to May 1975. Jour. Geophys. Res., 81, 6411-6519.

Hayes, S.P., J. Glenn and N. Soreide 1978. A shallow water pressure-temperature gage (PTG): Design, calibration and operation. NOAA Tech. Memo. (in press).

Hickey, B.M. 1977. The use of a numerical model as a diagnostic tool to interpret current and density measurements from the Washington shelf. EOS Trans. Am. Geophys. Union, 58, 1158.

Holbrook, J.R.and D. Halpern 1977. A compilation Of wind, current, bottom-pressure and STD/CTD measurements in the northeast Gulf of Alaska, February-Flay 1975. NOAA Tech. Memo. ERL/PMEL-1 O.

Ingraham, WJ., Jr., A. Bakun and F. Favorite 1976. Physical oceanography of the Gulf of Alaska. Northwest Fish. Ctr. Processed Rep., July 1976, 132 pp.

Kroll, J. and P.P. Niiler 1976. The transmission and decay of barotropic topographic Rossby waves incident on a continental shelf. J. Phys. Oceanogr., 6, 432-450.

Kundu, P.K. and J.S. Allen 1975. Three dimensional structure of low frequency current fluctuations near the Oregon coast. J. Phys. Oceanogr., 6, 181-199.

Lee, T.N. 1976. Florida Current spin-off eddies. Deep-Sea Res., 22, 753-765.

McEwen, G.F., T.G. Thompson and R. Van Cleve 1930. Hydrographic sections and calculated currents in the Gulf of Alaska, 1927 to 1928. Rep. Int. Fish. Comm.,4, 36 pp.

Mooers. C.N.K. 1973. A technique for the cross-spectrum analysis of complex-valued time series with emphasis on properties of polarized components and rotational invariant. Deep-Sea Res., 20, 1129-1141.

Mooers, C.N.K. 1976. Wind-driven currents on the continental margin. In: Marine Sediment Transport nd Environmental Management (Stanley and Swift, Eds.), John Wiley, N.Y., 29-52.

Muench, R.D. and G.M. Schmidt 1975. Variations in the hydrographic structure of Prince William Sound. Univ. of Alaska Sea Grant Rep. R75-1, 135 pp.

Munk, W.H. 1950. On the wind-driven ocean circulation. Jour. Met., 7, 79-93.

Munk, W.H. and G.F. Carrier 1950. The wind-driven circulation in ocean basins of various shapes. Tellus, 2, 158-167.

Mysak, L.A. and F. Schott 1977. Evidence for baroclinic instability of the Norwegian Current. Jour. Geophys. Res., 82, 2087-2095.

Reid, J.L. and A.W. Mantyla 1976. The effect of the geostrophic flow upon coastal sea elevations in the northern North Pacific Ocean. Jour. Geophys. Res., 81, 3100-31"10.

Reynolds, R.M. and B.A. Walter 1976. A study of convective activity in the Bering Sea and air-mass modification on the southern Alaska Coast. Bull. Am. Meteorol. Soc., 56, 139.

Royer, T.C. 1975. Seasonal variation of waters in the northern Gulf of Alaska. Deep-Sea Res., 403-416.

Royer, T.C. and R.D. Muench 1977. On the ocean temperature distribution in the Gulf of Alaska, 1974-1975. Jour. Phys. Oceanog., 7, 92-99.

Royer, T.C. 1977. Hydrographic data report, Northeast Gulf of Alaska, July 1975-June 1976. Univ. of Alaska, Fairbanks.

Smith, R.L. 1974. A description of current, wind and sea level variations during coastal upwelling off the Oregon coast, July-August 1972. J. Geophys. Res., 79, 435-443.

Sverdrup, H.U. 1947. Wind-driven currents in a baroclinic ocean; with application to the equatorial currents of the eastern Pacific. Proc. Nat'l Acad. Sci., 33, 318-326.

Thomson, R.E. 1972. On the Alaskan Stream. Jour. Phys. Oceanog., 2, 363-371.

Webster, F. 1969. Vertical profiles of horizontal ocean currents. Deep-Sea Res., 16, 85-98.

Welander, P. 1957. Wind action on a shallow sea: Some generalizations on Ekman's theory. Tellus, 9, 45-52.

Welander, P. 1959. On the vertically integrated mass transport in the oceans. In: The Atmosphere and The Sea In Motion (Bolin, Ed.), Oxford, N.Y., 95-101.